

CERN LIBRARIES, GENEVA



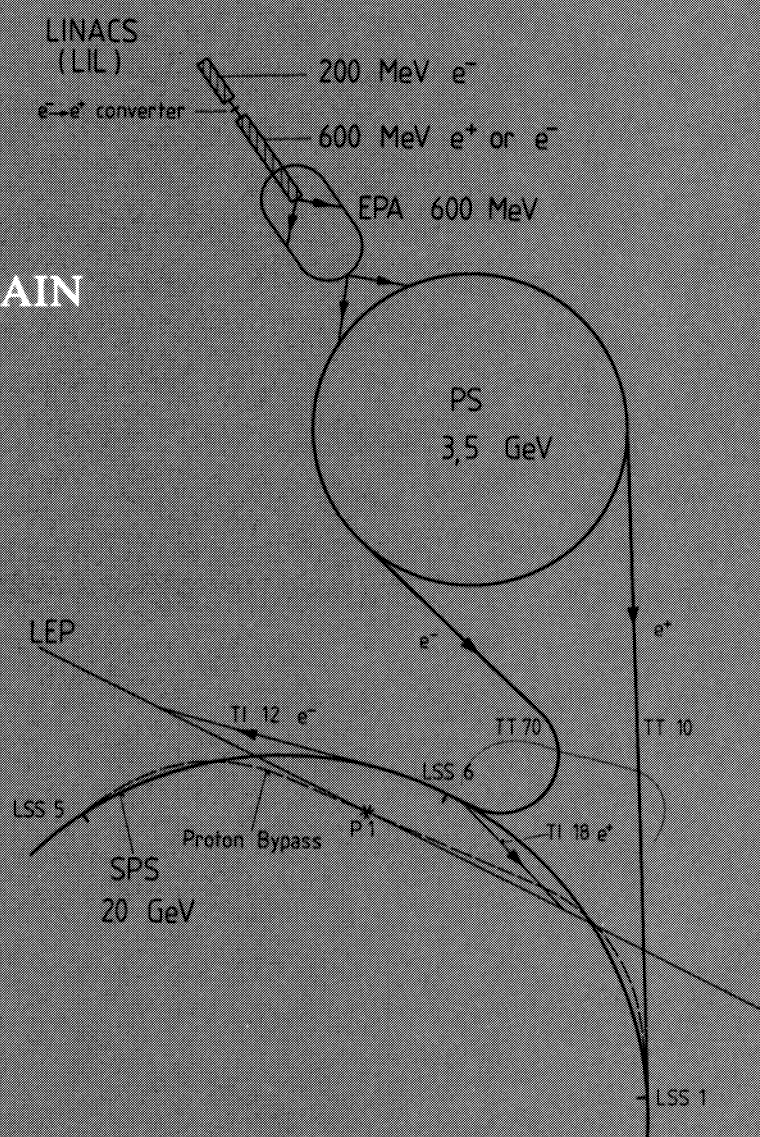
CM-P00047695

CERN-LEP/TH/83-29
CERN/PS/DL/83-31
CERN/SPS/83-26
LAL/RT/83-09
June 1983

LEP DESIGN REPORT

VOL. I THE LEP INJECTOR CHAIN

The LEP Injector Study Group



GENEVA
1983

© Copyright CERN, Genève, 1983

Propriété littéraire et scientifique réservée pour tous les pays du monde. Ce document ne peut être reproduit ou traduit en tout ou en partie sans l'autorisation écrite du Directeur général du CERN, titulaire du droit d'auteur. Dans les cas appropriés, et s'il s'agit d'utiliser le document à des fins non commerciales, cette autorisation sera volontiers accordée.

Le CERN ne revendique pas la propriété des inventions brevetables et dessins ou modèles susceptibles de dépôt qui pourraient être décrits dans le présent document; ceux-ci peuvent être librement utilisés par les instituts de recherche, les industriels et autres intéressés. Cependant, le CERN se réserve le droit de s'opposer à toute revendication qu'un usager pourrait faire de la propriété scientifique ou industrielle de toute invention et tout dessin ou modèle décrits dans le présent document.

Literary and scientific copyrights reserved in all countries of the world. This report, or any part of it, may not be reprinted or translated without written permission of the copyright holder, the Director-General of CERN. However, permission will be freely granted for appropriate non-commercial use.

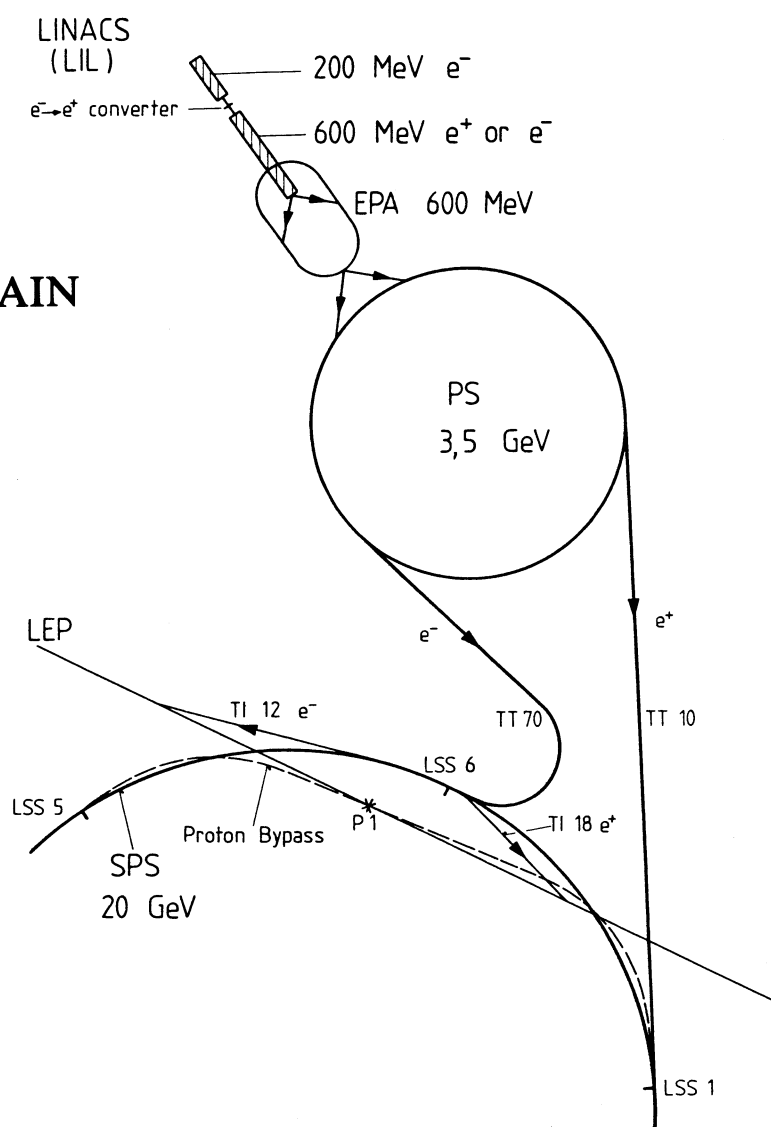
If any patentable invention or registrable design is described in the report, CERN makes no claim to property rights in it but offers it for the free use of research institutions, manufacturers and others. CERN, however, may oppose any attempt by a user to claim any proprietary or patent rights in such inventions or designs as may be described in the present document.

S

LEP DESIGN REPORT

VOL. I THE LEP INJECTOR CHAIN

The LEP Injector Study Group



CONTENTS

	Page
Chapter 1: Introduction	1
Chapter 2: Operation of the injector chain	2
2.1 Brief description of injectors	2
2.2 Modes of operation	2
Chapter 3: Description of individual systems	7
3.1 Pre-injector	7
3.2 PS modifications	20
3.3 Modifications and additions to the SPS	24
3.4 Beam transfer from the SPS to LEP	33
3.5 Injection into LEP	34
Appendix: List of nominal parameters	41
Figures	51

CHAPTER 1

INTRODUCTION

The last comprehensive report¹⁾ on the design of the CERN Large Electron–Positron Storage Ring (LEP) proposed a LEP injector consisting of a new 22 GeV slow-cycling synchrotron with a 600 MeV accumulation ring and linac as pre-injector. Subsequently, in order to reduce the cost it was suggested²⁾ to use the CERN 400 GeV Super Proton Synchrotron (SPS) as the LEP injector, taking advantage of the fact that LEP is close to the SPS in view of possible ep collisions. It was further proposed to accelerate the positrons or electrons in between the SPS proton acceleration cycles, during the dead-time that is imposed by the limit on the average power dissipation in the SPS magnets.

Studies of layout and parameters have been continued and have led to some evolution of the initial concept without changing its basic features. The pre-injector still consists of a small 600 MeV Electron–Positron Accumulation Ring (EPA) acting as a particle buffer between the slow-cycling synchrotrons and the 600 MeV S-band linac which cycles at a rate of 100 Hz; the positron source of this linac is a converter target preceded by a 200 MeV high-intensity electron linac. After accumulation in EPA, eight bunches are injected into the 28 GeV Proton Synchrotron (PS), accelerated to 3.5 GeV, and transferred via the existing proton and antiproton beam lines to the SPS, where the beam is accelerated to 20 GeV and sent to LEP.

As initially suggested, the electrons or positrons are accelerated in the dead-time of the SPS; but instead of one acceleration cycle (e-cycle), four e-cycles are inserted between the proton cycles in order to reduce the intensity of the e-beams in the injectors for beam stability reasons. This is possible because the SPS will operate at 450 GeV in the coming years, which implies a longer dead-time than at 400 GeV operation. Positrons are accelerated in the first two e-cycles and electrons in the second two, which leads to the SPS cycle pattern $pe^+e^+e^-e^-$. Both LEP beams, each consisting of four bunches, are accumulated almost simultaneously with a rate of $0.25 \text{ mA} \cdot \text{min}^{-1}$.

Thanks to this interleaving of cycles, the SPS proton programme is not affected at all by the insertion of the e-cycles during LEP filling and machine development. However, the filling of LEP and the use of the SPS as proton–antiproton collider are not compatible, but appropriate scheduling can take care of this problem.

This report, reflecting the status of the studies, describes the basic layout of the whole system and the conceptual design of the major components. After a brief description of the injector chain, the nominal mode of operation is presented in Chapter 2, including a discussion of possible variants. The individual parts of the chain are treated in Chapter 3. The layout and parameters of the new PS pre-injector are given in detail. For the existing synchrotrons, the emphasis is on the necessary additions and modifications, assuming that the reader is familiar with their basic features and functioning. The description also covers the beam transfer channels between the SPS and LEP, and the injection equipment in the LEP ring. Results of some prototype work are presented and a detailed parameter list is appended. A short summary of this report has been published³⁾.

CHAPTER 2

OPERATION OF THE INJECTOR CHAIN

2.1 BRIEF DESCRIPTION OF INJECTORS

Figure 2.1 shows a schematic diagram of the LEP injector chain. The 200 MeV electron linac consists of a high-intensity gun, a standing-wave buncher, and four travelling-wave S-band sections. Its intense electron beam produces the positrons in the converter target, just upstream of the 600 MeV low-intensity linac which has 12 travelling-wave sections nearly identical to the sections of the first linac. The electrons for electron filling of LEP are produced by a low-intensity gun located near the converter. Thus the high-intensity 200 MeV linac is not used during the electron fills and can stay tuned to high currents. Both linacs deliver 12 ns long beam pulses at a repetition rate of 100 Hz. The length of the two linacs together is approximately 100 m, and their position is about radial to the PS, with the second linac extending into the EPA in order to save on total length.

The linac pulses are stored in turn in eight bunches of the 600 MeV EPA, which has a circumference of 126 m, i.e. one fifth of the PS circumference. The racetrack shape was chosen for the EPA as being the one that makes best use of the available space. The EPA has its long axis on the linac axis and is sited close to the PS, to which it is connected by two new, short transfer lines.

Since the PS is a combined-function machine, the horizontal betatron oscillations are excited by synchrotron radiation at higher beam energies, whereas the energy oscillations are strongly damped, as was already pointed out when e-acceleration in the PS was considered for the first time⁴⁾. This damping behaviour would lead to a very small energy spread, insufficient for beam stability in the PS and for SPS injection. To modify and control the damping partition, a Robinson wiggler⁵⁾ must be installed in the PS. The wiggler together with the additional RF system for acceleration needs straight-section space, which is very scarce in this multifunction machine. For this reason, it cannot be envisaged to accelerate the particles much above 3.5 GeV in the PS, at least not in the initial phase. Since the electron/positron emittances are smaller than the proton emittances, the particles can be accepted by the SPS at this relatively low energy. However, in order to prevent instabilities and beam loss, the total charge to be accelerated per pulse must be distributed over many bunches. This is the reason for using eight bunches in all the injector machines in the basic mode of operation.

The positrons are sent to the SPS via the existing proton beam line TT10, and the electrons travel through the antiproton beam line TT70. The particles are accelerated to 20 GeV in the SPS by an additional 200 MHz RF system consisting of 32 single-cell cavities and, after extraction from the long straight section LSS6 of the SPS, they are sent to LEP through two new transfer channels.

The beams are injected in the arcs of LEP near a horizontally focusing quadrupole about 560 m away from the crossing point 1. A set of septum magnets makes the incoming beam travel parallel and close to the circulating beam; the latter is displaced towards the incoming beam by a closed-orbit bump created by three fast kicker magnets. Since this injection in the horizontal plane occurs at a point where the dispersion function is not vanishing, the injected bunch can be stacked in either betatron or synchrotron phase space close to the already circulating bunch of LEP.

2.2 MODES OF OPERATION

2.2.1 Basic mode of operation

The positrons and the electrons are accelerated in the dead-time of the SPS between the 450 GeV proton cycles. Thus the setting-up for the LEP filling, the filling itself, and all the machine development can be done without affecting the SPS proton programme. Time-consuming changes of magnet or timing cycles are completely avoided since these cycles, once established and tested, can remain switched on all the time between the LEP fillings.

Figure 2.2 shows the SPS dead-time T_0 between two proton cycles, which is imposed by the limit on average power dissipation in the magnets, and the repetition time T_{rep} of the SPS versus the duration of the 450 GeV flat-top. Subtracting 0.6 s stabilization time and the time it takes to inject b proton batches from the PS, we get the time t_e

available for the electron cycles, which virtually do not contribute to the power dissipation. Assuming for the nominal cycle a flat-top duration of 2.58 s and subtracting the time required for injection of three p-batches leaves about 5 s for the e-cycles. Taking into account the duration of n e-cycles,

$$t_e(s) = (n - 1) 1.26 + 1.02 ,$$

it can be seen in Fig. 2.2 that four e-cycles can easily be fitted between the proton cycles. The last e-cycle is shorter than the others because the magnetic field has to be decreased only to a value corresponding to 10 GeV/c, the proton injection momentum, instead of 3.5 GeV/c.

The precise value of these time intervals is determined by the necessity that all intervals must be multiples of 60 ms, the period of the SPS clock, and furthermore the repetition time of the SPS is quantized in steps of 0.84 s, which is the repetition time of the PS proton linac.

The first two e-cycles out of the four are used for positron acceleration, the last two for electron acceleration. Hence both beams in LEP are built up nearly simultaneously so that RF beam loading and space-charge detuning are the same for both beams, and correction of these effects is facilitated.

Figure 2.3 gives schematically the magnet supercycle of the SPS and PS, the total beam current in the EPA, and the pulsing periods of the linac versus time. In order to reduce the charge per bunch, all circular injector machines operate with eight bunches.

We now examine one period corresponding to an SPS supercycle in the middle of a LEP filling. It can be seen from Fig. 2.3 that the positrons are collected in the EPA during the relatively long SPS proton cycle because the linac positron current is low. The linac operates with a repetition frequency of 100 Hz, and each pulse is put in turn into another one of the eight collecting buckets of the EPA by stacking the pulse in betatron phase space close to the stored bunch. The time elapsing between two injections into the same bucket is 80 ms. This is sufficiently long compared to the EPA damping times ($\tau_x = 30$ ms, $\tau_z = 60$ ms)⁶⁾, so that the oscillations of the previously injected pulse are adequately damped and the stored beam does not suffer particle loss when bumped towards the septum during injection. The kickers generating the closed-orbit bump are fast enough so that only the stored bunch to which the pulse is added will be moved to the septum; the other seven bunches are virtually unaffected.

Once the required current is reached, each of the eight positron bunches is moved onto a thin electrostatic septum which cuts the bunch into two halves in betatron phase space and extracts one half for transfer to the PS. The other eight halves remain in the EPA and are saved for the next positron cycle. Radiation quickly re-establishes their equilibrium dimensions. The eight bunches injected into the PS are accelerated to 3.5 GeV and transferred to the SPS, where they are accelerated to 20 GeV and sent to LEP. In LEP, the eight bunches are injected close to the four circulating bunches by means of two-turn injection into either betatron or synchrotron⁷⁾ phase space. Hence each stored LEP bunch has, after injection, two companions performing damped betatron or synchrotron oscillations around it.

The second positron cycle starts with the transfer of the remaining eight positron bunches from the EPA to the PS, and this second positron batch is handled in the same way as the first batch in the rest of the injector chain. Since the radiation damping times in LEP are $\tau_x = 0.4$ s for the radial motion and $\tau_z = 0.2$ s for the longitudinal motion when the emittance control wigglers are switched on, more than three damping times elapse between the injection of the first and the second positron batch into LEP. The oscillations of the first batch will have sufficiently decayed so that its bunches will have already merged with the stored beam when the new injection takes place.

As soon as the positrons are extracted from the EPA the linac starts to inject electrons. The electron current provided by the linac is strong enough to fill, within 1.14 s, the eight bunches of the EPA to an intensity which is half the maximum positron intensity. The eight complete bunches are then transferred through the two synchrotrons to LEP in the same way as the positrons. After the second electron cycle, identical to the first one, the linac resumes positron injection into the EPA.

It can be seen from Fig. 2.3 that the linac must switch from positron production to electron production and back again within one SPS supercycle. A relatively long time-interval of 1.38 s is available for the commutation from positrons to electrons, but switching back must be fast in order not to encroach on the time available for positron filling. Since the electrons for the EPA electron filling are injected from a separate, low-intensity gun located off-axis between the 200 MeV high-intensity linac and the converter target, one can indeed aim at a short switching time of about 0.1 s although a revision of this parameter might be necessary once all the implications are known. The separate gun provides the additional advantage that the high-intensity linac is not needed during the electron filling and can stay tuned to the high current all the time.

Details of the bunch transfer schemes and the bunch positioning in the individual machines are given elsewhere⁸⁾ and under Chapter 3. Table 2.1 gives some key parameters and the nominal bunch intensities. The accumulation time of the EPA is shorter than the maximum possible because two damping times are reserved for the damping of the large energy spread of the last injected pulses prior to extraction. This time is also needed by the whole beam to attain its equilibrium dimensions after a change in longitudinal focusing, which is different during accumulation and during a short lapse of time before extraction. During accumulation, a large energy acceptance is required; before extraction, it

is the longitudinal matching to the PS which defines the RF focusing. The last column gives the transfer efficiencies which are global numbers taking into account losses during acceleration, extraction, transfer, and injection, plus RF trapping. Their estimate is based upon comparison with other electron machines and, to a certain extent, on the information available from the CERN proton machines. Given the uncertainty in the estimate of the transfer efficiencies, we still aim, in the design, at having a positron peak current of 12 mA in the linac as suggested previously²⁾. As a result of this injector performance, the current will be accumulated almost *simultaneously* in both LEP beams with a rate of

$$0.25 \text{ mA} \cdot \text{min}^{-1}.$$

Table 2.2 summarizes the ratio of calculated threshold intensity to the nominal intensity for longitudinal⁹⁾ and transverse turbulence, which are the most limiting effects found up to now. The ratios are given at injection energy for the PS and SPS where the stability margins are lowest.

The threshold values depend on the bunch dimensions, which are in turn determined by the detailed operating parameters. Since these parameters will still evolve, the ratios given in Table 2.2 should be considered as typical and not as final. The numerical values for the EPA given in Table 2.2 are based on the longitudinal bunch dimensions during accumulation with the 19 MHz RF system; the values for the PS and SPS have been worked out for longitudinal

Table 2.1

Basic scheme; main parameters and nominal number of particles per bunch N_b

Mode of operation:	Interleaved (pe ⁺ e ⁺ e ⁻ e ⁻)		Transfer efficiency (%)
e-cycles/supercycle:	4		
Supercycle period (s):	15.12		
Particles	e ⁺	e ⁻	
Number of bunches (EPA)	8	8	
Number of bunches (PS/SPS)	8	8	
Linac peak current (mA)	8.0	40	
pulse length (ns)	12	12	
repetition frequency (Hz)	100	100	
particles per pulse/10 ¹⁰	0.060	0.30	
Accumulation time EPA (s)	11.22	1.14	30
EPA N _b /10 ¹⁰	2.5	1.3	80
PS N _b /10 ¹⁰	1.0	1.0	80
SPS N _b /10 ¹⁰	0.81	0.81	90
at LEP septum N _b /10 ¹⁰	0.73	0.73	30
in LEP trapped N _b /10 ¹⁰	0.22	0.22	
LEP accumulation rate per beam (mA · min ⁻¹)	0.25	0.25	

Table 2.2

Typical threshold bunch intensity over nominal bunch intensity

Machine	E (GeV)	Longitudinal	Transverse
EPA	0.6	3	1.4–7
PS	0.6	3	2–7
SPS	3.5	2	0.5–1.5

bunch dimensions which are adjusted for maximum beam stability by proper choice of the RF parameters. The PS operates with a 114 MHz RF system and the SPS with 200 MHz (see Chapter 3).

Two values are given in Table 2.2 for the transverse safety margin. The first value is obtained from a scaling law derived from observations at machines with shorter bunches than those used in the LEP injectors¹⁰⁾. The second number is obtained from a stability criterion¹¹⁾ based on the hypothesis of transverse mode-mixing¹²⁾ and assuming the commonly accepted impedance model. This second procedure is considered to give a more accurate estimate of the threshold. More details on RF parameters and threshold calculations are given in separate notes^{13,14)} and in Chapter 3.

It can be seen from Table 2.2 that the stability margins in the EPA and in the PS appear to be sufficient, although measurements in the PS are still needed to confirm the calculations. The transverse stability in the SPS, however, seems to be marginal.

2.2.2 Variant schemes

It is obvious that the stability thresholds cannot be calculated precisely, certainly not better than to a factor of 2. Thus it is necessary to examine the possibilities for lowering the bunch current further in order to be prepared for the case that one of the thresholds turns out to be more unfavourable than expected. This is done under point (i) below. The estimates could also be too pessimistic, and it might happen that more particles could be loaded into the bunches than is estimated. This will lead to a simplification of the operation which is discussed under point (ii).

i) Operation with less bunch current

The preferred solution is to double the number of e-cycles inserted between the p-cycles, which allows for halving the bunch current in the PS and SPS. The period between two e-cycles becomes about 0.7 s, which is still nearly twice as long as the horizontal damping time constant of LEP with the wigglers switched on. The faster cycling does not require any hardware modifications, except that two additional 5 kV power supplies are needed for the dipoles in the SPS.

Figure 2.4 shows the SPS magnetic cycle, the total current in the EPA and the linac injection pattern for the case of a 0.66 s e-cycle. During the first three ejections from the EPA the electrostatic septum cuts the eight positron bunches such that one quarter of the initial intensity is extracted each time. The eight bunches remaining for the last positron cycle are transferred to the PS using standard extraction. The electrons are handled in the same way as in the basic scheme, except that there are four electron transfers during the supercycle instead of two. The LEP accumulation rate is expected to be approximately the same as in the basic scheme.

Table 2.3 gives the principal parameters and bunch intensities. It is clear that the e-cycle of the SPS could also be somewhat longer than 0.66 s since the dead-time is not yet fully used. This would reduce the linac electron current but would increase the positron current by a small, acceptable amount. Obviously, a certain margin in the choice of the cycle exists, and the supercycle, described by Fig. 2.4 and Table 2.3, should be considered as an example.

We have also investigated the possibility of operating the synchrotrons with 16 bunches. We find that this leads to a considerable complication of the transfer schemes between the circular machines; also, four-turn injection into LEP would be required, which would certainly reduce the injection efficiency. Furthermore, the scheme would require that also the electron bunches are cut in the EPA.

A further intensity reduction with each scheme could be achieved by using the dedicated mode where the PS and SPS would operate exclusively for LEP during a LEP filling. Consideration of the SPS duty factor shows that the intensity in the injectors would be reduced at most by an additional factor 3. The dedicated mode, however, has the serious drawback that the proton programme must be interrupted for each of the frequent LEP fillings and also for the setting-up and the machine development.

It would therefore appear that to achieve a given reduction of the intensity per bunch, one should start by making the number of e-cycles per SPS supercycle as large as possible and only thereafter start to increase the number of bunches simultaneously accelerated per e-cycle in the PS and SPS. It is not proposed to make initially any provisions for an intensity reduction scheme since it can be implemented later, when the necessity is proved, by simply adding equipment. The dedicated mode is considered to be a last resort to be tried only when all other means for reducing the intensity or making it acceptable have failed.

ii) Operation with more bunch current

If the bunch current in the PS and SPS could be increased by at least a factor of two, the PS and SPS could operate with four bunches only. Consequently, operation would be simplified, as bunch-cutting in the EPA and two-turn injection into LEP would no longer be necessary.

The pattern of cycles, similar to the pattern shown in Fig. 2.3, is shown in Fig. 2.5. After the accumulation of eight positron bunches in the EPA, four complete bunches are transferred to the PS for the first positron cycle. The remaining four bunches are used in the second positron cycle.

Only four electron bunches are accumulated in the EPA for each electron cycle. The time elapsing between two injections into the same EPA bucket is reduced to 40 ms compared to the 80 ms available in the basic scheme. This is taken into account when the aperture of the EPA is determined⁶⁾.

Since the total number of particles in the synchrotrons is the same as in the basic scheme, the LEP accumulation rate is not changed. Table 2.4 summarizes the main parameters and the bunch intensities.

Table 2.3

Main parameters and bunch intensities N_b in eight-e-cycle mode

Mode of operation:	Interleaved ($pe^+e^+e^+e^-e^-e^-e^-$)	
e-cycles/supercycle:	8	
Supercycle period (s):	15.12	
Particles	e^+	e^-
Number of bunches (EPA)	8	8
Number of bunches (PS/SPS)	8	8
Linac peak current (mA)	8.7	42
repetition frequency (Hz)	100	100
particles per pulse/ 10^{10}	0.065	0.31
Accumulation time EPA (s)	10.38	0.54
EPA $N_b/10^{10}$	2.5	0.63
PS $N_b/10^{10}$	0.51	0.51
SPS $N_b/10^{10}$	0.41	0.41
at LEP septum $N_b/10^{10}$	0.37	0.37
in LEP trapped $N_b/10^{10}$	0.11	0.11
LEP accumulation rate per beam ($\text{mA} \cdot \text{min}^{-1}$)	0.25	0.25

Table 2.4

Main parameters and bunch intensities N_b with four bunches in PS and SPS

Mode of operation:	Interleaved ($pe^+e^+e^-e^-$)	
e-cycles/supercycle:	4	
Supercycle period (s):	15.12	
Particles	e^+	e^-
Number of bunches (EPA)	8	4
Number of bunches (PS/SPS)	4	4
Linac peak current (mA)	8.0	40
repetition frequency (Hz)	100	100
particles per pulse/ 10^{10}	0.060	0.30
Accumulation time EPA (s)	11.22	1.14
EPA $N_b/10^{10}$	2.5	2.5
PS $N_b/10^{10}$	2.0	2.0
SPS $N_b/10^{10}$	1.6	1.6
at LEP septum $N_b/10^{10}$	1.5	1.5
in LEP trapped $N_b/10^{10}$	0.44	0.44
LEP accumulation rate per beam ($\text{mA} \cdot \text{min}^{-1}$)	0.25	0.25

CHAPTER 3

DESCRIPTION OF INDIVIDUAL SYSTEMS

3.1 PRE-INJECTOR

The LEP injector linacs (LIL) and the electron-positron accumulator (EPA) comprise the purpose-built pre-injector of the PS. In particular, the EPA converts the repetition rate and bunch charge of the linac to that suitable for the following machines. The choice of three basic linac parameters, namely operating energy, pulse repetition frequency, and beam charge per pulse delivered to the EPA, are treated here. In principle the design choices should lead to an optimized pre-injector for a given filling time for LEP. However, with increased constraints coming from the operating modes and the predicted performances of the PS and SPS, the equivalent result in a more pragmatic way is a pre-injector design, consistent in itself and which is well matched to the particular requirements of the other machines in the chain. A brief account of the linac beam quality in positron and electron acceleration modes essentially completes the parameter set required for a first look at the LIL/EPA interface.

The logic of the parameter choices is not fundamentally different from that of the Pink Book. The design filling rate for LEP, coupled with the cumulative transfer efficiencies between LIL and LEP (0.052), dictates the *mean* linac current requirements per SPS supercycle for both positrons and electrons (~ 7 nA). Since electrons are more readily produced, the relative timing for linac operation in the two modes can be 1:5 ($e^-:e^+$) as determined by the SPS supercycle and the “dead”-times (see Section 2.2). For a given required intensity in the EPA the necessary charge per positron pulse from the linac depends mainly on its repetition rate. The condition that the charge per bunch in the PS and SPS should be minimized leads to operation modes which maximize the product of the number of acceleration cycles and number of bunches. For the EPA the rise, flat-top, and fall-time of injection kickers (using “state-of-the-art” designs) determine the minimum possible distance between bunches and hence the approximate circumference of ring necessary to contain the desired (maximum) number of eight bunches.

The precise value of the EPA circumference is one fifth of the PS circumference in order to allow single-turn injection into the PS. The linac repetition rate must be such that the time between injections into the same bucket must be at least one transverse radiation damping time. In this case the existing bunch is small enough to take the injection bump without being scraped by the EPA injection septum. With the circumference fixed and the bending field set to the highest possible value for maximum damping, and the two damping partition numbers chosen $J_x = 2$, $J_z = 1$ (see subsection 3.1.2), the main parameter determining the damping time (τ_d) is the energy E ($\tau_d \propto E^{-2}$). The pair, $E = 600$ MeV and repetition frequency 100 Hz, satisfy the necessary condition that $\tau_d < 8/100$ s, and the required positron charge per linac pulse of 96 pC ($= 6 \times 10^8 e^+$) completes the basic parameter set. In practice this qualitative logic is a gross simplification of several detailed and iterative studies often involving critical assessment of other technical limitations in the two machines.

Some other linac parameters which influence the EPA design (and vice versa) are the pulse length, energy spread, and emittance, mainly of the positron beam. A pulse length of 12 ns is chosen as a compromise between high peak current in the first linac and the necessity, in the EPA, for the pulse to be compatible with the RF acceptance and kicker constraints. The accepted positron charge from the converter target depends on the kinetic energy of the electron impinging thereon within a 2 mm diameter spot. The high-current electron linac is thus a compromise solution in which a high but acceptable current (~ 2.5 A) is accelerated to the nominal energy of 200 MeV; the stored RF energy is sufficient to hold the transient energy drift to $\sim 10\%$ in order to satisfy the beam spot-size requirement. The energy spread of the 600 MeV positron beam is essentially correlated with its phase spread, and this in turn depends mainly on the phase spread of the electron beam at the converter target. With this model a spectrum peaked at the high-energy end is obtained with a tail to 2% below the peak corresponding to $\sim 23^\circ$ phase spread.

The emittance of the positron beam will be limited by the acceptance of the accelerating sections following the converter, where the beam is focused by solenoids on the sections. Assuming a solenoid field of $B_z = 0.3$ T, a limiting aperture diameter of 16 mm, and perfect transmission in the linac FODO focusing system, the maximum emittance at

600 MeV will be $\approx 4.8 \pi \cdot \text{mm} \cdot \text{mrad}$. The acceptance of the EPA is designed to handle this emittance and energy spread of the positron beam. For the 600 MeV electron beam, smaller energy spread ($< 1\%$) and much smaller emittance ($< 0.2 \pi \cdot \text{mm} \cdot \text{mrad}$) should be obtained.

The unusual layout of this pre-injector with the EPA passing 15 cm above the linac and injection taking place to the inside of the “racetrack”, results mainly from the limited space for the surface building near to the PS (see subsection 3.1.3 and Fig. 3.1).

3.1.1 Linacs

General parameters

A general description of the basic components of the injector linacs and their layout is given, essentially expanding the outline treatment of Section 2.1 and providing a background for the more specific information in the following subsections. A more detailed treatment of the LIL design is given in a report¹⁵⁾ produced by the “Laboratoire de l’Accélérateur Linéaire” (LAL) at Orsay in January 1982.

LIL consists essentially of two linacs in tandem: a high-current electron linac (V) of nominal energy 200 MeV, used for positron production, followed by a lower-current linac (W) accelerating either positrons or electrons to 600 MeV prior to injection in the EPA (see Table 3.1 and the schematic layout, Fig. 3.2). The first part of linac V will determine the eventual beam quality at the converter, hence the production rate and positron filling rate of the EPA and all the chain of machines to LEP itself. It was decided in 1979 that this region merited special attention, so the ensemble (“front end”) of electron gun (with its pulse modulator), prebuncher, and buncher was ordered and later installed at LAL (1981), and was equipped with sufficient diagnostic instruments to study the output beam quality in detail.

The triode electron gun operates up to 90 keV with a comfortable margin in output current which will allow the optimization of pulse length and limitation of beam diameter for the charge per pulse required during LEP operation. Between the gun and the buncher there are three solenoids providing the smoothly increasing field needed for confining the beam, and a re-entrant S-band cavity which prebunches the beam. Calculations have shown the importance of a proper adjustment of the RF field level and phase in this cavity if a highly bunched beam is required at the linac output^{16,17)}. The buncher is a triperiodic standing-wave structure¹⁸⁾, 2.24 m long, operating at 2.99855 MHz and accelerating to 30 MeV with 13 MW input power.

An important feature of the operation of all the accelerating sections in linac V is the transient beam loading¹⁹⁾. For the buncher accelerating 2.5 A during 12 ns to ~ 30 MeV, the acquired beam energy of 0.90 J must come from the RF stored energy, initially ~ 8 J, thus causing an output energy decrease of $\sim 6\%$ averaged over the beam pulse. In the four travelling-wave (TW) sections which follow the buncher, the relative energy decrease will be greater owing to the lower operating electric field, which is the main parameter determining stored energy and accelerating rate. These TW sections work in the $2\pi/3$ mode and are designed for an input power of 15 MW. The chosen length, 4.5 m, provides an efficient structure both for energy gain (linac W) and for stored energy (linac V). The focusing in linac V consists of solenoids before and on the buncher, with a short solenoid lens before the first TW section and quadrupole triplets between subsequent sections.

The 6 m long region between the two linacs contains the sources of positrons (converter target) and electrons (off-axis gun) for the 600 MeV linac (Fig. 3.3). In addition there is a spectrometer magnet and focusing triplet for the high-current beam, a 60 keV prebuncher/4 MeV buncher ensemble and its associated focusing solenoids for the low-current electron beam, and the necessary beam diagnostic equipment to supervise the rapid alternation between positron and electron injection. The converter itself will absorb 20% of the 600 W of incoming electron beam power, so the ensuing high-radiation levels require local shielding for equipment and personnel.

The RF power system of the linacs is based on 35 MW klystrons giving 15 MW input power at each of a pair of sections, or, when used in the preferred LIPS (LEP Injector Power Saver) energy-storage configuration, giving sufficient peak power output to feed four sections. More details of the LIPS scheme are given below under “Klystrons and modulators”. The waveguides (WR284), LIPS storage cavities, and other circuit elements of the microwave power distribution network for the TW sections are under vacuum. For vacuum purposes the accelerators are divided into nine sectors, and the design, except for the electron guns, is based on typical outgassing rates in unbaked systems with low-conductance paths unavoidable in the RF structure.

Problems of beam instrumentation are accentuated by the short pulse length (12 ns), large range of beam currents and emittances, and the need to operate alternately with two particle types. This also implies the application of a control system with a comprehensive range of diagnostic hardware and software adapted to the LIL problems (see brief description in subsection 3.1.2).

One important constraint on the design of the LIL has been the space available near the PS. By working near the maximum safe accelerating rate, using a FODO focusing system on linac W, carefully allotting the space between sections, and finally allowing the linac to overlap the EPA by 13.7 m (see Fig. 3.1), it has been possible to design a linac building which just avoids cutting Pauli Road.

The detailed parameters are given in the parameter list in appendix. Note that these are design and target values which have evolved and include engineering safety margins, whereas the parameters of Table 3.1 are the nominal parameters.

Table 3.1

Nominal linac parameters

General		
Frequency	2.99855	GHz
Klystron power	35	MW
No. of sections/klystron (LIPS)	4	
No. of sections/klystron (non-LIPS)	2	
Repetition rate	100	Hz
Beam pulse length	12	ns
High-current linac (V)		
No. of sections (incl. buncher)	5	
Input current	6	A
Input energy	90	keV
Output current	2.5	A
Output energy	200	MeV
Converter		
Type	Tungsten + $\lambda/4$ solenoid	
Conversion efficiency, e^+/e^-	0.04	GeV ⁻¹
Low-current linac (W)		
No. of TW sections	12	
Output energy	600	MeV
Positron operation		
Input energy (mean)	8	MeV
Resolved output current ^{a)}	12	mA
Emittance ^{b)}	≤ 4	$\pi \cdot \text{mm} \cdot \text{mrad}$
Energy spread ^{b)}	≤ 0.02	
Electron operation		
Input energy	60	keV
SW buncher energy	4	MeV
Output current	60	mA
Emittance ^{b)}	$\ll 1$	$\pi \cdot \text{mm} \cdot \text{mrad}$
Energy spread ^{b)}	< 0.01	

a) Defined as current within 2% energy spread.

b) Defined as containing $> 80\%$ output current.

Injection Systems

It has been necessary to develop two distinct injection systems for LIL to satisfy the operational requirement to have available high-quality beams with good reproducibility despite the frequent commutation between positron and electron operation. In particular, the settings of linac V used solely for positron production can be made nearly independent of the electron current operation in linac W and only a reduced amount of fast parameter switching is necessary. The two gun-prebuncher-buncher systems will operate in quite different current and energy regimes, yet have some common design features.

The injection ensemble for linac V (briefly described above) was built by industry and is at present installed at LAL, which provides the 3 GHz power source. The beam lines are equipped to measure the current and charge per pulse, the output energy and energy spread, the beam profile and transverse emittance, and the longitudinal profile (phase spread). The first series of measurements (acceptance tests) were completed in July 1982. They have led to a rather detailed knowledge of the electron gun characteristics, which can be summarized as follows. A series of four pulse shapers covers the range from 5 ns to 13 ns for which an output current of 10 A can be obtained with acceptable pulse shape. Maximum currents obtainable for each of the pulse shapers were ~ 14.5 A and ~ 17 A for output energies of 80 keV and 90 keV, respectively. At the buncher output the beam current, energy, and energy spread ($\Delta E/E$) have been measured. Typical results in terms of the accelerated charge are given in Table 3.2.

Table 3.2

Typical measured beam parameters after buncher

Q (nC)	τ (ns)	I_{\max} (A)	E_{\max} (MeV)	E (MeV)	$\Delta E/E$ (%)
3.1	3.4	0.9	29.9	29.2	5
52	5	10.4	28.3	25.3	11.5
104	9.8	10.6	29.5	24.5	19.6

Note that results for $\Delta E/E$ correspond to 80% of the output current and that the transient energy decrease during the pulse is clearly demonstrated. The measurements at currents near to nominal LEP requirements typically give a transverse emittance (H or V) of 6 to 10 $\pi \cdot \text{mm} \cdot \text{mrad}$ and a bunch length of 25° ($\Delta\phi$ at 3 GHz); all measurements correspond to 80% of accelerated particles with nominal output current of 3 A and pulse length 15 ns at an energy of 25 MeV. Further measurements are still necessary to provide reliable performance figures.

The injection system for linac W is in the design and specification state (Fig. 3.3). Based on experience with the high-current gun, it has been assumed that considerable reduction in size and complexity will be obtained by lowering the energy to 60 keV and the output current to 0.25 A. This gun will inject onto the linac axis via a 255° bending magnet (α magnet) which has a suitable gradient to make it essentially achromatic and to focus equally in horizontal and vertical planes. A compact prebuncher–buncher system operated in a standing-wave (SW) mode and powered with 2 MW at 3 GHz will provide a tightly bunched electron beam at 4 MeV for matched injection into linac W.

Accelerating sections

The LIL accelerating sections consist of disc-loaded waveguides working in the $2\pi/3$ TW mode with quasi-constant field gradient. Sections lengths of 4.5 m for linacs V and W result from a compromise between the number of S-band klystrons and associated modulators required, and the technical difficulties arising with longer structures. The basic performance calculated for the chosen design is an energy gain of 60.2 MeV for 15 MW input power, of which 11.7 MW is dissipated in the section, the rest going to the terminating load (Table 3.3).

The section is constructed from 135 elementary cells, each of which consists of an iris between two half cavities (Fig. 3.4 and Table 3.4). To reduce the number of different cell types required, the section consists of nine constant impedance landings with eleven identical cells per landing, except at the input and output landings which consist of thirteen cells. From one landing to the next, the iris diameter varies by 875 μm (in range 25 mm to 18 mm); this causes a corresponding change in the group velocity. Between landings there are four transition cells with smaller changes of

Table 3.3

Design characteristics of the accelerating sections

Frequency	2.99855 GHz
Accelerating mode	$2\pi/3$, travelling wave
Length	4.499 m
No. of cells	135
No. of constant impedance landings	9
Range of iris diameters	25 mm to 18 mm
Filling time	1.22 μs
Input power (non-LIPS)	15 MW
Energy gain (non-LIPS)	60.2 MeV
RF pulse length for 60.2 MeV energy gain with LIPS	< 4 μs

Table 3.4
Dimensions of unit cells (see Fig. 3.4)

Outer diameter (D)	102.00	± 0.01 mm
Inner diameter	$82 < 2b < 85$	± 0.01 mm
Iris diameter	$18 < 2a < 25$	± 0.01 mm
Length (h)	33.321	± 0.008 mm
Iris thickness (e)	5.000	± 0.004 mm
Profile radius	12.500	± 0.004 mm

175 μm in iris diameter, this smoother variation reducing reflections of the e.m. wave. Such an arrangement of cells keeps the power losses per metre (and hence accelerating rate) approximately constant along the accelerating section when it is powered by the conventional constant-amplitude RF pulse.

With LIPS the field distribution is non-uniform along the section, but the energy gain can be set to about the same by increasing the RF pulse length to $\sim 4 \mu\text{s}$ (see Fig. 3.5).

To assemble a section the cells are joined by silver diffusion at 320° , ensuring sufficient strength for the ensemble including input and output couplers. The whole is placed in a stainless-steel vacuum envelope.

A 1.5 m prototype section comprising three landings and two four-cell transitions has been built in order to make mechanical and RF tests (see photo, Fig. 3.6). The machining tolerances on cells are of the order of 10 μm , which introduces a maximum frequency spread of 500 kHz between cells. Thus the cells must be tuned individually to the working frequency of 2.99855 GHz at 30 $^\circ\text{C}$ (under vacuum) or, which is equivalent, to 2.99825 GHz at 20 $^\circ\text{C}$ (in air). Tuning is made by deformation of the cell walls using screw clamps. Previous local thinning of this wall (tuning recesses) permits several megahertz of frequency variation without significant reduction in the RF properties. First measurements in SW mode give a Q of ~ 13500 (90% of computed value), but the more significant results in TW mode cannot be made until completion of the rather lengthy iterative measurements required to match input and output couplers.

Klystrons and modulators

The RF power sources at 3 GHz are 35 MW klystron amplifiers fed by high-power modulators which, allowing for waveguide losses, give 15 MW input power to each of the two TW sections in normal non-LIPS operation. With one klystron and its associated modulator feeding the bunchers, a further eight klystron-modulator assemblies would then be required for the 16 TW-accelerating sections of the two linacs (see Fig. 3.2). However, at present the preferred powering scheme is the LIPS arrangement, which enables four sections to be powered from one klystron reducing the total requirement for klystrons/modulators to six. With LIPS, which is based on the SLAC SLED scheme²⁰, power is stored for the first part of the RF pulse, for example for 3 μs , before a 180° phase switch at the klystron input causes the storage cavities to be “emptied” into the accelerating sections, more than doubling the effective peak power. The maximum RF pulse length required is 4.5 μs for buncher(s) and LIPS, and 1.5 μs otherwise. Promising results have been obtained at LAL from tests of a prototype LIPS system, using a 20 MW klystron and working into a resistive dummy load²¹ (see Fig. 3.7).

Prototype klystrons designed for the above operation are under development in industry. All will use d.c. solenoid focusing and require special output window technology in order to approach the efficiency and reliability of the SLAC klystrons.

The specifications of the modulator components satisfy the more stringent demands of LIPS, namely 5.5 μs pulse flat-top to -3 dB, 280 kV, 290 A at 100 Hz. A prototype modulator is being studied at LAL; it contains all the elements necessary for the final version, including the high-voltage supply (23 kV), de-Q-ing circuitry (to 96%), delay line consisting of 25 sections ($> 5.5 \mu\text{s}$), thyatron switch tube, and klystron tank with its pulse transformer (1:13 ratio). This prototype modulator was first operated in July 1982, using a klystron as output load, and the results so far obtained give good controllable pulse shapes up to 73 MW (270 kV, 270 A). This modulator will eventually be used for the reception tests of the klystrons.

LIL-RF distribution and phase-control system

The signal from the master oscillator is amplified to the 25 kW level by a 3 GHz booster klystron situated at the beginning of the accelerator. A phase reference consisting of a rigid coaxial line distributes this signal along the accelerator, and ~ 1 kW power is coupled out to each high-power klystron. The initial phase adjustment of the accelerator can be made by maximizing the output energy, for example of linac W operating with electrons; this method

offers sufficient sensitivity given the small number of klystrons to adjust. It is important to hold these optimum phases during operation and this is done automatically in two ways. First, the beam phase is measured from the field induced in a cavity placed just after one or other of the bunchers, and this is compared with and controlled relative to the phase reference line. Then the phase of the RF signal from the input of one of the TW accelerating sections corresponding to each klystron is compared with and controlled relative to the phase reference and, hence, indirectly relative to the beam phase.

This ideal approach can, with some qualifications, be applied to the practical LIL situation where adjustments for different particles (positrons and electrons), accelerated to a fixed energy less than the maximum have to be made. Two phase shifters corresponding to operation with buncher V and buncher W, respectively, are switched, in synchronism with the positron and electron acceleration cycles, into the input line of the klystron which feeds both bunchers. To avoid introducing unnecessary energy spread in the beam bunch when reducing the beam energy, half the correction is made with a positive phase shift of the first 10 sections of linac W; in fact the corresponding buncher and hence beam phase is varied relative to the reference line. The rest of the energy correction is made with a negative phase shift of the last two sections of linac W. For the latter, two switchable phase shifters in the corresponding klystron input line, have different settings for positron and electron acceleration to 600 MeV, as there are different input conditions (energy, energy spread, and emittance) for the two particle types.

Positron production and focusing

The electron beam leaving buncher V is focused by a short solenoid and then by four quadrupole triplets, each placed after a TW accelerating section, to give eventually a beam spot corresponding to an emittance of $1.2 \pi \cdot \text{mm} \cdot \text{mrad}$ (at $\sim 200 \text{ MeV}$) on the converter. The useful positron production varies linearly with the energy deposited by the incident electron beam, but only when it falls within a small radius (1 to 2 mm) on the converter, owing to the limited geometrical acceptance beyond the converter. To keep within this spot size in spite of the chromatism in the focusing system, the beam energy spread, mostly arising from the transient beam loading, is typically limited to $\pm 5\%$ ²². The positrons are produced in a tungsten target, two radiation lengths thick ($2X_0 = 7 \text{ mm}$), with flat distribution in energy around 8 MeV within a radius of 0.6 mm and a mean angle of $\sim 20^\circ$ (point source). The yield of positrons should in this case be better than 8×10^{-3} for e^+/e^- at 200 MeV incident energy.

Matching of the positrons into the acceptance of the accelerating sections is made with a "quarter-wave transformer" system, which essentially converts the beam of small radius, large divergence (e.g. $2 \text{ mm} \times 160 \text{ mrad}$) to one of larger radius, smaller divergence ($8 \text{ mm} \times 40 \text{ mrad}$). Following the DESY design²³, a short pulsed solenoid ($\sim 1.5 \text{ T}$) is used followed by a long solenoid (0.3 T) which is mounted on the first two accelerating sections; with limiting apertures of $\varnothing = 18 \text{ mm}$ this 0.3 T field essentially determines the maximum transverse acceptance. The accelerating rate on these two sections has been chosen to be less than the nominal, $\sim 7 \text{ MeV} \cdot \text{m}^{-1}$ compared to $\sim 12 \text{ MeV} \cdot \text{m}^{-1}$, because of a possible reduction in breakdown strength in the high radiation environment just after the converter.

Subsequent focusing consists of a matching section of a quadrupole triplet followed by three quadrupoles mounted around the accelerating section to bring the beam into a FODO system (starting at $\sim 95 \text{ MeV}$) formed of 30 quadrupoles mounted around and between the sections where necessary. The separation of the quadrupoles increases with energy from 0.55 m at 100 MeV to 3.5 m at 550 MeV, with the need to avoid the input and output couplers providing severe additional constraints on the positioning (Fig. 3.8).

With the correct RF phases, gun trigger, and α -magnet excitation set, and the converter target retracted from the beam axis, the electron beam is easily transmitted through linac W as its emittance is much smaller than that of the positron beam.

Linac vacuum system

The two linacs V and W can be considered essentially as an extended vacuum system, mainly following the beam paths from cathodes onwards but also including much of the RF power distribution network and LIPS. Many of the components are connected by low-conduction paths (beam tubes) and can thus be considered as independent systems as far as pumping is concerned. The logical division into sectors separated by gate valves is made first by making one vacuum sector correspond to each of the six klystron-modulator ensembles, or rather their associated buncher, TW sections, waveguides, and LIPS, where applicable. There will be a further three sectors corresponding to the two electron guns and the converter region (see Fig. 3.2).

A critical item for the vacuum is the TW accelerating section. This consists of a cylindrical stainless-steel envelope with minimum internal diameter 144 mm, containing the copper accelerating structure (outer diameter 102 mm), which is 4.5 m long and is pumped (mainly) through 540 holes of 4 mm diameter in the copper outer wall. Measurements on the Orsay linac under RF power gave, for copper, an outgassing rate of $2 \times 10^{-10} \text{ Torr} \cdot \text{l} \cdot \text{s}^{-1} \cdot \text{cm}^{-2}$. For the design of LIL a value of $5 \times 10^{-10} \text{ Torr} \cdot \text{l} \cdot \text{s}^{-1} \cdot \text{cm}^{-2}$ has been retained and a nominal design pressure of 0.1 mPa (10^{-6} Torr) chosen. Rough vacuum will be made with turbopumps of $100 \text{ l} \cdot \text{s}^{-1}$ at section inputs, or of $\sim 40 \text{ l} \cdot \text{s}^{-1}$ on the waveguides. Mobile units dealing with each sector in turn are currently preferred. Thereafter the high vacuum will be maintained with ion pumps of $100 \text{ l} \cdot \text{s}^{-1}$ effective pumping speed mounted at the input and output ends

of each section. In addition, each waveguide branch will have $30\text{ l}\cdot\text{s}^{-1}$ pumps situated to maintain 0.01 mPa (10^{-7} Torr) at the RF windows; the converter region will have its own system, and the electron guns will need to keep $1\text{ }\mu\text{Pa}$ (10^{-8} Torr) to achieve good cathode lifetimes.

Beam instrumentation

Pulse shape, electric charge, and beam transverse position: The shape of the current pulse $I = f(t)$ as well as the corresponding charge can be measured by means of transformers made from high-quality ferrite toroids (rise-time $< 1\text{ ns}$). The pulse shape is invariant to first order along the machine, so it is sufficient to have access to it in one or two places. The transverse position of the beam is measured by microwave or stripline monitors.

Transverse profile: Knowledge of the beam profile and position of the beam is particularly important just before the converter, after the long solenoid, after the matching section, and in the transport lines between linac and EPA. Two possible secondary emission monitors under development at LAL use aluminium strips (secondary emission coefficient $\delta = 4\%$) in the high-current electron beam, or aluminium strips coated with CsI ($\delta = 100\%$) for the positron beam. A moving wire profile monitor based on either secondary emission or on the detection of scattered radiation is also being tested in the buncher V measuring line.

Longitudinal profile of the microbunches: This measurement has been successfully applied to low-energy beams (e.g. after buncher V) using a RF deflecting structure to sweep the beam across a slit. Within the limits placed by the beam size and divergence, a measure of the longitudinal bunch profile is obtained from the transmitted current as a function of the deflector RF phase. Since the phase spread, determined by the buncher V, is the principal contributor to the positron energy spread, it is important to monitor it. The slits are placed after the first TW section in order to obtain sufficient drift space between the deflector, installed after the buncher, and the slits.

Energy spectrum: The form and position of the energy spectrum peak is the main criterion for the (phase) adjustment of the accelerator. The first magnet in the beam transport to the EPA is used to provide the necessary dispersion, which can then be monitored by a horizontal profile monitor placed so as to minimize the errors due to finite beam emittance.

RF phase of microbunch: Two bunch-phase monitors and their associated phase comparison networks suitable for a 12 ns pulse (36 microbunches) are foreseen for the RF pulse phase stabilization loop.

Controls of LIL will be combined with those for the EPA. They will be an extension of the new PS controls system (see subsection 3.1.2).

3.1.2 The Electron–Positron Accumulation ring (EPA)

General design criterion and parameters

The electron–positron linac produces short particle pulses with a repetition frequency of 100 Hz . The number of particles in each linac pulse is low, and many pulses need to be accumulated in one bunch to achieve the intensity required. It is the role of the EPA to build up the required intense bunches at constant particle energy.

In the basic mode of operation of the LEP injection system — the interleaved $\text{pe}^+\text{e}^+\text{e}^-\text{e}^-$ mode — about 140 linac positron pulses need to be accumulated in each of the collecting buckets. One of the main design goals of the EPA is to accumulate the large number of linac pulses injected with high efficiency. The other design goal is to preserve bunch stability and to shape the bunches prior to ejection such that they are stable during the injection process in the PS.

The energy of the EPA is constant during an operational period. Although the nominal energy is 600 MeV , the design aims to enable operation at slightly higher energies as well, probably up to 650 MeV in order to match the potential of the linac.

The circumference is equal to one fifth of the PS and is thus 125.665 m . The ratio of the EPA and PS circumferences chosen provides an optimum cog-wheeling between the two machines and allows for the transfer of the EPA bunches in one PS revolution.

In the basic mode of operation all injector machines operate with eight bunches. Eight equidistant bunches can be stored in the EPA as the time between bunches is sufficient for fast kickers to handle the injection and the extraction of individual bunches. The required kicker performance is close to what is achievable with present technology and, therefore, it seems that from this point of view as well, the circumference chosen is the minimum.

In the basic mode the two positron cycles in the EPA are followed immediately by two electron cycles. To achieve a fast reproducible switching from e^+ operation to e^- operation and vice versa, the field in the magnets is kept constant. Consequently, the electrons and positrons circulate in opposite directions.

Each successive linac pulse is put into a different bucket so that injection into the same bucket takes place every 80 ms . The horizontal damping time is 32 ms and the betatron oscillations are well damped at injection of the following pulse.

The short horizontal damping time has been obtained by designing a lattice with combined function magnets, resulting in a horizontal damping partition number J_x equal to two. Hence the longitudinal damping partition number J_e becomes equal to one. This results in an energy spread in the bunch at equilibrium which is larger, by a factor of $\sqrt{2}$, than in a separate-function machine which has a $J_e = 2$. This choice of the partition number has two objectives: to achieve a good injection efficiency and a high bunch-stability threshold.

The RF voltage (50 kV) provides a relative half-bucket height of 1.2%; this is sufficient to capture the linac pulse, which has a maximum energy spread of $\pm 1\%$. In order to obtain some latitude in the choice of the linac pulse length and to keep the required RF voltage at minimum, the lowest possible RF frequency, 19.1 MHz ($h = 8$), is chosen.

The transverse emittance of the linac positron beam will be equal to or smaller than $4\pi \cdot \text{mm} \cdot \text{mrad}$. The emittance of the electron beam is much smaller. The acceptance of the EPA should be large enough to achieve high injection and accumulation efficiency. With this objective in mind, all possible errors which are likely to occur during normal operation are taken into consideration in deriving the minimum dimensions of the vacuum chamber, which are 105 mm in the horizontal plane and 35 mm in the vertical plane.

Table 3.5

Main lattice parameters of the EPA

Circumference	$C = 125.665 \text{ m}$
Machine tune	$Q_x/Q_y = 4.45/4.38$
Damping partition	$J_x/J_z = 2.0/1.0$
Damping time	$\tau_x/\tau_z = 32/61 \text{ ms}$
Transition energy	$\gamma_t = 5.5$
Twiss parameters (max)	$\beta_x/\beta_y = 14.9/14.3 \text{ m}$
Dispersion function (max)	$D_x = 2.3 \text{ m}$
Chromaticity	$\xi_x/\xi_y = -1.1/-2.6$

Table 3.6

Parameters of the EPA magnets

Bending magnets			
Number	16		
Field strength ^{a)}	1.4 T		
Field gradient	$-1.0 \text{ T} \cdot \text{m}^{-1}$		
Magnetic length	0.56 m		
Gap height ^{a)}	45 mm		
Quadrupoles	Number	Strength ($\text{T} \cdot \text{m}^{-1}$)	Length (m)
F_1	8	2.8	0.38
F_2	8	3.5	0.38
F_3	12	1.35	0.39
D	12	-1.35	0.39

a) At central orbit.

A long beam-lifetime is not required for operation of the EPA as the LEP injector, and a lifetime greater than a few minutes would suffice. An ultra-high vacuum is therefore not required. However, to avoid perturbations on the beam due to trapped ions, a vacuum pressure of equal to or below $1 \mu\text{Pa}$ (10^{-8} Torr) is aimed at — a pressure which can be obtained with conventional vacuum techniques. Adequate pumping capacity will be installed in the bending sections of the accumulator in order to cope with the important degassing rate produced by the synchrotron radiation. The synchrotron radiation has a critical energy of 0.33 keV in the bending magnets and is absorbed in the vacuum chamber.

A thin electrostatic septum is foreseen for cutting the positron bunches into two parts at extraction, as described in Section 2.2. A high- β insertion at this septum reduces the losses inherent in this process. Since the electrons are more abundant, no cutting of the electron bunches is needed, but space is available for an electrostatic septum so that electrons could also be cut, if required, at a later stage.

The extraction kickers are able to eject a bunch every 262 ns; consequently, the PS can be filled in one turn with eight equidistant bunches. This fast extraction scheme allows for injection with a rising magnetic field in the PS, which is advantageous for the reproducibility of injection and results in a simple injection kicker. In order to facilitate the extraction kicker design, the lattice provides high β_x and vanishing dispersion at kicker and septum positions; the phase advance between the elements is optimum. The electron and positron bunches are deviated into the beam transfer lines to the PS by a common extraction septum.

Lattice and magnets

The layout of the elements forming the racetrack-shaped ring is shown in Fig. 3.9. The shape of the ring is chosen to fit the constraints imposed by existing roads and buildings (see subsection 3.1.3). From the position of the injection points and the common extraction point it can be seen that the ring can be divided into two identical and symmetric parts. Each part consists of three sections: one straight section, with a 90° bending section on each side.

The bending section contains the combined-function magnets B_1 to B_4 and the quadrupoles F_1 to F_2 . The structure is F–D–D–F and provides a regular alternating transverse focusing. Figure 3.10 shows the lattice functions in one EPA quadrant. The dispersion function D_x is created and cancelled by the bending magnets B_1 and B_4 . The distances between the bending magnets are adjusted so that the normalized transition energy γ_t becomes 5.50. The resulting maximum dispersion function D_x is 2.3 m.

A fairly high magnetic field (1.4 T) in these relatively short bending magnets has been adopted to enhance the radiation damping and the energy spread in the beam at equilibrium. With the same objective, a gradient of $-1 \text{ T} \cdot \text{m}^{-1}$ has been introduced in the field of the bending magnets in order to obtain the desired damping partition numbers, $J_x = 2$ and $J_y = 1$. The larger energy spread does not entail a larger aperture in the EPA because the aperture is determined by the injection process.

The Twiss parameters in the bending section are adjusted by the distance between the elements and the strength of quadrupoles F_1 (see Fig. 3.10). Table 3.5 summarizes the main lattice parameters.

The 36 m long dispersion-free straight section is composed of three identical symmetrical quadruplets which are matched to the bending sections and create optimum conditions for the injection and extraction elements.

The working point ($Q_x = 4.45$ and $Q_y = 4.38$) has been adjusted to stay clear of betatron resonances up to the fourth order. The transverse chromaticities are -1.1 and -2.6 in the horizontal and vertical plane, respectively. The chromaticity is corrected by sextupoles in the bending section, as shown in Fig. 3.9. The parameters of the bending magnets and quadrupoles are given in Table 3.6.

The quadrupoles are at present in use in the ISR. They will become available for installation in the EPA in 1984. More details of the lattice design are given elsewhere^{6,24}.

The RF system

The 19.1 MHz RF system has as tasks:

- i) to capture the e^+ and e^- pulses coming from the linac;
- ii) to assure accumulation of the pulses in the bunches with good efficiency;
- iii) to compensate the energy loss caused by synchrotron radiation (8 keV/turn);
- iv) to prepare the bunches for a stable injection in the PS.

To capture the linac pulses, the RF voltage must provide sufficient bucket height to achieve a large enough energy acceptance for the linac pulse. Taking into account the expected energy spread of the positron pulse ($\pm 1\%$) (electron spread much smaller) and the pulse length, a bucket height of $\pm 1.2\%$ is required, which implies an RF voltage of 50 kV.

To match the EPA bucket trajectories to the linac pulse, an impractically high RF voltage (250 kV) would be needed. However, it is acceptable to capture the linac pulse without full matching. The non-matched pulse will rotate in longitudinal phase space and thus lengthen. The longitudinal damping acts upon it, and the resulting gap between bunches remains sufficiently long to accommodate the rise-time and fall-time of the injection kickers. Figure 3.11 shows the longitudinal phase plane at the moment of injection into the bucket to the left in the figure. The bucket height determined by the trapping requirements provides a very large quantum lifetime for the bunch in equilibrium after damping.

Table 3.7

RF parameters of the EPA

Peak voltage/turn	50	kV
Radiation energy loss/turn	8	keV
Radiofrequency	19.1	MHz
Harmonic number	8	
Synchrotron tune (accumulation)	1.6×10^{-3}	
Norm. shunt impedance ^{a)} r/Q_0	37	Ω
Quality factor Q_0	9100	
RF power (zero current)	3.7	kW
RF power (into beam)	0.61	kW
Beam current	76	mA

a) Equivalent circuit convention.

After the last linac pulse has been injected, a damping period of 120 ms is introduced to allow for longitudinal and transverse damping of the last pulses. During this damping period the bunch can be prepared for the transfer to the PS (RF matching).

As explained in Section 3.2, acceleration in the PS can be performed either with the existing RF system (7.6 MHz) or with the new RF system (114 MHz)¹⁴⁾. The equilibrium r.m.s. bunch length during accumulation is 26 cm and this bunch is well matched to the trajectories of the PS 114 MHz bucket. It can be transferred without further manipulation to the PS. If 7.6 MHz is used at the PS then the bunch must be lengthened to make it fit the longer RF wavelength. To this purpose the RF voltage in the EPA is adiabatically reduced until a bunch length of about 50 cm is obtained¹³⁾.

Considering the low RF frequency, the RF cavity is relatively small, about 1 m length and 1 m diameter; these dimensions are obtained by strong capacitive loading. A ceramic cylinder seals the accelerating gap, so that the cavity structure is separated from the vacuum of the beam pipe.

The RF parameters are given in Table 3.7. The parameters for cavity and generator are still tentative. The quality factor refers to a cavity made from an AlMgSi alloy.

The RF amplifier has to provide a minimum of ≈ 6 kW, including transmission losses. It is equipped with a single tetrode, driven by a transistor amplifier.

Larger cavities optimized for highest shunt impedance have been ruled out because of their bulkiness and their very limited benefit in the presence of the strong and varying reactive beam loading during accumulation and partial extraction. Even the far less sensitive “low-Q” approach above necessitates special precautions in this respect. Moderately fast mechanical tuners in addition to a set of binary tuners actuated by PIN diodes, or local RF feedback, are possible solutions that are presently under study.

Beam stability

The design of the EPA has been guided by the objective to avoid longitudinal⁹⁾ and transverse^{10,11)} turbulent instabilities of the single bunches in the EPA and at injection in the PS.

The longitudinal turbulent instability, also known as microwave instability, is avoided in the EPA for the nominal bunch intensities by an appropriate choice of the machine parameters. The number of particles per bunch at the longitudinal stability threshold is given by:

$$N_{\text{bth}} \sim \gamma^3 \sigma / (J_e \rho \gamma_t^2 |Z/n|).$$

Small values have been taken for the longitudinal partition number J_e and the bending radius (1.0 and 1.43 m, respectively). The transition energy is low as well: $\gamma_t = 5.5$. For the impedance $|Z/n|$ the value of 10Ω is aimed at. With the 19.1 MHz RF the r.m.s. bunch length σ is 26 cm, taking into account the potential well effect at the end of the accumulation process. Using these values at 600 MeV the threshold per bunch becomes $N_{\text{bth}} = 6.4 \times 10^{10}$, which is well above the 2.5×10^{10} required in the basic mode of operation.

It is even more important to avoid bunch turbulence at injection in the PS. Both experiment and theory show that a bunch which is turbulent at injection will not only lengthen until the threshold is reached but will overshoot, which can cause beam loss. The measures taken to avoid turbulence in the EPA are also favourable for a turbulent-free injection

in the PS, and the calculated threshold for the PS is 2.6×10^{10} per bunch, again well above the intensity (1.0×10^{10}) required in the basic mode (see Table 2.1).

The transverse stability threshold has also been estimated for the EPA and the PS. The threshold is about 2×10^{11} ppb in the EPA and is thus well above the longitudinal stability threshold. At injection in the PS the estimated transverse stability threshold is about a factor of 3 above the one calculated for the longitudinal stability.

Multibunch instabilities have not yet been examined because they can be damped with a feedback system if necessary. The need to avoid transverse beam instabilities originating from the ions trapped by the beam is discussed in the section on vacuum.

Injection and extraction

There are two identical injection systems for the two kinds of particles. Injection takes place in the straight section of the ring. Two bumpers first move the closed orbit somewhat towards the injection septum in order to bring the machine acceptance to the edge of the septum. This orbit deformation stays on during the whole injection/accumulation process. The EPA bunch receiving a linac pulse is kicked by a fast kicker and moved close to the injection septum. At the same time the linac pulse appears on the other side of the septum, which makes the pulse travel parallel to the bunch. The fast orbit deformation is cancelled by a fast kicker downstream of the injection septum. The bunch follows again the central orbit, now having as companion the linac pulse which performs a damped oscillation until it finally merges with the bunch.

The injection and accumulation process determines the betatron acceptance required for the EPA. The resulting acceptance required is $105 \pi \cdot \text{mm} \cdot \text{mrad}$ and $10 \pi \cdot \text{mm} \cdot \text{mrad}$ for the horizontal and vertical plane, respectively.

The strength of the injection kickers is relatively weak ($46 \text{ G} \cdot \text{m}$) owing to 90° advance between kicker and septum and the relatively high β_x at the septum (13.7 m). Each injection kicker consists of two C-core ferrite transmission-line type magnets of cellular construction. A single-cable pulse-forming network (PFN) excites the two magnets via thyatron switches located at its extremities. The PFN is resonantly charged up to 35 kV in $\approx 1 \text{ ms}$ from a 100 Hz pulsed supply. Kick rise-time or fall-time (10–90%) of 30 ns and a $\pm 5\%$ flat-top of 25 ns are expected.

The space available for the injection septa is only 1.5 m, and the bending angle between the transfer line and the EPA orbit is high (30°). The septum which is parallel to the central orbit in the EPA gives a deflection of 7.25° and the preceding septum a deflection of 21.75° . Both septa are 0.5 m long and are energized in series with a d.c. current of 2500 A. The first septum is 6 mm thick (Cu) and the second 18 mm. Both septa are located outside the vacuum envelope.

The electrons and the positrons are extracted from a common extraction septum located between the two bending sections near the PS ring. Two of the injection bumpers are used to form a closed-orbit bump at the extraction septum. The fast kickers are located in the middle of the bending section opposite the extraction point (see Fig. 3.9). The required kick strength is $36 \text{ G} \cdot \text{m}$ only; the rise-time and fall-time of the kicker pulse (10–90%) is 30 ns, flat-top time 10 ns. The kicker system provides eight shots spaced by 262 ns in order to eject the eight bunches in one PS turn.

The positron bunches are cut in half prior to ejection. The cutting is done by a thin electrostatic septum preceding the extraction septum and located in the long straight section. Before being kicked onto this septum, the beam is widened in the horizontal plane in order to reduce the losses on the septum. This beam widening is achieved with a local β_x bump generated by two quadrupoles (Q_d) shown in Fig. 3.9. For the positron extraction the fast kicker system needs to provide 16 shots: eight shots to eject half of each bunch, and eight shots to cancel after one turn the oscillation of the half-bunches remaining in the machine. The kicker system contains four magnets, similar in construction to the injection magnets. Each magnet is excited by a four-pulse burst derived from a series combination of cable PFNs and thyatron switches, each pulse of the burst providing one of the desired shots. The PFN charging systems for injection and ejection kickers are very similar.

Vacuum

The vacuum system is designed to keep the gas pressure at $\leq 1 \mu\text{Pa}$ (10^{-8} Torr) in the presence of a stored beam. With this pressure and a typical gas composition of 50% H_2 and 50% H_2O , the beam lifetime is greater than 3 min, which has been set as a limit to avoid beam losses during accumulation and storage. The beam lifetime is calculated taking into account bremsstrahlung interactions and Coulomb scattering.

The ions created by the beam in the chamber may jeopardize stable accumulation and storage. The ions produced by the e^+ beam will not become harmful, but those due to the e^- beam can become trapped by the beam. The time for ion build-up until its charge neutralizes the e^- beam is short compared with the accumulation time. The building-up of the ion charge causes an incoherent space-charge tune shift. A mechanism needs to be introduced to disturb the ion build-up, as otherwise beam loss due to resonances will occur. This could be a transverse bunch oscillation caused by an imbalance in the injection kick every 10 ms²⁵⁾. Ions could also be removed by means of clearing electrodes. A reduction of the gas pressure to about $0.01 \mu\text{Pa}$ (10^{-10} Torr) would not be sufficient to avoid the undesirable ion build-up.

The synchrotron radiation produces a high degassing rate in the bending sections exposed. The critical energy is 333 eV (at 600 MeV) and the peak synchrotron radiation power about 600 W (at the nominal current of 76 mA). To cope with the high degassing, a $200 \text{ l} \cdot \text{s}^{-1}$ ion pump is installed at both ends of each bending magnet. To obtain a static

gas pressure of $\leq 1\mu\text{Pa}$ (10^{-8} Torr) in the sections not exposed to the synchrotron radiation (about 92% of the EPA circumference), the straight sections are equipped every 3 m with a $200\text{l}\cdot\text{s}^{-1}$ pump.

The vacuum chamber is made of stainless steel and is manufactured using standard techniques. In order to achieve an ultimate static outgassing rate of $\leq 10^{-10}\text{ Torr}\cdot\text{l}\cdot\text{s}^{-1}\cdot\text{cm}^{-2}$ and to ensure a residual gas composition made of the lightest gas species, the standard UHV cleaning techniques and high-temperature degassing prior to installation will be applied but the vacuum system will not be baked *in situ*. Additional pumps are needed on the tanks containing the kickers and septa.

Beam transfer from the linac to the EPA

Leaving the linac, electrons and positrons are separated by a $2 \times 30^\circ$ splitter magnet (see Fig. 3.9). The particles are steered symmetrically by two EPA-type 22.5° bending magnets towards the EPA injection points, and the injection septa (see above) bend them parallel to the closed orbit of the accumulator. In the preliminary design²⁶⁾ seven quadrupoles in each branch, with focusing strength up to 2 T, are needed. The β -values vary between 0.3 and 60 m horizontally, and between 0.4 and 20 m vertically; the dispersion function does not exceed -1.3 and $+1.5$ m. For an emittance of $10\pi\cdot\text{mm}\cdot\text{mrad}$ and an energy spread of ± 0.01 , the maximum total width of the beam is 50 mm horizontally and 27 mm vertically in the transfer line.

The possibility to incorporate energy stabilizers²⁷⁾ between the linac and the EPA has been kept open. An energy stabilizer consists of a magnetic debuncher and RF structure for energy correction. Space has been reserved for debunchers, providing a path length dispersion of about $6 \times 10^{-5}\text{ m}/(\Delta p/p)$, followed by straight sections where the beam dimensions stay below 20 mm over 1.4 m compatible with a 3 GHz RF structure.

Beam transfer from the EPA to the PS

The schematic layout of these lines²⁶⁾ is shown in Figs. 3.12 and 3.13. The layout is chosen such that disturbance of the PS operation during the construction of the lines is minimized. This leads to the use of part of the existing neutrino channel for e^- transfer and the (10 m) penetration of the PS wall with a simple beam duct, free of focusing elements.

Both channels start from the common (15°) ejection septum at the EPA. With four EPA-type bending magnets (15.5 – 22.5° bending angle) in each branch, the following takes place: i) Electrons are steered to straight section SS74; ii) positrons to SS92 of the PS. At the injection points two identical septa (9°) bend the particles parallel to the closed orbit of the PS. For beam focusing 9 (for e^- transfer), respectively 11 (for e^+), quadrupoles with focusing strengths ≤ 2.1 T are needed. Particles with emittances of $0.14\pi\cdot\text{mm}\cdot\text{mrad}$ horizontally, $0.07\pi\cdot\text{mm}\cdot\text{mrad}$ vertically, and momentum spread of $\pm 0.6 \times 10^{-3}$ (all values refer to 1σ of a Gaussian distribution) can be transferred. The range of betatron functions is $0.3 \leq \beta_H \leq 150\text{ m}$, $2 \leq \beta_V \leq 270\text{ m}$, and the dispersion function D_x oscillates between -2.7 and 1.1 m. The small emittances and the low momentum spread due to the “cooling” effect of the EPA, lead to beam diameters limited to $\leq 20\text{ mm}$ horizontally and $\leq 15\text{ mm}$ vertically.

Beam observation

The successful running-in and the efficient routine operation of the EPA and its transfer lines depend largely on the quality of the beam observation systems and the controls. No final choice of the type of beam detectors has yet been made. They will be of the type commonly used on electron synchrotrons.

It is likely that the bunch and beam intensity will be measured with current transformers. With these devices the longitudinal bunch profile can be found as well. For the bunch position detectors, electromagnetic pick-up loops may be chosen, but the electrostatic pick-up type is examined as well. Screens with TV observation are required. The transverse bunch profile will be measured in the transfer lines with SEM grids or wire scanners. In the EPA this profile can best be measured with a synchrotron radiation-light observation system.

The beam detectors will be necessary for:

- i) measuring the beam characteristics at the end of the linac (bunch form and intensity, beam position and angle, beam emittance, beam energy and energy spread, jitter);
- ii) steering the beam through the transfer lines (beam position at a number of locations);
- iii) matching the beam phase plane ellipse at the injection points of the EPA and the PS (beam profile at a number of locations);
- iv) adjusting the injection and accumulation in the EPA;
- v) observing beam and bunch during accumulation and at equilibrium (position, intensity of beam and individual bunches, beam profile, bunch length, beam loss at septa);
- vi) adjusting the beam cutting and ejection;
- vii) determining the EPA machine parameters: $Q, \beta, D, \xi, J_x, J_e, \gamma_{tr}$.

Controls

The controls for both the LIL and the EPA will form a natural extension²⁸⁾ of the new PS control system. This is a logical consequence of the fact that the LIL and EPA become an integral part of the PS accelerator complex and will thus be normally operated from the present PS main control room. For both the LIL and the EPA the operator at the

consoles and the process hardware on the interface side will be presented with control properties and hardware similar to those of the present PS.

Interfacing to the process and to the consoles will be through CAMAC, using the adopted standard spectrum of modules, which may be somewhat extended in order to allow for recent technological progress. Close to every CAMAC crate there will be an Auxiliary Crate Controller (ACC), which can autonomously execute resident programs using resident data tables. A new, more powerful ACC with substantially increased memory capacity is planned, thus allowing high-level language programming throughout the controls system.

The software structures will be essentially the same as those for the new PS controls system, but they will be adapted and extended in order to benefit from the potential performance improvements given by the new ACC. This means that, where appropriate, the applications programs may be further decentralized. This may also, in certain cases, work for local control sequences, diagnostics, surveying, and autonomous checkout. Applications programming languages will be NODAL and P+.

As for other machines, the LIL and EPA timing will be locally derived by preset counters from pulse trains and key pulses. The intricate interplay between the LIL, EPA, PS, and SPS, however, suggests some rethinking of the Programme Line Sequencer (PLS), the central system for cycle coordination and programming in the PS.

The NODAL compatibility for message transfer between the PS and SPS computer networks will, of course, be conserved.

3.1.3 Buildings, infrastructure, and shielding

Location

The linacs and the accumulator ring are situated in what was the car park to the East of the PS ring, between the East and South-East Experimental Halls. By minimizing the over-all length of the linac and by overlapping the linac and the EPA, it has been possible to avoid closing the main north/south road (Pauli) at its junction with Bakker Road (see Fig. 3.1).

The EPA beam will be at the same level as the PS (433.66 m). The linac beam level will be 15 cm lower, giving about 5 cm clearance between the vacuum envelopes of the two machines at their crossing point. Both machine tunnels will have the same floor level (432.31 m), which is about the existing ground level in the EPA area. The linac beam height will accordingly be 1.20 m and that of EPA 1.35 m.

The neutrino tunnel (which contained the beam lines for Gargamelle) and its associated power supply building have been demolished, but use is being made of three existing buildings: 179, which formerly housed the (g-2) ring, and 278, at present housing power supplies for the East Hall, are used for auxiliary equipment, local control position, and power supplies. The water-cooling plant is installed in building 176, the former Gargamelle cooling room.

Buildings

The two linear accelerators are housed in an above-ground reinforced concrete tunnel, 3.0 m wide, 2.5 m high, and 101 m long (see Fig. 3.14). To minimize the length of the waveguide runs between klystrons and accelerator sections and to avoid blocking the Pauli/Bakker road junction, the klystron gallery is superimposed on the accelerator tunnel. The gallery, 6.5 m wide and 3.6 m high, contains, besides the klystrons and their modulators, all electronic equipment associated with the linacs (with the exception of high-power d.c. supplies), and pumps and control equipment for the temperature-stabilized water supply (30 ± 0.2 °C) system for the accelerator sections.

A 3 t goods lift is provided, its capacity being determined by the power supply tanks of the klystron modulators.

The linac building is supported on piers anchored in the molasse, since the ground is unstable, consisting of moraine and backfill above a sloping molasse roof.

The accumulator ring is contained in a racetrack tunnel, 3.0 m high by 3.2 m wide over most of its length (see Fig. 3.15). The twin transfer lines from the linac to the accumulator ring will pass through a Y-tunnel whose width is sufficient to accommodate the transfer line containing the energy stabilizer should this be required in the future (see Fig. 3.1). The e^- transfer line from the EPA to the PS follows the old PS proton ejection line which fed Gargamelle. A new transfer tunnel for the e^+ line enters the PS ring near octagonal point 8.

Auxiliary equipment which needs to be close to the accumulator ring for performance reasons or to reduce cable costs, is placed in an equipment hall, of light construction, south of the EPA ring. It houses injection and ejection kicker and septum supplies, the EPA RF supplies, and beam observation equipment. High-power d.c. supplies are installed with those for the linacs in the existing rectifier building 278. Other electronic equipment and the vacuum system racks are installed in building 179. This building also contains the service and test area for the linac klystrons, the spare modulator, and the accelerating waveguide section, as well as machine documentation and the local control position during the running-in period.

Infrastructure

Electricity. The pre-injector is fed by three 18 kV/380 V transformers: two 2 MVA for the accelerators and one 800 kVA for general services. Longitudinal cable runs for the linacs are in the klystron gallery, with access to the linac tunnel at each accelerator section.

There are no cranes in the accelerator tunnels or auxiliary buildings, and equipment handling will be done with forklift trucks. Consequently, overhead cable trays are used and there are no floor ducts.

Cooling-water systems. The total heat load to be water-cooled is about 2 MW. Most of this load consists of standard accelerator elements, but about 100 kW is dissipated in the accelerating waveguide sections of the linacs, whose temperature must be held to 30 ± 0.2 °C.

The existing Gargamelle cooling room (building 176) is used for the central cooling plant. The relative costs of using the Gargamelle cooling tower or of using Industrial Cold Water (8–13 °C), which will be available in sufficient quantity after the closure of the ISR, are being studied. There will be a single secondary demineralized-water circuit, running in existing pipework as far as building 179, and continuing via the klystron gallery to the EPA tunnels. Pumps and control equipment for individually regulated cooling circuits for the set of accelerating sections fed by a klystron are situated in the klystron gallery. The normal pressure differential available will be 0.6 MPa (6 bar); booster pumps will be used where necessary (electromagnetic septa).

Air cooling and ventilation. Buildings 179 and 278 are already equipped with adequate air conditioning and ventilation equipment. The heat load for the accelerator tunnels, the klystron gallery, and the EPA auxiliary buildings is not yet completely determined but should not greatly exceed 500 kW. Standard air conditioning units ($50\,000$ – $60\,000$ kcal·h⁻¹) will be used. Smoke extraction fans for the accelerator building will be installed on the EPA/PS transfer tunnels.

It may be necessary to install local ventilation to deal with ozone and nitrogen oxides produced by irradiation of the air near the electron-positron converter. Methods of reducing the quantity of corrosive molecules by local shielding of the converter and for containment of the air in its vicinity are being studied²⁹⁾.

Shielding

The shielding criteria used³⁰⁾ are that the dose level in freely accessible areas (i.e. at the outside wall of the building), averaged over a LEP accumulation cycle of e⁺ and e⁻, will be less than 0.25 mrem·h⁻¹ and inside the klystron gallery (which will be a radiation controlled area) will not exceed 2.5 mrem·h⁻¹.

The major source of radiation is the electron-positron converter situated at the input of linac W. During positron production, the mean power of the 200 MeV beam dissipated in the converter region is 600 W.

The building construction and shielding has been strongly influenced by the availability of standard shielding blocks from the West Experimental Area. These blocks are used for all lateral shielding, so only the roof shielding has to be incorporated into the building structure.

A 2 m thick concrete roof slab is sufficient between the linac and the klystron gallery, except for the region above the converter, where a composite shield is used. This consists of 40 cm of iron^{*)}, 130 cm of baryte concrete, and 30 cm of normal concrete in order to keep the slab thickness constant.

Since there is no building on top of the EPA tunnels, the roof shield thickness is determined by sky shine. Concrete of 80 cm thickness is sufficient to keep the level due to sky shine to 0.1 mrem·h⁻¹ at 20 m, provided that local shielding (5 cm of steel) is used above concentrated loss points such as scrapers and dumps.

The lateral block shielding for the linac and outer sides of the EPA tunnels will not exceed 2.40 m; 0.80 m is sufficient for the inner walls of the EPA tunnels.

The three dead spaces enclosed by the EPA tunnels and totalling about 400 m² will be available for the storage of active waste.

3.2 PS MODIFICATIONS

3.2.1 General

The amount of additional hardware required for using the PS as a 3.5 GeV electron synchrotron is surprisingly modest³¹⁾. All its existing equipment is compatible with the acceleration of electrons and positrons. Not more than a few metres of straight section will have to be made available for the installation of a new RF accelerating system, wiggler magnets, the injection systems for e[±], and some additional instrumentation.

The new injection system can be installed without compromising the performance with proton beams. The extraction channels are the same as for p \bar{p} operation.

The PS will be the only electron synchrotron that has both a combined-function lattice and a long acceleration cycle. This has imposed the use of a Robinson wiggler to ensure the stability of the beams. The same wiggler will help to match the longitudinal bunch size to the SPS.

An important effort is required in order to cope with the increased complexity of the operation. A number of additions or improvements to the instrumentation and the control system are foreseen.

*) A convenient active waste storage area.

3.2.2 Injection

The ratio of the PS and EPA circumferences is chosen to be an odd integer so that the eight bunches from the EPA can be injected within a single turn of the PS. Single-turn injection is desirable because it makes the beam transfer very fast so that a slowly rising PS magnetic field can be tolerated, providing a better reproducibility than a constant field.

The design^{32,33)} of the injection channels takes into account the constraints imposed by the position of the EPA (see subsection 3.1.3) and the operation of the PS with proton beams. Symmetric injection trajectories are chosen to standardize equipment, and the angle of incidence is large (160 mrad) for reducing the effect of the magnet stray field. The injection septa are put in mid-D short straight sections; the positron septum is in straight section SS92 and the electron septum in SS74. Since the septa are only 40 cm long, enough space is left in the straight section for the installation of a vertical correction dipole and a position monitor.

The injection kickers are located in mid-D straight sections, one eighth of a betatron wavelength downstream from the septa, with the positron kicker in the SS94 and the electron kicker in SS72. Both kicker magnets are of the lumped inductance type. Each is powered from a resonantly charged high-voltage pulse generator of 8 Ω impedance. The kicker fall-time (the rise-time is unimportant) is less than 250 ns, corresponding to less than one eighth of the PS circumference. The kick strength (9 mrad) is sufficiently strong, so that no provisions for a slow injection bump have to be made. The layout of the positron injection channel is shown in Fig. 3.16.

3.2.3 Acceleration

Apart from beam acceleration, the RF system has the task of compensating for the synchrotron radiation loss at high energy (200 keV/turn at 3.5 GeV) and of providing an RF bucket that is large enough for adequate lifetime in the presence of quantum fluctuations. Furthermore, the bunches must have the appropriate longitudinal dimensions at peak energy so that they get trapped by the SPS RF system without instabilities. In order to fit the bunches into the SPS bucket with a sufficient margin,

$$\sigma_s \leq (1/3\pi)\lambda_{\text{RF}}(\text{SPS}) = 0.16 \text{ m}$$

must hold¹⁴⁾. Transverse stability¹¹⁾ of the single bunch at nominal intensity requires, at 3.5 GeV,

$$\sigma_s(\sigma_\epsilon/E) \geq 1.4 \times 10^{-4} \text{ m}.$$

If these two criteria are fulfilled, then the bunch is also longitudinally⁹⁾ stable.

The PS as it is, without any modifications ($J_\epsilon = 4$), can provide at 3.5 GeV

- with the 7.6 MHz RF system: $\sigma_s = 0.46 \text{ m}$ and $(\sigma_\epsilon/E)\sigma_s = 1.1 \times 10^{-4} \text{ m}$,
- with the 200 MHz RF system: $\sigma_s = 0.05 \text{ m}$ and $(\sigma_\epsilon/E)\sigma_s = 0.13 \times 10^{-4} \text{ m}$.

In the first case the bunch is too long, and the bunch area is too small in both cases. Two approaches are suggested for obtaining the proper bunch dimension: i) “bunch expansion”¹⁴⁾ or ii) “bunch compression”¹³⁾.

In the first approach, a 114 MHz ($h = 240$) RF system providing 1 MV of peak RF voltage is used to accelerate the beam from injection (0.6 GeV) to the peak energy (3.5 GeV). The required beam relative energy spread of 1×10^{-3} at a bunch length of 16 cm is obtained by decreasing the longitudinal damping through adjustment of the damping partition number J_ϵ . Two Robinson wiggler magnets³⁴⁾ occupying two short straight sections are used for this purpose; each wiggler changes J_ϵ by -1.9 . Table 3.8 shows the machine parameters at injection and extraction for the bunch expansion. Figure 3.17 gives an example of the voltage programme and shows the evolution of bunch length and energy spread versus time³⁵⁾.

The acceleration rate, defining the magnetic cycle, is $\dot{E} = 2.1 \text{ GeV} \cdot \text{s}^{-1}$ ($\dot{B} = 0.1 \text{ T} \cdot \text{s}^{-1}$) during the first 50 ms after injection, and then $\dot{E} = 11.2 \text{ GeV} \cdot \text{s}^{-1}$ ($\dot{B} = 0.53 \text{ T} \cdot \text{s}^{-1}$) for 250 ms before the 180 ms long 3.5 GeV flat-top is reached.

Table 3.8
Machine parameters at injection and extraction with bunch expansion

	N_b	E (GeV)	σ_s (m)	σ_ϵ/E	J_ϵ	V_{RF} (kV)	f (MHz)	Q_s ($\times 10^{-3}$)	\dot{B} ($\text{T} \cdot \text{s}^{-1}$)
Injection	1×10^{10}	0.6	0.2	0.6×10^{-3}	0.2	40	114	8.2	0.1
Extraction	1×10^{10}	3.5	0.16	1.0×10^{-3}	0.2	950	114	16.5	0

Table 3.9

Machine parameters at injection, before and after compression

	N_b	E (GeV)	σ_s (m)	σ_e/E	J_e	V_{RF} (kV)	f_1 (MHz)	Q_s ($\times 10^{-3}$)	V_{RF} (kV)	f_2 (MHz)	Q_s ($\times 10^{-3}$)
Injection	1×10^{10}	0.6	0.5	0.6×10^{-3}	3.1	120	7.6	3.7	–	–	–
Before compression	1×10^{10}	3.5	0.5	0.3×10^{-3}	3.1	220	7.6	1.5	5	114	1.2
After compression	1×10^{10}	3.5	0.16	1.0×10^{-3}	3.1	220	7.6	1.5	1000	114	17

About 150 ms after the beginning of the flat-top, the beam reaches the required energy spread and a first batch of four bunches is ejected. The second batch waits for the reloading of the kicker magnets and is then extracted. During this reloading time, the blow-up of the bunch dimension due to the quantum excitation is less than 5%.

The second method, bunch compression, uses the existing 7.6 MHz RF system as the accelerating system, the acceleration rate being the same as for bunch expansion. This low-frequency system provides a large bunch area, but the bunch is too long. Thus, once the beam has reached the 3.5 GeV flat-top, a second RF system, operating at 114 MHz, is adiabatically switched on. Since the voltage increase from 5 kV to 1 MV is fast with respect to the radiation damping time, the large bunch area is conserved and only the bunch length is compressed. Table 3.9 shows machine parameters at injection, before and after compression.

Since the value of J_e is close to the natural value of 4, only one Robinson wiggler is necessary, providing $\Delta J_e = -0.9$, but because of the short damping time ($\tau_e \approx 24$ ms) the RF manipulation has to be repeated twice, once for each batch. This introduces operational complications and makes the bunch expansion the preferred solution.

Bunch expansion has also the potential for reaching higher energies and higher intensities if wigglers and RF cavities are added¹⁴⁾. For example, stable transfer of four bunches of $N_b = 1.6 \times 10^{10}$ particles per bunch (second variant scheme, see Section 2.3) at 5 GeV could be possible with four wigglers ($J_e = 0.32$) and 2.7 MV of peak RF voltage at 114 MHz.

However, bunch expansion needs strongly excited Robinson wigglers and operation with a very small J_e . Since these are operating conditions which have never been tested in a synchrotron and which are difficult to assess in all ramifications, it is suggested to keep the bunch compression option open.

The two acceleration modes also give different transverse emittances because the horizontal partition number J_x is very different in the two cases. The solution of the differential equation describing the evolution of the horizontal emittance during acceleration³⁵⁾ leads to $\epsilon_{x0}(1\sigma) = 0.04 \pi \cdot \text{mm} \cdot \text{mrad}$ in the case of bunch expansion, where $J_x = 2.8$. With bunch compression J_x is still negative (-0.1) because the wiggler is weak. This makes the transverse emittance larger, and it grows during the kicker reloading. Consequently, the second batch will have a larger transverse emittance, $\epsilon_{x0}(1\sigma) = 0.32 \pi \cdot \text{mm} \cdot \text{mrad}$, than the first batch which has $\epsilon_{x0} = 0.22 \pi \cdot \text{mm} \cdot \text{mrad}$. As the horizontal, uncoupled emittance of the second batch is too large for the SPS electron injection channel, strong coupling between the horizontal and the vertical plane is produced by powering the existing skew quadrupoles in the PS. This brings the transverse emittances at transfer to $\epsilon_x = \epsilon_y \leq 0.11 \pi \cdot \text{mm} \cdot \text{mrad}$ and $0.16 \pi \cdot \text{mm} \cdot \text{mrad}$ for the first and second batch, respectively. These emittances can be accepted by the SPS. Consideration of the transverse beam size might eventually influence the choice of the acceleration mode, as neutralization-induced space-charge effects in the SPS could be reduced by working with a beam of lower transverse density.

At present, however, no choice needs to be made between these two schemes because both of them require the same additional equipment: a 1 MV, 114 MHz, RF system and Robinson wigglers.

The choice of the radio frequency is a compromise. A too low frequency needs excessive voltage to produce the short bunch length required by the SPS, and the cavities become very voluminous. A higher frequency does not give the bunch area needed for stability with an acceptable quantum lifetime. The RF wavelength must also be long enough to trap the bunch for bunch compression after it has been accelerated by the 7.6 MHz system. The exact value of the harmonic number (240) is chosen so that it can support 4, 6, 8, 12, 16, and 20 bunches, which is attractive for a possible multipurpose RF system.

A single copper cavity provides the required peak voltage of 1 MV. It is 1.75 m in diameter, 1 m in length and will be located in a short straight section of the PS. Computations indicate that a normalized shunt impedance $r/Q_0 = 93 \Omega$ (equivalent circuit convention) and a quality factor $Q_0 = 40000$ can be expected. This figure includes allowance for non-ideal copper conductivity and for additional losses due to tuners, high-order mode couplers, and a damping device for the fundamental mode. The damping device has to reduce the fundamental shunt impedance by a factor of ≈ 5000

during the proton cycles in order to prevent coupled-bunch oscillations. This damping factor is rather high because of the high proton bunch intensity; consequently the damping device would be of an elaborate design. For this reason a mechanical short circuit of the cavity is also under consideration. A total RF power of 160 kW is provided by the RF power amplifier, using two tetrodes working in a power combiner. A system of two such cavities, each driven by only 40 kW of RF power, could increase the flexibility at the expense of one additional short section and a moderate increase in cost; this alternative needs further study. The low-level part of the RF system generating the voltage programmes, the necessary timing, and synchronization signals for bunch transfer is under study³⁶⁾.

Since the RF of the EPA is exactly one sixth of 114 MHz, synchronization between the EPA and the PS is straightforward. A subharmonic common to the RF in the PS and the SPS is used to synchronize the PS to the SPS, which operates with an RF higher by a factor of 7/4 than the PS. The expected jitter in the synchronization between the PS and the SPS is less than ± 0.1 ns, which is acceptable given an r.m.s. bunch length of 0.5 ns and an SPS bucket length of about 5 ns.

One Robinson wiggler magnet consists of four approximately equal blocks of identical pole profile located in a short F straight section of 1.00 m free length, where the dispersion function D_x equals 2.7 m. The orientation of the pole profile is the same in all four blocks, but the field of the two centre blocks has opposite polarity of the field of the two outer blocks. In first order this localizes the closed-orbit perturbation and compensates the quadrupole focusing. The product of the central field and field gradient is $-0.66 \text{ T} \times 8.2 \text{ T} \cdot \text{m}^{-1}$. A layout of the four blocks in the straight section and a side view of one block are given in Fig. 3.18.

3.2.4 Extraction and transfer to the SPS

The extraction system is the same as that used for $p\bar{p}$ operation. The positrons are extracted at straight section SS16 and transferred to the SPS via the transfer lines TT2 and TT10, and the electrons are extracted at SS58 and transferred via TT70 and TT60.

In the nominal operating mode and its first variant (see Section 2.2), eight equidistant bunches circulate in the PS. After bunch shaping, a family of four is extracted first in such a way that the bunches are equidistant in the SPS³⁷⁾. The time between two bunch extractions, allowing for reloading of the SPS electron injection kicker, corresponds to $4^{1/4}$ turns in the SPS, and the four bunches are extracted within 294 μs . As a matter of fact, the SPS positron injection kicker does not need reloading and extraction could be performed in one SPS revolution. However, in order to standardize operation, the same procedure is proposed for both kinds of particles.

After extraction of the first family of four, the kickers are reloaded within 30 ms³⁸⁾, and the remaining family is moved by $\pm 3/56^{\text{th}}$ or $\pm 5/56^{\text{th}}$ of the PS circumference depending on the desired position of the second family in the SPS. This position is determined by the choice of the number of LEP turns elapsing between the injection of the first and the second family into LEP. The waiting time between the two successive injections into the same LEP bucket depends upon whether injection into synchrotron or betatron phase space is chosen, and upon the tune of LEP. Thus the waiting time is considered as a variable parameter which will be optimized empirically. The rephasing of the second family in the PS is obtained within 20 ms by letting the four bunches run with a mean radial displacement of 1 mm during the reloading of the kickers. Then, if required, bunch compression is performed, the RF systems in the PS and the SPS are synchronized again, and the second family is extracted. More details on eight-bunch transfer are given elsewhere⁸⁾.

The extraction kick for each individual bunch is provided by firing 2 out of 12 modules of the full-aperture kickers located in straight sections SS71 and 79. The extraction system can cope with a 3.5 GeV beam of $1.5 \pi \cdot \text{mm} \cdot \text{mrad}$ horizontal emittance (1σ) and a relative energy spread of 10^{-3} . At 3.5 GeV, in the worst case of bunch compression where the beam is antidamped, the emittance is less than $1 \pi \cdot \text{mm} \cdot \text{mrad}$ and the relative energy spread is around 10^{-3} . Since the extraction of one family takes longer than the presently available current pulse for septa and orbit bumpers, their power supplies must be modified.

As only four bunches circulate in PS and SPS in the second variant scheme (see Section 2.2.2), no rephasing takes place in this case and extraction is completed after 294 μs .

3.2.5 Synchrotron radiation and vacuum

The synchrotron radiation³⁹⁾ does not penetrate the wall of the PS vacuum chamber at 3.5 GeV. The critical energy of the photons is only 1.4 keV, and the photons are absorbed upon traversing a few micrometres of metal.

With 8×10^{10} particles circulating in the PS on the flat-top at 3.5 GeV, the power lost in the vacuum chamber around the bending magnets is about $1 \text{ W} \cdot \text{m}^{-1}$. Therefore, no noticeable heating of the vacuum chamber will occur.

Recent extrapolations^{40,41)} from measurements⁴²⁾ done on DCI (LAL Orsay) indicate that the initial increase in outgassing rate due to synchrotron radiation might be more than one order of magnitude above the actual outgassing level with protons and what had been assumed so far for electrons/positrons. If this is confirmed, the gas pressure could rise to the 0.01 mPa (10^{-6} Torr) range.

Under these conditions, rapid accumulation ($\tau_i \simeq 1$ ms) of ions up to full neutralization of the beam would certainly occur⁴³⁾, entailing a large tune shift $\Delta Q \sim 0.040$. Furthermore, emittance growth due to multiple scattering

might become a problem, the time constant of growth being of the order of 100 ms at 10^{-6} Torr. Thus an improvement programme for the PS vacuum system has to be undertaken.

3.2.6 Beam stability

The most dangerous single-bunch instabilities are the fast-growing, so-called turbulence effects generated by mode coupling via the broad-band impedance. These effects need special attention at injection. There the beam energy is low, and the bunch suddenly finds itself in a new environment to which it has not yet had time to adapt. The RF parameters of the sending machine must be properly chosen so that the bunch energy spread is sufficient and the peak current remains below threshold in the receiving machine. For this reason, as described before, the PS acceleration mode is strongly conditioned by beam stability considerations at injection in the SPS. In order to obtain a sufficient energy spread at PS injection, the lattice of the EPA has a reduced damping partition number J_x (see subsection 3.1.2). All calculations are based on the longitudinal low-frequency impedance of $|Z/n| = 20 \Omega$ in the PS and the SPS, as indicated by measurements with proton beams^{10,44}. The high-frequency impedance is evaluated by extrapolation using the $Q = 1$ resonator model with a resonance frequency at 1.3 GHz.

If multibunch instabilities driven by the low-frequency impedance occur, the existing proton feedback systems will help. Whether high-frequency resonators, not detectable with the proton bunches, will contribute to the multibunch modes remains to be seen. If required, new damping systems will be developed after the first tests. A good control of chromaticity is certainly imperative so that the growth rate of the head-tail modes can be minimized.

3.2.7 Instrumentation³¹⁾

At the EPA-PS hand-over point a beam position monitor, a profile monitor, and a current transformer will provide data on the incoming beam properties. Matching of both injected beams will be measured by means of a single set of three SEM grids centred around straight section SS30 or 80 and used in conjunction with one or two beam stoppers.

The electronics of the 40 electrostatic pick-up stations (PUs) at present used in the closed-orbit digital display can handle the very short e^\pm bunches if the signal from the electrode is shaped by a filter. The surface of the electrodes is not exposed to synchrotron radiation, except for the 14 PUs located in the enlarged vacuum chamber. Since the PUs are located in the fringe field of the main magnet, the secondary electrons will be trapped before they can spoil the signals of the electrodes⁴⁵⁾. Six new beam position monitors, not affected by synchrotron radiation, will be installed to evaluate the amplitude of coherent betatron oscillation and the mean radial position at injection.

The equipment used to measure the mean radial position derived from the revolution frequency can easily be adapted to the requirements of e-operation. The existing wide-band directional coupler located in SS98 will allow for the observation of the bunch structure.

A precise measurement of bunch length as well as beam size will be possible with a synchrotron light monitor, to be installed. The present beam current transformers are, in principle, suitable for the e^\pm beams.

3.2.8 Controls

The PS control system will handle all variants of the e-cycle in the interleaved mode. However, the e^\pm operation differs in many respects from a proton operation and an appreciable amount of new equipment is to be installed. Software and controls hardware has to be developed, mainly to cope with speed and sequencing problems⁴⁶⁾.

3.3 MODIFICATIONS AND ADDITIONS TO THE SPS

3.3.1 Introduction

The SPS has been built as a 400 GeV proton accelerator for fixed-target physics. Since 1981 it is also operating part-time as a proton-antiproton collider at 270 GeV, and now the work has started to adapt the SPS to its further task as the largest component of the LEP injector chain. The present section first reviews some basic problems related to e^\pm acceleration, i.e. beam stability and synchrotron radiation, and thereafter describes the required modifications and additions to the SPS.

3.3.2 Beam stability

Single-particle stability

At the design injection momentum of 10 GeV/c for protons the magnetic field in the main ring dipoles is 0.045 T, whereas the e^\pm will be injected at 3.5 GeV/c, corresponding to a field of 0.0158 T. The magnitude ΔB of the field fluctuations caused by remanent field errors is roughly independent of the absolute field level, so that the resulting closed-orbit deformations at 3.5 GeV/c are expected to be about three times larger than at 10 GeV/c. This problem will be dealt with by pulsing the existing orbit correction dipoles during the e^\pm acceleration cycle, as described in subsection 3.3.8.

Similarly the systematic sextupole field component in the dipoles, produced by their remanent field and by eddy currents in the vacuum chamber during the rise of the magnetic field, produces a chromaticity change of the machine

which is about inversely proportional to the injection momentum. For the same reason the widths of the stopbands caused by fluctuations of sextupole and higher-order fields are roughly inversely proportional to the injection momentum.

Nevertheless, the existing system of multipoles for correcting the betatron oscillations around the closed orbit is thought to have enough degrees of freedom to cope with this unfavourably low injection momentum. In particular, the four sextupole and two octupole families are theoretically capable of correcting the large natural chromaticity, produced by the sextupole field components in the dipoles, with sufficient precision up to second order for an r.m.s. momentum spread of 10^{-3} . The existing quadrupole, sextupole, and octupole stopband correctors can be used, if necessary, to increase the single-particle stability.

Synchro-betatron resonances should not be observable, since at the injection energy Q_s is too small, whilst at high energy, synchrotron damping will dominate.

The effect of higher-order stopbands strongly depends on the amplitude of the betatron oscillations. Therefore, the above-mentioned corrections are facilitated by the fact that the emittances of the 3.5 GeV/c electrons and positrons are smaller than those of the 10 GeV/c protons injected for fixed-target physics. The expected 2σ emittances for e^\pm are $\varepsilon_x \cong \varepsilon_y \leq 0.64 \pi \cdot \text{mm} \cdot \text{mrad}$, and this is to be compared to $\varepsilon_x \cong \varepsilon_y \cong 2 \pi \cdot \text{mm} \cdot \text{mrad}$ for the currently injected proton beam.

Turbulent instabilities

The most dangerous of the known collective instabilities which could affect the electron beams in the SPS is the single-bunch high-frequency transverse instability¹⁰⁾, sometimes called transverse “turbulence”. It has been observed in two e^+e^- storage rings (SPEAR and PETRA), and is thought to arise from the interaction of the transverse modes of the bunch with the high-frequency broad-band transverse coupling impedance of the machine. This coupling impedance is known in the SPS with a good accuracy from measurements with protons which give $Z_\perp = 38 \text{ M}\Omega \cdot \text{m}^{-1}$. An existing theoretical model allows the determination of the threshold intensity for given bunch parameters¹¹⁾. With a bunch length $\sigma = 16 \text{ cm}$ and energy dispersion $\sigma_e/E = 1.0 \times 10^{-3}$, stability is predicted for intensities below 1.0×10^{10} electrons per bunch. This model is known to be valid for the short bunches of the present e^+e^- storage rings, but unfortunately no experimental check can be made for the long bunches expected for electron acceleration in the SPS, since in this case details of the approximations and the particularities of the coupling impedance play a more important role. Therefore it appears advisable to base the LEP injection scheme on a nominal electron bunch intensity in the SPS of 0.8×10^{10} , provided that in view of the uncertainties in the calculation of the stability limit the option of a somewhat more elaborate solution which requires only half this bunch intensity is kept open (see subsection 2.2.2).

The corresponding phenomenon in the longitudinal phase plane (the microwave instability) is much better known. Its threshold is predicted at three times the nominal intensity and therefore it should not pose any problem.

Effects of the RF system for electron acceleration

The impact on the SPS performance of the 32 standing-wave cavities which will be installed to accelerate the e-beams has been assessed for the different machine utilizations: acceleration of electrons and positrons, acceleration of high-intensity proton beams, and the acceleration and storage of protons and antiprotons in the collider mode. In contrast to the situation in modern e^+e^- storage rings designed with a smooth vacuum chamber, the contribution of these cavities to the broad-band coupling impedance of the machine is negligible in the SPS. Therefore, the transverse and longitudinal “turbulence” thresholds discussed above will be very little affected. However, coupled-bunch instabilities would be strongly excited by both the fundamental and the first higher transverse and longitudinal modes of the cavities⁴⁷⁾. The worst situation arises for high-intensity proton acceleration, where injection of 5×10^{13} protons at 10 GeV/c in 4620 bunches requires a damping of the fundamental mode by a factor of around 200 to ensure stability. The damping loops foreseen for the cavities will exceed this requirement, since a damping factor of 500 on the fundamental has already been measured on a prototype. It can be expected that even the higher modes will be sufficiently damped by these loops.

During electron acceleration, the interaction of the dense bunches with the fundamental mode of the standing-wave cavities will generate the Robinson instability, where all the bunches oscillate in phase. This will be damped, as is customary in electron machines, by a small detuning of the cavities. Other coupled-bunch modes, with bunches oscillating out of phase, could be excited by higher-order modes of the cavities. These instabilities, which usually have longer growth times, will have to be damped by suitable feedback loops similar to those used for protons.

3.3.3 Synchrotron radiation

Introduction

The data given in this subsection are based on the nominal design figures, i.e. a beam intensity in the SPS of eight bunches, each with 0.81×10^{10} particles, corresponding to a total current of 0.45 mA and a maximum energy of 20 GeV. Some data are also given to permit extrapolation to higher energies.

The power loss of the beam during the flat-top of an electron cycle, with energy and current as defined above, is $1.85 \text{ W} \cdot \text{m}^{-1}$ in the dipole magnets. Taking into account the duty cycle leads to an average power for the entire

supercycle of about $0.024 \text{ W} \cdot \text{m}^{-1}$. Therefore thermal effects should be negligible in the SPS, but we have to review the following effects of synchrotron radiation:

- i) radiation dose deposited in the coils of the magnets;
- ii) production of ozone and nitric acid in the air;
- iii) secondary emission of electrons;
- iv) desorption of gas molecules.

It is expected that LEP will operate 3000 hours per year and will need to be filled during 22 min about every 3 hours. Since one cannot afford to lose valuable machine time in setting up for each new fill, the entire injection chain could remain cycling continuously when LEP operates, although possibly without e^\pm beams in, say, three out of four supercycles, thus enabling the operator to verify once per minute that all settings are still correct. In addition, all setting up and machine development of the LEP injection chain will also have to be done during these 3000 hours of LEP operation (which are compatible with SPS fixed-target physics) since electron acceleration or LEP filling is not compatible with proton-antiproton operation of the SPS.

It seems reasonable, therefore, to estimate the effect of synchrotron radiation in the SPS on the basis of 2000 hours of operation with a supercycle with electron and positron beams of the nominal intensity, i.e. a total of 5×10^5 supercycles with e-beams per year.

Radiation dose to the magnet coils

Inside the SPS dipoles^{48–50} the synchrotron radiation impinges on the vacuum chamber at a grazing angle which varies between 10 mrad and 20 mrad. This incident radiation is strongly absorbed by the stainless steel of the vacuum chamber and therefore the dose received by the coil insulation is due to Compton scattering at large angles to the incident radiation. The highest radiation dose is received in the median plane of the machine by the insulation of the conductors inside the gap of the MBB dipole magnets, which are at only a few millimetres from the vacuum chamber with a wall thickness of 1.5 mm (against 2 mm for the MBA magnets). Curve (a) of Fig. 3.19 shows the dose rate for the most exposed part of the MBB insulation for a current of 0.45 mA during the flat-top of an electron cycle as a function of the flat-top energy⁵¹). The dose rate is a strong function of the flat-top energy, since the total power of the emitted synchrotron radiation is proportional to E^4 and the fraction of energy absorbed in the vacuum chamber wall slowly decreases with increasing beam energy.

Outside the dipoles the vacuum chamber has transition pieces where locally the chamber wall is perpendicular to the direction of the synchrotron radiation, so that limited regions of coil insulation could be irradiated by the almost unattenuated synchrotron radiation from about 1 m length of electron orbit. At these locations a protective lead collar must be mounted to reduce the radiation dose to an acceptable level. Curves (b) and (c) of Fig. 3.19 show the dose rate for a current of 0.45 mA as a function of the flat-top energy, for a thickness of 10 mm and 15 mm, respectively, of the protective lead collar. It is worth noting that curves (b) and (c) are even steeper functions of energy than curve (a).

It is clear from Fig. 3.19 that the dose rate from synchrotron radiation becomes significant only when the beam energy is close to the flat-top energy, and therefore it is convenient to express the total radiation dose per electron cycle in terms of an equivalent time T_{eq} corresponding to the time during which a beam circulating on the flat-top would produce that same radiation dose. For the cycle parameters given in subsection 3.3.7, we find that $T_{\text{eq}} = 50 \text{ ms}$ is a typical, slightly conservative value. This means that one supercycle is equivalent to 0.2 s at flat-top beam energy for the coils inside the magnet, and 0.1 s at flat-top energy for the coil ends because the latter are only irradiated by synchrotron radiation from either the positron or electrons. Therefore the 5×10^5 supercycles per year are equivalent to 10^5 s at top energy for curve (a) and $5 \times 10^4 \text{ s}$ at top energy for curves (b) and (c). The latter numbers, multiplied with the dose rates of Fig. 3.19, then give the doses in rad per year shown in Table 3.10.

Whereas around 20 GeV the dose inside the magnet is larger than the dose to the coil ends, the latter would rapidly become dominant for higher electron energies. In order to remain smaller than the dose deposited for the present proton operation, the yearly dose should not exceed 10^6 rad .

Table 3.10

Estimated radiation doses (rad/year)

Flat-top energy	20 GeV	22 GeV	24 GeV	26 GeV
Coil inside the magnet	6.6×10^4	2.0×10^5	4.6×10^5	1.0×10^6
Coil ends with 10 mm Pb collar	1.6×10^3	5.5×10^4	4.4×10^5	2.4×10^6
Coil ends with 15 mm Pb collar	1.6×10^2	1.0×10^4	1.4×10^5	8.7×10^5

Production of ozone and nitric acid

Detailed numerical data have been worked out^{51–53}. Here we shall restrict ourselves to more qualitative arguments. Calculations made using the MORSE⁵⁴ and EGS⁵⁵ Monte Carlo programs confirm that the dose received by the air between the vacuum chamber and the coil insulation in the dipoles is close to the dose received by the superficial layer of the insulation itself.

If the average dose rate due to electron acceleration (see above) is kept below the average dose rate due to the present proton acceleration, the production rate of ozone and nitric acid during e^\pm acceleration should also remain below the respective production rates associated with proton acceleration in the SPS. The latter do not present any problem, since at present the ozone concentration in the SPS is far below the permissible level for ventilation exhausts or for access to the tunnel during machine stops, whilst no corrosion effects have been observed which are directly attributable to the production of nitric acid.

Just outside the transition pieces of the vacuum chamber where the synchrotron radiation can emerge almost perpendicular to the chamber wall, the local dose rate between the vacuum chamber and the lead collar is some 10^5 times larger than the values downstream of the lead collar shown in Fig. 3.19. Since it would probably be difficult to achieve an airtight fit between collar and vacuum chamber it may be better to leave some space for the dilution of the nitric acid concentration by air convection.

Effects of synchrotron radiation inside the SPS vacuum system

The synchrotron radiation must be prevented from hitting a number of components inside the SPS vacuum system. A first review has shown the following cases.

- i) The outer electrodes of the radial position beam monitors would give a spurious signal due to secondary electron emission. They will be shielded by copper masks (see subsection 3.3.8).
- ii) The cathodes of the electrostatic septa for proton extraction which are at -250 kV during the interleaved cycle would spark because of secondary electron emission. It may be possible to prevent this breakdown by inserting movable shutters upstream of the electrostatic septum during the e-cycles. If this is not sufficient, the electrostatic septa must be rapidly turned on and off for the p- and e-cycles, respectively.
- iii) The ferrite of the existing kicker magnets could suffer radiation damage from synchrotron radiation. Since the yokes are C-shaped this can be prevented, where necessary, by turning the kicker magnet around so that the yoke is radially on the inside of the orbit.

Gas desorption

The total number of photons produced per second and metre by the circulating beam in the dipoles is⁴⁸

$$dn_\gamma/dt = 1.6 \times 10^{17} (E \cdot I)/\rho,$$

where E (GeV) is the particle energy, I (mA) the beam current, and ρ (m) the bending radius. Gas desorption from the vacuum chamber walls by these photons will initially be very important during the running-in, but will gradually decrease because the chamber is slowly cleaned.

The desorption rate as function of the dose (product of beam current times operating time) has been measured in DCI⁴². Scaling to the SPS⁴⁰ yields an estimate of the pressure-rise factor shown in Fig. 3.20. Since this pressure-rise factor corresponds to steady-state operation at 20 GeV, it is an upper limit expected to occur if the pressure were proportional to the instantaneous flux of photons. In order to give some typical values, the upper pressure limit is calculated for the case where the SPS has been operating with the nominal current of 0.45 mA for one day with the 1.26 s long nominal e-cycle and, secondly, for one year (2000 h) with the nominal SPS supercycle. Taking into account that the total number of photons per e-cycle is equivalent to the number produced during 0.12 s at 20 GeV, the dose becomes 1 mA·h after one day and 30 mA·h after one year. Hence the expected upper limits for the pressures are 0.3 mPa (2×10^{-6} Torr) and 0.03 mPa (2×10^{-7} Torr). These pressures are substantially higher than estimated earlier⁴⁸. The previous values were averages over the e-cycle and were based on desorption yields of the PETRA vacuum chamber, which had already been exposed to prolonged beam cleaning.

Observations indicate that the time constant of the pressure rise is relatively long⁵⁶. Thus the actual peak pressure during the e-cycles will be between the upper limit and the 10 times lower average pressure calculated from the average desorption during the e-cycle.

Even under the pessimistic assumption that the pressure at injection equals the upper limit at 20 GeV, the beam lifetime is much longer than the time the beam is in the machine. However, accumulation of ions in the electron beam could upset the cancellation of electric and magnetic space-charge forces and could lead to significant tune shifts at injection. If, initially, the effects turn out to be bothersome or if the pressure rise disturbs the proton operation, the beam cleaning must be speeded up by running for a few days in storage ring mode or with cycles with a long flat-top. Another possible measure is to use the sublimation pumps, but their very limited lifetime does not make them suitable for continuous operation.

3.3.4 Transfer of e^+ and e^- from the PS to the SPS

The schematic layout of the transfer channels is shown in Fig. 3.21. The positrons are transferred through the existing transfer line TT10 at 3.5 GeV/c in alternation with the 10 GeV/c protons. At present, TT10 is operated in d.c. mode, and modifications to the power supplies for pulsing between these two field levels are necessary. With the exception of one dipole which will be changed, all TT10 magnets have laminated cores and are suitable for pulsed operation.

The electrons are transferred through the antiproton transfer line TT70 and through the upstream part of the proton extraction line TT60. The magnets of TT70 are at present connected to power supplies which, during the periods of fixed-target physics, feed the downstream part of TT60. The change-over from one load to the other is done by mechanical switches. With the interleaved mode of operation for electrons and protons, this double use is no longer possible, and independent new power supplies are required for TT70. It is proposed to make these new power supplies just strong enough for the 3.5 GeV/c electron transfer and to continue to switch to the stronger ones of TT60 for the transfer of 26 GeV/c antiprotons.

The first part of TT60 must be pulsed between 3.5 GeV/c and 450 GeV/c. The required relative precision at 3.5 GeV/c cannot be achieved with the present strong power supplies, and additional small ones will be added to take over at the moment of the electron transfer. Before the magnets can be switched to these small power supplies, the currents of the strong power supplies must be rapidly brought to zero level, and some power supplies must be modified accordingly.

Beam observation of electrons and positrons will be done with the existing secondary emission monitors which are now used for protons and antiprotons.

3.3.5 Injection and extraction

Injection of e^+ in LSS1

The injection of e^+ in long straight section LSS1 makes maximum use of the existing equipment for proton injection but will need some modifications and additions. Similar to TT10, the four injection septum magnets MSI must be pulsed and therefore their solid cores must be replaced by laminated ones. The most important modifications concern the proton injection kicker system MKP⁵⁷⁾, which must be adapted to the injection of eight independent e^+ bunches per e^+ cycle.

The minimum distance between bunches in the SPS required for two-turn injection into LEP is 1/14 of an SPS circumference, i.e. $1.65 \mu\text{s}$. The flat-top duration of the inflector pulse can be adjusted between $1 \mu\text{s}$ and $12 \mu\text{s}$, whilst the rise- and fall-times of the kick strength are $0.15 \mu\text{s}$ and $0.7 \mu\text{s}$, respectively. Thus adjacent bunches are not disturbed if the flat-top duration of the pulse is chosen to be $1 \mu\text{s}$.

Proton injection at 10 GeV/c makes use of eight separate kicker magnet modules powered in pairs by four pulse generators. Injection at 3.5 GeV/c requires a kick strength of $0.053 \text{ T} \cdot \text{m}$ which can be obtained from two kicker modules operating at a generator voltage of 53 kV. To place four of the eight bunches in their correct azimuthal positions, four pairs of kicker modules will be pulsed successively with a time interval of $89 \mu\text{s}$, each pair injecting one bunch. The pulse-forming networks are then recharged within about 30 ms and pulsed a second time to inject the remaining four bunches. During the 30 ms charging time, the latter four bunches are rephased in the PS in order that they get into the correct positions in the SPS. The implementation of this injection scheme requires the following:

- a new attribution of the existing transmission cables between generators and magnets, to conserve the same deflection centre when different magnet pairs are powered;
- a second set of capacitor banks for the resonant charging power supplies;
- additional equipment for timing and voltage setting.

During initial operation it may be sufficient to operate LEP with stored beams of only two bunches each, and in that case it could be desirable to transfer the eight SPS bunches to LEP by four-turn injection into each of the two LEP bunches. In order that the bunches fall in the correct SPS positions for this mode of operation, the PS must be rephased three times, each time after the transfer of two bunches from the PS to the SPS. The equipment for the transfer scheme described above is also capable of this mode of operation.

Injection of e^- and extraction of e^\pm in LSS6

Electron injection and positron extraction is through the existing magnetic channel in LSS6, which was originally built for the extraction of 400 GeV/c protons and is now also used for the injection of 26 GeV/c antiprotons. The extraction of electrons requires a complete new system. The schematic layout of LSS6 is shown in Fig. 3.22.

The 3.5 GeV/c electrons are transferred to the SPS via TT70 and part of TT60. After passing through the extractor magnet MSE and through the thin septum magnet MST for proton extraction, they are deflected onto the SPS closed orbit by a new kicker magnet MKLP to be located upstream (as seen by the protons) of the defocusing lattice quadrupole QDA 6171. For the MSE, a small thyristor rectifier must be coupled in parallel to the output of the high-current rectifier, since the stability of the latter is insufficient at less than 1% of its design current. The MST is not excited during e^- injection, but must be demagnetized. For this purpose, a new, small power supply will be connected to an existing correction winding around the back yoke of the MST.

The extracted e^+ at 20 GeV follow the same trajectories as the injected e^- at 3.5 GeV/c, apart from the fact that the positrons move in the opposite direction. All hardware is used in common until the e^+ leave TT60 via a vertical switch and enter the transfer line TI18, which transports them to LEP (see Section 3.4).

The extraction of e^- in LSS6 is done in the vertical plane to avoid interference with the transfer schemes described above. A kicker MKLE located downstream of QDA 6191 deflects the beam vertically by 0.8 mrad into a copper septum magnet installed downstream of the lattice quadrupole QDA 6171. The septum magnet is located above the circulating beam without limiting the vertical aperture of the SPS, and deflects the electrons just enough to clear the top of QDA 6171.

The septum magnet is of conventional design, very similar to the design of the existing septum magnets in LSS6 for proton extraction. It consists of two units with an effective length of 2 m each. The field strength of about 1 T can conveniently be reached with a septum thickness of 12 mm.

Apart from the above layout and hardware modifications, the injection and extraction of e^+ and e^- requires a number of smaller modifications and additions, mainly concerning the vacuum system and the system of horizontal dipoles which produce the bumps required to bring the circulating beam close to the septum magnets at the moment of beam transfer through the existing proton channel.

Kicker magnets for e^\pm extraction and e^- injection

In view of the good experience with the existing SPS kicker magnets, which are single-turn, C-cored ferrite magnets housed in vacuum tanks, it is proposed to use the same type of magnets for e^\pm extraction and e^- injection.

Because of the short bunch length and the relatively large interbunch gap, it is not necessary to make pulses with a short rise- and fall-time and a long flat-top, as is usual for the injection or extraction of proton beams which fill the entire machine circumference, but it is sufficient to use pulse generators which produce pulses of half-sine-wave shape. The bunch traverses the magnet during the peak of the pulse.

Half-sine-wave pulsers operate at considerably lower voltages than square-wave generators for the same maximum current because of the longer rise-time. Air rather than oil is used as the insulating medium and they are therefore much cheaper. The generator consists of a capacitor and a low-cost, single-stage ceramic thyatron, such as type EEV CX 1154. It must be housed in the accelerator tunnel close to the magnet, which is purely inductive and therefore does not need matching capacitors. The pulser is connected via a single coaxial cable to the high repetition rate, resonant charging supply, which is located, with all its control and interlock electronics, in the service building. The supply produces one charging pulse per bunch to be injected or extracted.

The same type of excitation system will be used for the LEP injection kickers and pulsed septa, where the saving in the cost of coaxial power cables is particularly important.

Thyatron filament lifetimes between 10000 h and 30000 h, depending on the required duty, have been obtained in the SPS in recent years. The location of the thyatrons in the accelerator tunnel, i.e. in a position which does not permit a fast exchange in case of failure, should therefore be acceptable.

The pulse rise- and fall-times are chosen $< 1.5 \mu\text{s}$ and are short enough to allow extraction or injection of individual bunches which are 1/14 of the SPS circumference apart. The minimum repetition time of the kickers is $89 \mu\text{s}$, corresponding to one LEP revolution.

The e^+ extraction kicker (MKLP), which is also used for e^- injection, produces a horizontal deflection of 1.7 mrad. The e^- extraction kicker (MKLE) produces a vertical deflection of 0.8 mrad. The main parameters of the two kicker systems are given in Table 3.11.

Table 3.11
Main parameters of new SPS kickers for e^\pm

	MKLP		MKLE
	e^- injection	e^+ extraction	e^- extraction
Deflection direction		horizontal	vertical
Deflection angle (mrad)		1.7	0.8
Number of modules		3	1
Aperture (h \times v) (mm)		112 \times 54	120 \times 54
Module length (m)		0.835	2.5
Pulse rise/fall-time (μs)		< 1.5	< 1.5
Minimum repetition time (μs)		89	89
Beam momentum (GeV/c)	3.5	20	20
Current amplitude (kA)	0.43	2.4	2.4
Charging voltage (kV)	3.6	20.7	13.9

3.3.6 The accelerating system for positrons and electrons

For e^\pm acceleration in the SPS, a peak RF voltage of about 30 MV is needed to compensate for the energy loss caused by synchrotron radiation, to make provision for parasitic mode losses, and to adapt the bunch shape to the 352 MHz buckets of LEP. The present 200 MHz accelerating system of the SPS consists of TW structures which are well suited for proton acceleration but can provide at most 8 MV. An extension is not practical since the effective energy gain per unit length is relatively low in this system, which was designed to cope with the large frequency swing and heavy beam loading during proton acceleration. Since the e^\pm intensity is low and the beam loading not severe, it is planned to use a new 200 MHz system made of single-cell SW cavities which will provide a much higher energy gain per metre and which can therefore be fitted into the available straight section space. The TW system must be retained for the normal proton acceleration and for $p\bar{p}$ collider operation.

The new system has two sets of 16 individual modules, each consisting of a single-cell accelerating cavity with its own power amplifier on top of it. Figure 3.23 shows a cross-section of the SPS tunnel at the location of the new cavities. A schematic layout of the existing and additional accelerating systems near and in LSS3 is shown in Fig. 3.24. The two sets of modules will be installed in the two missing magnet sections on either side of LSS3, downstream of quadrupole QF3141 and upstream of quadrupole QF3221. Although the horizontal dispersion is of the order of 2 m in these two regions, synchro-betatron resonances should not be harmful because of the very low Q_s at low energy. The 16 cavities of each set will occupy 12 m out of the 13.3 m available in each missing magnet section, just leaving space for vacuum pumps and valves. The equipment at present installed in these sections will be moved to other places in the SPS ring, mainly to the missing magnet section upstream of LSS4, without influencing the machine performance.

As shown in Fig. 3.25, each cavity is formed from two half-shells of thick copper sheet, which are joined together by electron beam welding, with nose-cone inserts brazed onto the shells. The beam hole in the noses has a diameter of 144 mm, which is imposed by the aperture required for the beam during proton acceleration. Two prototypes of such a cavity have been constructed, and one of these has already been installed in the SPS machine to measure its effect on the proton beam.

Each cavity has a servo-controlled mechanical tuner which corrects for mechanical tolerances, thermal expansion, and varying beam loading condition. The frequency range of the tuner is large enough to cover also the 130 kHz frequency swing between the 26 GeV/c injection momentum and the 270 GeV/c coasting beam momentum in $p\bar{p}$ collider operation. Therefore these new cavities could also be used during $p\bar{p}$ operation, in which case the much higher peak RF voltage would improve the longitudinal bunch stability.

When the SPS is accelerating protons, these new cavities cannot be used and must be damped, since the proton beam, with a bunch structure whose frequency is close to the resonant frequency of the cavities, would otherwise induce excessive voltages in the cavities and would become itself unstable as these voltages act back on the beam. Damping of each cavity is obtained by a loop which is connected to an external load and is driven into the cavity by a pneumatic actuator before proton acceleration starts. A damping factor of about 500 has been obtained with such a device mounted on the cavity which has already been installed in the ring. This factor should be sufficient, according to theoretical estimates of the thresholds for coupled bunch longitudinal instabilities⁴⁷⁾. Higher-order resonating modes in the cavities also need to be damped for both proton and e^\pm operation, and this will be obtained with two additional static loops per cavity.

The amplifier of each cavity consists of a single tetrode which is directly coupled to the cavity. A prototype tetrode has already delivered more than the design RF power of 65 kW into a resistive load. Taking advantage of the location of the new cavities on either side of LSS3, it is planned to use the rectifier plant of one of the two existing RF transmitters associated with the TW structures for supplying the 10 kV anode voltage needed by the new amplifiers. The alternating operation of the TW structures for proton acceleration and of the new cavities for e^\pm acceleration requires only the correct pulsing of the grids of the tetrodes in the corresponding transmitters, thus allowing the saving of a 4 MW rectifier plant.

Synchronization between LEP and the SPS will make use of the same principle as for synchronization between the SPS and the PS during $p\bar{p}$ operation. Since the ratio between the two radio frequencies of LEP and SPS is not an integer but is equal to the ratio of two integers (58/33), each frequency will be suitably divided to obtain a subharmonic which is common to both frequencies. The relative phase of these two subharmonics is then used to control one frequency so that the required ratio is always maintained. It is estimated that the total jitter of such a system will be lower than 30 ps, which should be acceptable for the expected bunch lengths in each machine during transfer of the bunches from the SPS to LEP.

3.3.7 Magnet power supplies

The e^\pm cycles (see Fig. 2.3) have a length of 1.26 s. The rate of rise of the magnetic field can be smaller than for proton acceleration, but must remain reasonably fast to limit the exposure of the SPS to synchrotron radiation. A suitable value, consistent with the power supply ratings given below, is $dE/dt = 90$ GeV/s. For the same reason, the round-off at the beginning of the flat-top will be kept to about 20 ms. The flat-top itself can be short, since in all transfer schemes under consideration the eight bunches are always extracted within 5 ms. The fall-time of the field is not critical, provided that it fits within the total cycle duration of 1.26 s.

The existing power supplies of the SPS main-ring magnet which enable protons to be accelerated to 450 GeV, have been designed for a minimum current corresponding to an injection momentum of 10 GeV/c and are not suitable for injection at 3.5 GeV/c or for cycles with a short round-off.

The best technical and most economical solution is to insert dedicated power supplies for the e-cycles in the SPS main magnet circuits, as is shown schematically for the dipole circuit in Fig. 3.26. The present dipole circuit has 14 rectifiers, each rated at 2.4 kV, 6 kA peak, which are distributed around the SPS ring and are used in such a way that the voltage to ground in the magnet circuit always remains within ± 3 kV. For the e-cycles, two new power supplies rated at 5 kV/500 A peak will be inserted at symmetrical points in the existing circuit so that the voltage to ground is kept within the limits ± 2.5 kV. Each of the two new power supplies must have a 6 kA bypass to conduct the main current during proton acceleration to 450 GeV. Similarly, all 14 large rectifier stations must have small 500 A bypasses which conduct during e-acceleration. Each power supply for e-acceleration has two voltage levels, i.e. 5 kV for acceleration and 0.6 kV for the other parts of the cycle. This arrangement gives an important saving on the filtering and also makes it possible to reduce the length of the round-off at the beginning of the flat to about 20 ms.

Each of the two SPS quadrupole circuits has at present one rectifier station for proton acceleration, and will be equipped with one 2.5 kV/250 V/200 A rectifier station for e-acceleration and the appropriate current bypasses for interleaved operation.

All four new power supplies described above will be located in the SPS equipment building BA3, which houses all the present current regulating electronics and is adjacent to the main control room.

The regulating system of the new power supplies will be independent and will have its own computer, which sends out voltage references at a repetition time of 5 ms (instead of 60 ms for proton cycles) to be consistent with the shorter time-scale and short round-off for the e-cycles. This arrangement also leads to the following important practical advantages:

- i) independent commissioning of the electron power supplies with interleaved cycles during periods of proton acceleration;
- ii) independent adjustment and trouble-shooting of the regulation systems for electron and proton cycles during interleaved operation.

3.3.8 Beam observation and closed-orbit control

The pick-up electrodes

In the SPS the horizontal closed orbit is measured with 108 electrostatic pick-up stations located near the 108 horizontally focusing lattice quadrupoles. The principle of operation of the pick-up (PU) stations is shown in Fig. 3.27. The horizontal displacement of the closed orbit is proportional to the ratio Δ/Σ . This ratio is obtained from a direct subtraction and summation of the signals in a "hybrid ring junction".

Without special precautions, the outer electrode of the PU station would be hit by synchrotron radiation during the e^+ cycles and generate a spurious signal caused by the emission of photoelectrons which would falsify mainly the difference measurement from which the beam position is derived. Measurements of this effect have been made on a test set-up⁵⁸⁾ at DCI (LAL/Orsay), and have also shown that its magnitude can be reduced to a negligible value by placing, upstream of the outer electrode, a mask which shadows it from the direct synchrotron radiation. Thus it is proposed to equip all horizontal PU stations with two masks, one on either side, to shadow the synchrotron radiation from the e^+ and e^- beam, respectively. The masks consist of rectangular copper frames which protrude a few millimetres into the aperture.

No masks are foreseen for the 108 vertical PU stations, since in this case the two electrodes should receive the same amount of synchrotron radiation if the beam is in the median plane of the SPS, so that the emission of photoelectrons has very little effect on the difference signal.

Electronics and data acquisition

In order to allow for the observation of the single bunches as well as for the detection of the proton beam with 4620 bunches used for fixed-target physics, the electronic circuits of all 216 electrostatic position monitors must be modified.

It is expected that the modified electronics can cope with single-bunch intensities as low as 2×10^9 particles per bunch. Observation of the same bunch by all PU stations around the ring can be achieved using synchronization by the beam itself. The number of the bunch is selected by adjusting the timing.

As shown in Fig. 3.27, the centres of the two electrodes are 62.5 mm apart along the beam direction. The resulting time difference of the induced signals is corrected by a corresponding difference of the electrical length of the two cables which connect the electrodes to the hybrid junction, so that the latter delivers the correct sum and difference signals. This adjustment has been made for protons and is therefore also valid for e^+ . However, for e^- which travel in the opposite direction, the resulting phase error is 30° at a frequency of 200 MHz and introduces large errors for which it is difficult to correct electronically. Therefore it is planned to adjust the closed-orbit corrections during the e^+ cycles and then to assume that the same corrections are valid for the e^- cycles. It will be possible to ascertain the correctness of this assumption with the help of 16 existing position-sensitive directional couplers which have the same accuracy for

particles travelling in either direction. The latter have been installed at critical positions around the SPS ring as part of the proton-antiproton project.

The present beam observation system can acquire the closed-orbit position at three different times during the same proton cycle. This, for instance, permits independent adjustments of injection and extraction during the setting up of the SPS. It is planned for the interleaved SPS supercycle ($e^+e^+e^-e^-p$) to maintain the three orbit acquisitions for the proton cycle and to add for the lepton cycles a total of four new acquisitions which can be chosen at will, i.e. one acquisition for each cycle, or four acquisitions for the first e^+ cycle, etc. Instead of transferring all data directly to the general-purpose computers which are located in the equipment buildings around the SPS ring and which are limited in real-time acquisition capability, it is best to use a front-end microcomputer in each sextant for all acquisitions of the beam position.

Closed-orbit correction

Adjacent to each of the 216 lattice quadrupoles of the SPS is an orbit correction dipole which is d.c. powered. These are used to correct the horizontal and vertical closed orbits to within a few millimetres at the 10 GeV/c injection momentum of protons. As the protons are accelerated, the field in the orbit dipoles remains constant and the closed-orbit deformations gradually increase to the high field values, which are determined mainly by misalignments of the SPS quadrupole magnets and small geometrical defects of the SPS dipole magnets. Because of the relative importance of remanent and stray magnetic fields at the low field levels during the lepton cycles, the above procedure is not suitable in this case, and the correction dipoles must be pulsed, each with its own current programme. The existing orbit correctors are laminated and their power supplies have enough voltage, so that the system can be used for pulsed operation. It is sufficient to use a relatively coarse current programme, and this can be achieved economically by controlling the power supplies with a single microprocessor in each sextant.

Synchrotron light observation

The SPS is already equipped with instrumentation to observe the synchrotron light from protons and antiprotons at high energy³⁹⁾. In order to achieve a good time resolution for e^\pm bunch length measurements, mirrors will be installed which can direct the light onto photodiodes instead of onto the image intensifiers.

3.3.9 Controls

The implications of the e^\pm acceleration for the SPS controls system can be discussed under three different headings, as follows:

i) Master timing generator

In order to generate the various machine cycles for LEP injection, SPS fixed-target physics, and $p\bar{p}$ collider operation, a new programmable Master Timing Generator and new multitrigger timing modules will be developed. This Master Timing Generator must also implement the proper synchronization of the PS, the SPS, and LEP.

ii) Increased traffic in the computer control network

The present duration of the SPS cycle for proton acceleration is about 12 s. The architecture of the SPS computer control network takes advantage of this long repetition time by calling most programs from a central library and by storing locally only the ones most frequently used. With the addition of the much shorter interleaved electron cycles, a number of the local computers will have to execute many more programs on a much shorter time-scale. To avoid congestion of the message transfer system, additional local memory will have to be installed for these computers.

One can also reduce the network traffic by installing more front-end intelligence between the local computer and the equipment to be controlled, such as the present SPS microprocessor-based autonomous crate controllers or equivalent intelligent crates to be developed for LEP.

More detailed studies will be made to define the exact requirements and optimal technical solutions.

iii) Additional computers and interfaces for new equipment

The changes in the proton injection beam line TT10 are relatively modest and can be handled by the existing injection computer in BA1. Similarly, it is expected that e^- injection and e^\pm extraction in LSS6 can be handled by the existing two West-extraction computers. Of course, the appropriate interfaces must be added for the additional magnet power supplies, etc.

The new cavities represent a new RF system and will require an additional computer. The new control electronics (about 40 crates) could possibly be built according to LEP standards, based on local microprocessors.

The new main-ring power supplies for the e-cycles will have their own computer interfaces.

The beam observation will mainly add to the increased traffic density in the network which was discussed under (ii).

The controls of the e^+ and e^- transfer lines from the SPS to LEP will probably be located in LEP Building SR1. Since this is a new installation it seems appropriate, in this case, to use LEP standards throughout, including the two process computers built as microprocessor assemblies. The latter will be connected to the computer control network of both SPS and LEP.

3.4 BEAM TRANSFER FROM THE SPS TO LEP

3.4.1 General layout

The electrons and positrons, extracted from the SPS in LSS6, are transferred along two new tunnels to the LEP injection points situated symmetrically on either side of interaction point P1, in the beginning of the regular arc. A schematic layout of these transfer lines is shown in Fig. 3.21.

From LSS6, the transfer tunnels slope downwards in order to overcome the difference in altitude between the two machines, which is 50 m for the e^- line (TI12) and 37 m for the e^+ line (TI18). The unequal differences in altitude result from the tilt of LEP with respect to the SPS, which is about 1.2% in the region of P1.

It is of interest to move the injection points close to P1 to make the transfer lines as short as possible. The minimum length of TI18 is limited, however, by the maximum slope of the tunnel, which is practical for installation and maintenance of the beam transfer equipment. The injection points are therefore placed at two period lengths from the beginning of the regular LEP lattice, which gives for TI18 a length of 255 m and a slope of 15.5%. The figures for TI12 are 540 m and 10.3%, respectively. Both tunnels join LEP at a distance of 488 m from P1. A more detailed layout of the transfer lines is shown in Fig. 3.28.

e^+ transfer line (TI18)

The positrons are ejected through the existing proton extraction channel towards TT60 (see subsection 3.3.5). A vertical dipole, downstream of quadrupole QTLD 6101, acts as a beam switch and deflects the beam out of TT60 with an upward angle of 2° . After it has reached a height of 1.25 m above the SPS orbit, four tilted dipoles again make the beam horizontal and deflect it by 11.5° towards the inside of the SPS. In this way the passage is crossed at a height of 2.45 m, which preserves the free circulation of the SPS transport vehicles. The tunnel wall is traversed at an angle of 8.5° , through a small diameter hole about 10 m long.

Almost immediately after it has entered TI18, four dipoles bend the beam vertically downwards by 8.9° and horizontally by 8° towards the injection region of LEP. Shortly before the junction with LEP, another set of four tilted dipoles bend the beam such that vertically it remains at 1.05 m above the machine orbit and horizontally it approaches LEP at an angle of 5.4° . After it has crossed the junction region of the transfer tunnel and LEP tunnel, two tilted dipoles installed on top of the LEP machine bend the beam vertically downwards and horizontally nearly parallel to the LEP orbit. A vertically deflecting steel-septum magnet again makes the beam horizontal, such that it runs at machine level at a distance of about 80 mm from the orbit on the inside of LEP.

e^- transfer line (TI12)

The electrons are ejected from the SPS by a vertically deflecting septum magnet, such that they just clear the quadrupole QDA 6171 (see subsection 3.3.5). Between this quadrupole and the electrostatic septum (ZS), where the beam has reached a height of 0.95 m above the SPS orbit, a pair of tilted dipoles bend the electrons onto a trajectory directed vertically slightly downwards and horizontally 3.5° towards the outside of the SPS. In this way, the beam travels behind the ZS, remaining clear of existing equipment and allowing free access to the ZS from the passage side. The beam leaves the SPS tunnel through the wall at the beginning of the LSS6 enlargement and enters the TI12 transfer tunnel through a 10 m long hole of small diameter.

In the TI12 tunnel, the beam is first bent 5.2° downwards by two vertical dipoles, and thereafter it is bent horizontally twice 6.1° by a total of four dipoles. At the bottom of TI12, a second vertical bend made by two dipoles brings the beam parallel to LEP at 1.05 m above the orbit. The junction with LEP is then achieved in the same way as for the positron beam.

3.4.2 Beam optics

In view of achieving the best possible injection into LEP, the optics of the transfer lines is designed to allow for different matching conditions at the injection points, and this for both LEP tunes (60° and 90° phase advance). These options include betatron matching with variable horizontal β values, dispersion matching to make the beam either achromatic or to match its dispersion to that of the LEP lattice, and the provision to exchange the horizontal and vertical emittances. The necessity for these options is discussed under Section 3.5.

Constraints in obtaining dispersion matching and in limiting the peak values of the dispersion function arise from the geometry of the transfer lines which necessitates lumped bends at fixed positions, in particular the bends on top of the SPS and LEP and the main vertical bends, which are spaced as far apart as possible to reduce the tunnel slopes. Further restrictions come from the aim to reduce the number of power supplies for the main bends by choosing, in each line, the same strength for as many dipoles as possible to connect them in series.

The solution adopted for these transfer lines is a regular FODO structure with a period length of 61 m in TI12 and of 30 m in TI18, so that in both lines the main vertical bends are separated by eight periods. Since some freedom existed in both lines for placing the horizontal bends, their location was chosen such as to obtain the best compromise in beam characteristics along each line for the different beam tunes.

The phase-plane exchange is achieved in the same way as for the SPS injection line TT10, i.e. by inserting three series-connected skew quadrupoles into the regular FODO structure. These are placed halfway between adjacent lattice

quadrupoles and are separated from each other by one period length. The four lattice quadrupoles between the skew ones are tuned to give 90° phase advance per period in both planes. The phase-plane exchange sections are located in both lines in the straight part between the main vertical bends.

The series of F and D lattice quadrupoles between the beginning of the transfer tunnels and the phase-plane exchange sections are each powered separately to allow independent adjustment of phase advance in the horizontal and vertical planes. The quadrupoles at the beginning of each line, i.e. two in TI12 and three in TI18, are powered independently and are mainly used to keep the β values within acceptable limits. Downstream of the phase-plane exchange sections, all quadrupoles are powered individually, providing the required number of variables to satisfy the matching conditions at injection.

Examples of beam optics calculations are shown in Figs. 3.29 and 3.30. In case (a) of each figure the beam is achromatic and betatron matched at the injection point; in case (b) it is both dispersion and betatron matched. All cases shown provide phase-plane exchange and are for a LEP tune of 60° phase advance.

3.4.3 Equipment

The layout of the beam lines has been made with the aim of re-using the beam transfer magnets of the ISR. This was achieved for 80% of the required bending magnets and for nearly all the quadrupoles. The apertures of these magnets are adequate and their strength is sufficient to go beyond the nominal energy of 20 GeV if this should be required in the future.

The magnets which are required in addition and which must be built are: the first quadrupole in the e^- line, which must be slim to fit into the space left free by the SPS machine elements; the dipole magnets which are installed on top of the SPS and LEP; a number of small steering dipoles; and the steel-septum magnets. A schematic cross-section of the steel-septum magnets is shown in Fig. 3.31.

It is also assumed that power supplies of the ISR beam transfer lines will be re-used. The number of supplies which can be re-used and the requirements of new supplies are at present under study.

All power supplies will be housed in the new LEP rectifier building SR1. The routing of the cables for the equipment in LSS6 will be via the existing pit PA6 of the SPS, and for the equipment in the transfer tunnels and in the junctions, via pit PM15 of LEP.

The beam observation equipment for beam steering and diagnostics will be mainly of the secondary emission type plus some scintillation screen monitors. Also, in this case it is foreseen to re-use existing equipment, mainly that which has become available from closing-down part of the TT60 lines in connection with the upgrading of the SPS West Experimental Area.

3.4.4 Tunnels and equipment buildings

At the junction with the transfer lines, the LEP tunnel is enlarged. Excavation of the transfer tunnels will start from these junctions towards the SPS. This can proceed independently of the SPS operation schedule, except for the last parts, which must be done while the beam in the SPS is off. Finally, the breakthroughs to LSS6, i.e. the holes for the vacuum chambers and the passages for personnel access, must be made during a long shutdown of the SPS machine. A tunnel diameter of 3.5 m has been adopted for the transfer lines. The installation of magnets on a slope of 15.5% is under study and might require some special transport equipment.

In addition to the power supplies, all the electronics and controls for the equipment in the beam lines, including that in LSS6, will be housed in SR1.

3.5 INJECTION INTO LEP

3.5.1 Injection procedure

The number of particles injected into LEP per SPS e-cycle is two orders of magnitude smaller than the total number of particles stored in each beam. This necessitates an accumulation scheme which is similar to the scheme in use at other e^+e^- storage rings such as PEP and PETRA. The injected beam is deposited in the LEP vacuum chamber as close as possible to the circulating beam and nearly parallel to it. The injected particles then start large-amplitude oscillations about the central orbit. These oscillations, which in the beginning are almost coherent, are damped owing to the emission of synchrotron radiation, so that the injected particles are integrated into the equilibrium distribution of the stored beam. With a typical damping time constant of 0.4 s (LEP wigglers on), the damping process is fast enough to avoid particle loss when the next pulse is injected after 1.26 s.

If the energy of the injected beam is equal to the energy of the beam which is already circulating in LEP, the large-amplitude oscillations which are launched at the beginning of the injection process are pure betatron oscillations. This type of accumulation (betatron accumulation) is used in both PEP and PETRA and is one of the procedures for which provision is made in LEP.

Since injection takes place at an azimuth where $D_x \neq 0$, a second type of accumulation (synchrotron accumulation) can also be envisaged⁷⁾. In this case, the energy of the particles coming from the SPS is about 1.5% lower than the energy to which the LEP ring has been adjusted. The injected beam is deposited on an off-momentum

orbit exactly corresponding to its energy. The particles then start slow large-amplitude synchrotron oscillations about the central orbit and reach the equilibrium distribution of the stored beam after damping of the oscillations with a typical time constant of 0.2 s.

For both betatron and synchrotron accumulation the same injection equipment is used, and the choice between the two schemes can be made later when LEP has come into operation.

In the nominal operating mode, eight bunches are accelerated in the SPS, whereas each of the beams stored in LEP consists of only four bunches. Therefore, large-amplitude oscillations of two injected bunches about the same bunch in LEP must be launched nearly simultaneously. After the injection of the first of these bunches, one or a few LEP turns elapse, depending on the accumulation scheme and on the machine tune, before the bunch has left the area of the LEP acceptance into which it was initially deposited. The second bunch can then be injected into this area. The described stacking process can be extended to more than two injected bunches⁷⁾. The positions which must be occupied by the eight bunches in the SPS before they are transferred to LEP depend on the number of LEP turns elapsing between successive injections⁸⁾.

In order to keep the amplitude of the injection oscillations to a minimum, the injected beam must be deposited very close to the stored LEP beam, as was mentioned before. This leads to the choice of a 2 mm thin septum magnet as the last element of the beam transfer line. At the moment of injection, the stored beam is brought close to the septum by a fast orbit bump. This bump must then be removed within less than one LEP turn in order to make room for the large-amplitude oscillations of the injected particles.

3.5.2 Layout of the LEP injection system

As mentioned in Section 3.4, the injection points for electrons and positrons are situated symmetrically on either side of interaction point 1, just inside the regular arcs. The LEP injection equipment—septum and kicker magnets—must therefore be installed in positions which are normally occupied by main dipoles. This leads to an unavoidable local perturbation of the bending pattern, which will be described in a forthcoming report on the LEP lattice. In order to keep the perturbation as small and localized as possible, a rather compact layout of the injection system has been chosen (Fig. 3.32).

A steel-septum magnet (Lambertson magnet) deposits the incoming beam in the horizontal plane of LEP not far from the radially focusing quadrupole QF 20, which is located at two period lengths from the beginning of the regular arc. The beam then passes through a ferrite kicker, which also acts on the circulating beam, before it enters the injection septum magnet. This magnet has a copper septum with an effective thickness of about 2 mm. It gives a deflection of some 3 mrad to the particles, so that they start the injection oscillations on trajectories which are nearly parallel to the circulating beam. The latter is brought close to the other side of the septum by a fast local orbit deformation produced by a system of three full-aperture ferrite kickers. The rise- and fall-times of the kickers have been chosen sufficiently short to deflect only the stored bunch to which the injected particles are to be added, as will be discussed in more detail in subsection 3.5.4.

In addition to considerations concerning the layout of the main dipoles, several other aspects have dictated the design of the injection system:

- Synchrotron accumulation is an interesting option. Injection should therefore take place in the horizontal plane, preferably near a radially focusing quadrupole, where the dispersion is large.
- Synchrotron radiation, which is enhanced in the injection region owing to the perturbation of the main bending pattern, must not hit the septa directly. Accordingly, the septa must be placed on the inside of the LEP aperture. Approach of the injected beam from above through a steel-septum magnet is then the only way to avoid blocking the passage in the tunnel.
- The system consisting of three ferrite kickers provides a well-compensated fast orbit deformation for both possible LEP phase advances. In order to keep their strength as small as possible, the kickers should be installed at positions where the horizontal amplitude function β_x is large. Furthermore, kickers 1 and 3 should have a phase advance, with respect to the injection septum, which is not too far from 90°. The layout of Fig. 3.32 fulfils these requirements. For the 90° phase advance, kickers 1 and 3 are at optimum positions and kicker 2 is very weak; for 60° phase advance, all kickers have nearly equal strengths which remain quite moderate (see subsection 3.5.4).

3.5.3 Aperture considerations

In order to avoid undue restrictions of its lifetime, the colliding beam requires a free aperture which is about 10 times the r.m.s. beam width. However, during a time which is short compared to the damping time, the available space can be reduced considerably. This is the case when the circulating beam is bumped towards the copper septum at the moment of injection. In the nominal injection scheme, each stored bunch is displaced twice per SPS e-cycle, and this process is repeated about 100 times. In order that the particle losses on the thin septum stay below 1%, it is then necessary to keep a distance between beam centre and septum of at least 4 standard deviations σ_{xc} of the equilibrium distribution in LEP.

The injected beam can be brought closer to the copper septum since it passes through the septum magnet just once. A minimum distance of $2.5\sigma_{xi}$ is considered to be sufficient.

The beam disposition at the exit of the copper-septum magnet is schematically shown in Fig. 3.33 for injection into a 60° lattice. The (1σ) emittance $\varepsilon_x = 0.13 \pi \cdot \text{mm} \cdot \text{mrad}$ and the energy spread $\sigma_e/E = 1.3 \times 10^{-3}$ assumed for the circulating beam correspond to a wiggler adjustment which gives a horizontal damping time of 0.4 s. The dimensions of the injected beam are based on the following assumptions: the emittance ratio $\varepsilon_y/\varepsilon_{x0}$ is equal to 1/5 in the SPS; the horizontal and vertical emittances (about $0.15 \pi \cdot \text{mm} \cdot \text{mrad}$ and $0.03 \pi \cdot \text{mm} \cdot \text{mrad}$, respectively) are exchanged in the beam transfer line; the beam is both dispersion and betatron matched at the injection point. As indicated in Fig. 3.33, safety margins of 1 mm for the circulating beam and of 5 mm for the injected beam are assumed at the copper septum in order to allow for misadjustments which are unavoidable in operation.

Figure 3.34 shows beam trajectories and envelopes which correspond to injection via betatron accumulation under the above assumptions. Since the septa are positioned at the limit of the horizontal LEP aperture, scaled from the maximum of 59 mm in the QF-quadrupoles, the injected beam has completely entered the standard LEP aperture only about 18 m downstream of QF 20. In QF 20 itself, the beam passes far outside the region where the gradient is constant. The accumulation through radiation damping in LEP is, however, a forgiving process, and small errors at injection do not affect the final equilibrium particle distribution. Therefore, the only criterion for the quality of the magnetic fields, which are traversed by the injected beam, is their effect on the amplitude of the injection oscillations. As long as the resulting increase of the maximum amplitude stays within a few millimetres, magnetic field non-linearities seem acceptable. From this point of view the field distribution⁶⁰ in QF 20, which is shown in Fig. 3.35a, is considered to be good enough near the horizontal mid-plane up to a distance of ~ 87 mm from the centre. The edge of the injected beam, defined as the $2.5\sigma_x$ limit, stays some 6 mm within this boundary. Likewise, sufficient mechanical aperture can be made available in the quadrupole if a specially shaped enlarged vacuum chamber is built (Fig. 3.35b).

Figures 3.33 and 3.34 are based on a natural width and energy spread of the stored beam, which correspond to strong wiggler fields ($\tau_x = 0.4$ s) and can be considered as maximum values. The half-aperture needed in LEP for the injection process is then the distance which is measured at the exit of the copper septum between the outer edge of the injected beam and the centre of the circulating beam. This distance amounts to 42 mm, which is well below the horizontal LEP half-aperture of 57 mm at the septum. Sufficient margin is therefore left for some mis-steering, closed-orbit deformations and longitudinal turbulence of the stored beam.

3.5.4 Injection equipment

In addition to the steel-septum magnet which is described in subsection 3.4.3, a copper-septum magnet and three ferrite kickers are needed for each of the two LEP injection channels.

As regards the kickers, it is proposed to use single-turn C-cored ferrite magnets in air, in combination with ceramic vacuum chambers. Compared to a vacuum tank, a ceramic chamber does not need special pumping equipment, and does not produce higher-order mode losses which would adversely affect beam stability. A C-shaped yoke avoids a closed magnetic flux path through the ferrite, induced by the beam, and facilitates the access to the chamber. The chamber is metallized on the inside in order to provide a conducting path for the wake fields of the bunches. The metallization is, however, sufficiently thin so that the magnetic field pulse of the kicker is not attenuated or significantly distorted. The chamber is slightly wider than the standard LEP vacuum chamber to avoid it being hit by direct synchrotron radiation.

For each bunch to be injected, each pulse generator produces one half-sine-wave pulse with voltage and current amplitudes comparable to those of the SPS extraction kickers (see subsection 3.3.5). Electrons travel through the central positron kicker about $3.7 \mu\text{s}$ before and $18.5 \mu\text{s}$ after the passage of the positrons to be injected. For the upstream and downstream kickers, these values change by $0.5 \mu\text{s}$. The inverse pattern holds for the central electron kicker. The pulse duration has then been chosen as $3.7 \mu\text{s}$. This value avoids kicking the other beam and provides convenient parameters for the power supply.

All six kicker magnets have the same design. Their magnetic length is 1.0 m, with an inner aperture of the elliptical vacuum chamber of 200 mm horizontally and 46 mm vertically. For a phase advance of 60° , all kickers have about the same maximum deflection angle of 0.55 mrad. Their current amplitude at the nominal injection energy of 20 GeV is 2.1 kA and the charging voltage is about 16.2 kV. For a phase advance of 90° , the charging voltage of the central kickers is lower than the minimum voltage required to turn on the thyatrons. The voltage must then be artificially increased by means of a series resistance. The main parameters of the systems are listed in Table 3.12.

As described for SPS extraction, the pulse generators are located in the tunnel, whereas the high-repetition-rate resonant-charging systems together with all command and interlock electronics are housed in the service building. It is foreseen to install the pulse generator on top of the kicker magnets because of the low beam height in the tunnel.

The moderate deflection angle of 3.5 mrad, required for the thin septum magnets, can be provided by a ferrite magnet powered from the same type of fast pulse generator as is used for the kicker magnets. Compared to a slowly pulsed magnet, the proposed solution avoids a water-cooled septum and allows for a decrease in thickness from about 4 mm to not more than 2 mm. Furthermore, important savings in the costs for the power supply, the transmission line, and the magnet construction can be made. The septum magnet has a magnetic length of 2.0 m and operates at a field strength of about 0.12 T for an injection energy of 20 GeV. The amplitude of the excitation current is 2.3 kA and the charging voltage is about 17.7 kV. The main parameters are listed in Table 3.12.

Table 3.12

Main parameters of LEP injection kickers and septum magnets at 20 GeV

	Kickers (IKP/IKE)	Septa (IKSP/IKSE)
Max. deflection angle (mrad)	0.55	3.5
Number of magnets	2×3	2×1
Aperture (h \times v) (mm)	200×46	30×25
Magnet length (m)	1.0	2.0
Pulse duration (μ s)	3.7	3.7
Minimum repetition time (μ s)	89	89
Current amplitude (kA)	2.3	2.3
Charging voltage (kV)	17.7	17.7

Beam observation equipment is foreseen at the exit of the septum magnets in order to measure the positions and profiles of the injected beam. As for the transfer lines, the beam monitors will be mainly of the secondary-emission type plus one or two luminescent screen monitors.

Absorbers for synchrotron radiation are needed upstream and downstream of the kicker and septum magnets. Their layout has been based on a maximum linear power flux of $100 \text{ W} \cdot \text{cm}^{-1}$, which results in an adequate safety margin in the thermal design of the absorber. For a beam energy of 100 GeV, the absorbers then require a length between 300 mm and 650 mm, depending on their azimuthal position.

REFERENCES

- 1) The LEP Study Group, CERN/ISR-LEP/79-33 (1979).
- 2) Y. Baconnier, O. Gröbner and K. Hübner, LEP Note 212 (1980).
The LEP Study Group, CERN/ISR-LEP/79-33/Add. (1980).
- 3) LEP Injector Study Group, The chain of LEP injectors, paper submitted to the Particle Accelerator Conf., Santa Fe, 1983.
- 4) H.G. Hereward, Proc. Int. Conf. on High-Energy Accelerators, Brookhaven, 1961 (Brookhaven Nat. Lab., Upton, NY, 1961), p. 222.
- 5) K.W. Robinson, Phys. Rev. **111** (1958) 373.
- 6) J.-P. Delahaye and A. Krusche, LEP Note 408 (1982).
- 7) S. Myers, LEP Note 334 (1981).
S. Peggs, LEP Note 358 (1981).
- 8) K. Hübner, LEP Note 411 (1982).
- 9) Y. Baconnier and J. Madsen, LEP Note 325 (1981).
- 10) J. Gareyte, LEP Note 356 (1982).
- 11) B. Zotter, LEP Note 363 (1982).
B. Zotter, CERN/ISR-TH/82-10 (1982).
B. Zotter, LEP Note 418 (1982).
- 12) R.D. Kohaupt, DESY 80/22 (1980).
- 13) K. Hübner and J.H.B. Madsen, LEP Note 378 (1982).
- 14) R. Cappi, LEP Note 416 (1982).
- 15) R. Belbéoch, G. Bienvenu, J.-C. Bourdon, P. Brunet, R. Chaput, R. Chéhab, S. Costa, Y. Dabin, G. Dannon, G. Dardenne, F. Dupont, J.-M. Hasselsweiller, J. Le Duff, G. Le Meur, L. Mélard, G. Michaud, M. Mossetti, B. Mouton, G. Nalin, C. Nguyen Ngoc, J.-P. Perrine, M. Renard, M. Roch, J. Rodier, P. Roudier and J.-L. Villain, LAL/PI 82-01/T (1982).
- 16) B. Mouton, LAL/PI/81-22/T and LAL/PI/81-27/T (1981).
- 17) D.J. Warner, PS/DL/LIL/Note 81-4 (1981).
- 18) A. Bensussan and J.M. Salome, Nucl. Instrum. Methods **155** (1978) 11.
- 19) K. Hübner, LEP Note 265 (1980).
- 20) Z.D. Farkas, H.A. Hogg, G.A. Loew and P.B. Wilson, IEEE Trans. Nucl. Sci. **NS-22** (1975) 1299.
- 21) A. Fiebig and R. Hohbach, PS/LPI/RF/Note 82-16 (1982).
A. Fiebig and R. Hohbach, Study of peak power doublers with spherical resonators, paper submitted to the Particle Accelerator Conf., Santa Fe, 1983.
- 22) R. Chéhab, LAL-PI/81-10/T (1981).
- 23) G. Stange, IEEE Trans. Nucl. Sci. **NS-26** (1979) 4146.
- 24) J.P. Delahaye and A. Krusche, Lattice design of the LEP electron-positron accumulator, paper submitted to the Particle Accelerator Conf., Santa Fe, 1983.
- 25) E.J.N. Wilson, CERN/SPS-DI(LTD)/80-9/Rev. (1980).
- 26) H. Kugler, PS/LPI/Note 82-3 (1982).
- 27) H. Herminghaus and K.H. Kaiser, Nucl. Instrum. Methods **113** (1973) 189.
- 28) B. Kuiper, forthcoming CERN PS/CO report.
- 29) A.H. Sullivan, private communication.
G. Dardenne, LAL-PI/82-57/T (1982).
- 30) A.H. Sullivan, LEP Note 354 (1982).
A.H. Sullivan, CERN/HS-RP/TM/82-37 (1982).
- 31) J.H.B. Madsen (ed.), CERN/PS/DL/LEP Note 80-4 (1980).
- 32) M. Bouthéon, CERN/PS/DL/LEP Note 80-3 (1980) and CERN/PS/OP/LEP Note 80-26 (1980).

- 33) M. Bouthéon and J.-P. Potier, CERN/PS/OP/Note 82-24 (1982).
- 34) Y. Baconnier, LEP Note 185 (1979).
- 35) W. Hardt, CERN/PS/DL/LEP Note 80-5 (1980).
Y. Baconnier, R. Cappi, R. Garoby, W. Hardt, K. Hübner and J.H.B. Madsen, Electron beam dynamics in the CERN PS, paper submitted to the Particle Accelerator Conf., Sante Fe, 1983.
- 36) R. Garoby, CERN/PS/RF/Note 82-8 (1982).
- 37) J. Boillot and J.-P. Riunaud, LEP Note 336 (1981).
- 38) D. Fiander, CERN/MPS/SR/Note 71-30 (1971).
- 39) M. Höfert, CERN/HS-RP/TM/82-21 (1982).
- 40) O. Gröbner, Technical Note ISR-VA/OG/tn-4 (1982).
- 41) A. Poncet, PS/ML/Note 82-10 (1982).
- 42) O. Gröbner, A.G. Mathewson, H. Störi, P. Strubin and R. Souchet, CERN-ISR-VA/81-31 (1981).
- 43) Y. Baconnier and G. Brianti, CERN/SPS/DI/80-2 (1980).
- 44) D. Boussard, E. Brouzet, R. Cappi and R. Garoby, CERN/PS/OP/LR/Note 80-16 (1980).
- 45) L. Burnod, private communication.
- 46) P. Heymans and M. Overington, CERN/PS/CO/Note 82-9 (1982).
- 47) B. Chen, S. Chen, E.J.N. Wilson and B. Zotter, IEEE Trans. Nucl. Sci. **NS-28** (1981) 2537.
E.J.N. Wilson and B. Zotter, LEP Note 338 (1981).
- 48) G. Brianti, CERN/SPS/DI/80-03/Rev. (1980), or LEP Note 246 Rev. (1980).
- 49) G.R. Stevenson, CERN/HS-RP/IR/80-59 or LEP Note 266 (1980).
- 50) O. Gröbner, CERN/ISR-VA/OG/sm (1980).
- 51) G.R. Stevenson, CERN/HS-RP/IR/82-55 (1982).
- 52) A. Fasso, K. Goebel, M. Höfert, C. Nuttall and A. Perrot, CERN/HS-RP/IR/82-23 (1982), or LEP Note 379 (1982).
- 53) A. Perrot, LEP Note 225 (1979).
- 54) M.B. Emmett, ORNL-4972 (1975).
- 55) R.L. Ford and W.R. Nelson, SLAC-210 (1978).
- 56) O. Gröbner, private communication.
- 57) E. Frick, H. Kuhn, M. Mayer, V. Rödel, G.H. Schröder and E. Vossenberg, CERN/SPS/82-14 (ABT) (1982).
- 58) R. Bossart, J. Bosser, B. Bouchet, L. Burnod and V. Rossi, CERN/SPS/ABM/LB/Note 82-08 (1982).
- 59) R. Bossart, J. Bosser, L. Burnod, E. d'Amico, G. Ferioli, J. Mann and F. Méot, CERN/SPS/80-8 (ABM) (1980).
- 60) C. Wyss, private communication (1982).

APPENDIX: LIST OF NOMINAL PARAMETERS

(Status beginning 1983)

A.1 GENERAL

LEP injection energy	20	GeV
Mode of SPS operation	interleaved with 450 GeV protons	
Cycles in SPS supercycle	$pe^+e^+e^-e^-$	
Nominal length of SPS supercycle	15.12	s
Nominal length of one e-cycle	1.26	s
Minimum length of one e-cycle	1.20	s
LEP accumulation rate per beam ^{a)}	0.25	mA · min ⁻¹
Number of bunches in LEP	4	

a) Almost simultaneous for both LEP beams

A.2 BEAM TRANSFER SPS TO LEP

A.2.1 LEP injection

Distance of LEP injection points (exit septum) from LEP crossing point 1	≈ 558		m
Distance from septum exit to face of next downstream QF quadrupole	≈ 2		m
LEP lattice functions in QF			
phase advance	60	90	degrees
β_x	135	132	m
β_y	46.3	23.6	m
D_x	2.22	1.20	m
Injection mode	2 SPS bunches are stacked in betatron or synchrotron phase space close to each one of the 4 LEP bunches		
Number of LEP turns elapsing between 2 injections into same bucket ^{a)}	(1,3,4,6) + 7n n = 0, 1, 2, 3, ...		
Injection type	Fast bump of circulating bunch towards septum		
Length of fast bump	2 cells in LEP arc		
Kicker magnets	IKP (e ⁺)/IKE (e ⁻)		
Number of kicker magnets	3/3		
Distance between IKPs or IKEs	≈ 1 cell of LEP arc		
Requirements			
Deflection angle	0.56		mrad
Rise-time/fall time ^{b)}	3.2/18.0		μs
Flat-top (6 r.m.s. bunch lengths)	1		ns
Repetition time	89		μs
Pulsed septum magnets	IKSP (e ⁺)/IKSP(e ⁻)		
Number of magnets	1/1		
Effective septum thickness	2		mm
Requirements			
Deflection angle	3.49		mrad
Rise-time/fall-time ^{b)}	3.7/18.5		μs
Flat-top (6 r.m.s. bunch lengths)	1		ns
Repetition time	89		μs

a) n adjusted by choice of bunch positions in SPS

b) Bunch centre to bunch centre

A.2.2 Beam transfer in SPS-LEP

Beam optics—adjustable betatron matching to LEP

—achromatic or dispersion matched to LEP

—exchange of horizontal and vertical emittance of SPS

Beam line characteristics	TI 18 (e ⁺)	TI 12 (e ⁻)	
Total length	386	655	m
Total horizontal deflection	31.0	22.3	degrees
Difference in height (SPS-LEP)	37	50	m
Maximum downward slope	15.5	10.0	%
Total vertical deflection	27	18	degrees
Total number of dipoles	16	14	
Focusing structure	FODO	FODO	
Period length of regular part	30	61	m
Total number of quadrupoles	25	24	

A.3 SPS

A.3.1 Over-all machine parameters

Nominal energy	20	GeV
Injection energy	3.5	GeV
Circumference	6911.562	m
Horizontal tune	26.6	
Vertical tune	26.6	
Momentum compaction factor	0.00186	
Horizontal damping partition J _x	1	
Dispersion of damping d(J _x)/(dE/E)	-185	
Horizontal damping time (20 GeV)	48	ms
Separated function lattice		
Superperiodicity	6	
Layout of one half superperiod	1 cell straight ½ cell bending ½ cell half-bending 7 cells bending	(4 dipoles) (2 dipoles) (7 × 8 dipoles)

A.3.2 Performance at 20 GeV

Total number of e ⁺	6.5 × 10 ¹⁰	
Total number of e ⁻	6.5 × 10 ¹⁰	
Number of bunches	8	
Horizontal emittance/π = σ _{x0} ² /β _x ^{a)}	0.094	μm
Vertical emittance/π = σ _y ² /β _y ^{b)}	0.019	μm
Max. emittance ratio (max. parasitic coupling)	0.25	
Energy spread (σ _e /E)	0.063	%
Bunch length (σ _s)	4	cm

a) Zero coupling

b) Maximum parasitic coupling

A.3.3 Beam and lattice parameters

	Arc	Straight section	
Location	64.00	64.00	m
Length of cell	89	89	degrees
Average phase advance per cell	108	108	m
Structure parameters β _{x max}	20	20	m
β _{x min}	108	108	m
β _{y max}	20	20	m
β _{y min}	4.45	-0.45	m
D _{x max}			m
D _{x min}			m
Max. r.m.s. beam size at 20 GeV			
Horizontal (no coupling)	4.2 ^{a)}	3.1 ^{a)}	mm
Vertical (max. parasitic coupling)	1.4	1.4	mm

a) Includes contribution of energy spread

A.3.4 Magnet parameters

	Dipoles		Quads QF, QD	
Bending radius	741.3	m		
Field/Gradient at 20 GeV	0.090	T	1.04	$\text{T} \cdot \text{m}^{-1}$
Field/Gradient at 3.5 GeV	0.016	T	0.18	$\text{T} \cdot \text{m}^{-1}$
Peak acceleration rate	82	$\text{GeV} \cdot \text{s}^{-1}$		

A.3.5 Synchrotron radiation

Element	Dipole	Quad	
Peak critical energy	24	0.75	keV
Emitted peak power/length	1.9	0.002	$\text{W} \cdot \text{m}^{-1}$
Emitted energy per e-cycle/length	0.091		$\text{J} \cdot \text{m}^{-1}$

A.3.6 Vacuum parameters

Linear pumping speed in dipoles	3.5	$\text{l} \cdot (\text{m} \cdot \text{s})^{-1}$
Base pressure	0.4 (3)	μPa (nTorr)
Beam-dose ^{a)}	30	$\text{mA} \cdot \text{h}$
Upper limit for peak pressure	0.03 (0.2)	mPa (μTorr)
Bremsstrahlung lifetime	10	min

a) After running for 2000 h in interleaved mode

A.3.7 RF parameters (20 GeV)

Frequency	200.3948	MHz
Harmonic number	4620	
Number of cavities	32	
Length of one cavity	0.75	m
Shunt impedance/metre ^{a)}	10	$\text{M}\Omega \cdot \text{m}^{-1}$
Unloaded quality factor	5.0×10^4	
Diameter of beam hole	144	mm
Number of tetrodes	32	
Max. RF power per cavity	60	kW
Peak voltage	30	MV
Synchrotron radiation loss/turn	19.1	MeV
Parasitic ring impedance $ Z/n $	20	Ω
Total beam current	0.45	mA
Parasitic loss per turn	0.6	MeV
Quantum lifetime	> 1	min
Synchrotron tune	0.040	
Synchrotron phase angle	141	degrees

a) Equivalent circuit convention

A.3.8 Kicker magnet requirements

	Injection		Ejection		
	e ⁺	e ⁻	e ⁺	e ⁻	
Kicker magnet	MKP	MKLP	MKLP	MKLE	
Deflection angle	4.5	1.7	1.7	0.79	mrad
Rise- and fall-time ^{a)}	1.64	1.64	1.64	1.64	μs
Flat-top ($6\sigma_s$)	3	3	1	1	ns
Shots without reload	4				
Reloads per e-cycle	1	7	7	7	
Reloading time	30	0.085	0.085	0.085	ms

a) Bunch centre to bunch centre minus flat-top

A.4 PS

A.4.1 Over-all machine parameters

Nominal energy	3.5	GeV
Injection energy	0.6	GeV
Circumference	628.324	m
Horizontal tune	6.23	
Vertical tune	6.32	
Momentum compaction factor	0.0267	
Dispersion of damping $d(J_x)/(dE/E)$	-274	
Horizontal damping time (3.5 GeV, $J_x = 1$)	76	ms
Combined function lattice		
Superperiodicity	10	
Layout of one half superperiod (L/2) DF O FD O DF O FD O DF (L/2)		

A.4.2 Performance at 3.5 GeV

Total number of e^+	8.0×10^{10}	
Total number of e^-	8.0×10^{10}	
Number of bunches	8	
Mode of bunch preparation	Expansion	Compression
Horizontal emittance/ $\pi = \sigma_{x0}^2/\beta_x$	0.05^a	0.16^c μm
Vertical emittance/ $\pi = \sigma_y^2/\beta_y$	0.01^b	0.16^c μm
Energy spread (σ_e/E)	0.10	%
Bunch length (σ_s)	16	cm

a) Zero coupling

b) Max. parasitic coupling ($\epsilon_y/\epsilon_x = 1/4$)

c) Full coupling

A.4.3 Beam and lattice parameters

Structure parameters

$\beta_{x \max}$	23 m
$\beta_{x \min}$	12 m
$\beta_{y \max}$	23 m
$\beta_{y \min}$	12 m
$D_{x \max}$	3.2 m
$D_{x \min}$	2.2 m

Partition numbers

	Bunch expansion	Bunch compression
J_e	0.2	3.1
J_x	2.8	-0.1
J_y	1	1

Max r.m.s. beam size at 3.5 GeV ^{a)}

Horizontal ^{b)}	3.4	3.7 mm
Vertical	0.5	1.9 mm

a) For nominal emittances

b) Includes contribution of energy spread

A.4.4 Magnet parameters

Main magnet

Bending radius	70.08	m
Field at 3.5 GeV	0.17	T
Field at 0.6 GeV	0.029	T

Robinson wiggler

Number of wigglers	2	
J_x change per wiggler	+1.9	
Location	short Mid-F	
Structure	B A A B	
Block	A	B
Block length	0.146	0.314 m
Peak dipole field	+0.66	-0.66 T
Peak gradient	-8.2	+8.2 $\text{T} \cdot \text{m}^{-1}$

A.4.5 Synchrotron radiation

Element	Magnet	Wiggler	
Peak critical energy	1.4	5.7	keV
Peak emitted power/length	2.6	46	$\text{W} \cdot \text{m}^{-1}$
Emitted energy per e-cycle/length	0.14	2.2	$\text{J} \cdot \text{m}^{-1}$

A.4.6 Vacuum parameters

Linear pumping speed in bending magnets	15		$\text{l} \cdot (\text{m} \cdot \text{s})^{-1}$
Base pressure	1.3	(10)	μPa (nTorr)
Beam dose ^{a)}	500		$\text{mA} \cdot \text{h}$
Peak pressure	< 8	(60)	μPa (nTorr)
Bremsstrahlung lifetime	> 27		min

a) After running for 2000 h in interleaved mode

A.4.7 RF parameters (3.5 GeV + wiggler)

Frequency	7.63409	114.5113	MHz
Harmonic number	16	240	
Number of cavities	11	1	
Sunt impedance/cavity ^{a)}	0.02	3.7	$\text{M}\Omega$
Unloaded quality factor	$\cong 70$	4.0×10^4	
Mechanical length of cavity	2.40	1	m
Number of tetrodes	11	2	
RF power per cavity	10	160	kW
Peak RF voltage	0.22	1.0	MV
Synchrotron rad. loss/turn		0.20	MeV
Parasitic ring impedance $ Z/n $		20	Ω
Total beam current		6.1	mA
Parasitic loss/turn		0.002	MeV
Quantum lifetime (expansion)		16	min
(start/end of compression)	25	19	min
Synchrotron tune (expansion)		0.017	
(start/end of compression)	0.0015	0.017	
Stable phase angle (expansion)		170	degrees
(compression)	128	0	degrees

a) Equivalent circuit convention

A.4.8 Kicker magnet requirements

	Injection	Extraction	
Kicker magnet for e^+	KFA 94	KFA 71	
Kicker magnet for e^-	KFA 72	KFA 71	
Deflection angle	9.0	2.2	mrad
Rise-time/fall-time ^{a)}	slow/250	255	ns
Flat-top ($6\sigma_s$)	10	3	ns
Shots without reload	1	4	
Reloads per e-cycle		1	
Reloading time		30	ms

a) Bunch centre to bunch centre minus flat-top

A.5 ACCUMULATION RING (EPA)

A.5.1 Over-all machine parameters

Nominal energy	600	MeV
Circumference	125.665	m
Horizontal/vertical tune	4.45/4.38	
Momentum compaction factor	0.0328	
Horizontal damping partition J_x	2	
Dispersion of damping $d(J_x)/(dE/E)$	-17.51	
Horizontal damping time	32	ms
Superperiodicity	2	
Layout of half superperiod	half of arc + half of straight section	
Half of arc	QF1 B B QF2 QF2 B B QF1	
Half of straight section	QF3 QD QD QF3 QF3 QD	

A.5.2 Performance

Total number of e^+	2.0×10^{11}	
Length of accumulation cycle	11.22	s
Total number of e^-	1.0×10^{11}	
Length of accumulation cycle	1.14	s
Number of bunches	8	
Horizontal emittance/ $\pi = \sigma_{x0}^2/\beta_x$ ^{a)}	0.14	μm
Vertical emittance/ $\pi = \sigma_y^2/\beta_y$ ^{b)}	0.03	μm
Max. emittance ratio (max. parasitic coupling)	0.25	
RF frequency in PS	Positrons 7.63	Electrons 114.5 MHz
Energy spread σ_e/E	0.060	0.060 %
Bunch length σ_s	50	25 cm

a) Zero coupling

b) Maximum parasitic coupling

A.5.3 Beam and lattice parameters

Structure parameters

$\beta_{x \max}$	14.9 m
$\beta_{y \max}$	14.3 m
$D_{x \max}$	2.29 m
$D_{x \min}$	0.0 m
max. of β_x and D_x do not coincide	

Max. r.m.s. equilibrium beam size	Horizontal (no coupling) ^{a)}	1.6 mm
	Vertical ($\epsilon_y/\epsilon_x = 1/4$)	0.6 mm

a) Includes contribution of energy spread

A.5.4 Magnet parameters

Type of magnet	Quad		Bending magnet			
Total number	40		16			
	QF1	QF2	QF3	QD	Bends	
Dipole field					1.40	T
Bending radius					1.43	m
Field gradient	2.8	3.5	1.4	-1.4	-1.0	$\text{T} \cdot \text{m}^{-1}$
Magnetic length	0.38	0.38	0.39	0.39	0.56	m

A.5.5 Synchrotron radiation

Critical energy	0.34		keV	
Emitted peak power in bending magnet	69		$\text{W} \cdot \text{m}^{-1}$	
Emitted energy in e^+ cycle in bending magnet	0.39		$\text{kJ} \cdot \text{m}^{-1}$	

A.5.6 Vacuum parameters

Linear pumping speed in bending magnets	50		$\text{l} \cdot (\text{m} \cdot \text{s})^{-1}$	
Base pressure	1.3	(10)	μPa	(nTorr)
Beam dose ^{a)}	75		$\text{A} \cdot \text{h}$	
Peak pressure	1.3	(10)	μPa	(nTorr)
Single Coulomb scattering	22		min	
Bremsstrahlung	4		h	

a) After running for 2000 h in interleaved mode

A.5.7 RF parameters

Frequency	19.0852		MHz	
Harmonic number	8			
Number of cavities	1			
Length of cavity	1		m	
Shunt impedance ^{a)}	0.34		$\text{M}\Omega$	
Unloaded quality factor	9.0×10^3			
Number of tetrodes	1			
Minimum RF power	4.3		kW	
Peak RF voltage	50		kV	
Synchrotron radiation loss/turn	8.0		keV	
Parasitic ring impedance $ Z/n $	< 10		Ω	
Total beam current	76		mA	
Parasitic loss per turn	< 0.07		keV	
Total bucket height (injection)	2.4		%	
Quantum lifetime	> 20		h	
Synchrotron tune (injection)	1.55×10^{-3}			
Stable phase angle (injection)	170		degrees	

a) Equivalent circuit convention

A.5.8 Kicker magnet requirements

	Injection	Extraction	
Number of kicker magnets	4	2	
Deflection angle	2.2	1.7	mrاد
Rise-time/fall-time ^{a)}	40	42	ns
Flat-top	12 ^{b)}	5 ^{c)}	ns
Repetition time	0.010	1.26	s

a) Bunch centre to bunch centre minus flat-top

b) Full width at half height of beam pulse

c) $6\sigma_s$

A.6 LINACS

A.6.1 General

Linac V	Energy	Particles
Linac W	200 MeV	e^-
	600 MeV	e^+ or e^-

Frequency (at 30 °C under vacuum)	2.99855	GHz
Total number of TW accelerating sections	16	
Total number of klystrons with LIPS	3	
Total number of klystrons without LIPS	3	
Total length (inside building)	101.0	m
Commutation time (e^- to e^+ operation)	0.1	s

A.6.2 Performance at 600 MeV

Pulse repetition rate	100	Hz	
Beam pulse length ^{a)}	12	ns	
Beam pulse rise-time	3	ns	
	e^+	e^-	
Pulse current ^{b)}	12	60	mA
Max. hor. and vert. emittance/ π ^{c)}	4	$\ll 1$	mm · mrad
Max. relative energy spread	2	< 1	%

a) Full width at half height

b) Within nominal energy spread

c) Containing $> 80\%$ of resolved output current

A.6.3 Linac V

Electron gun		
Beam energy	90	keV
Pulse current	6	A
Prebuncher type	SW, single-gap	
Peak energy modulation	± 40	keV
Buncher type	SW, tri-periodic	
Mode	$2\pi/3$	
Length	2.24	m
Power input	11	MW
Non-load energy gain	33	MeV
Pulse current	2.8	A
Number of TW accelerating sections	4	
Number of klystrons without LIPS	1 ^{a)}	
with LIPS	1	
Focusing after buncher 1 short solenoid		
4 quadrupole triplets		
between sections		
Performance at 200 MeV		
Pulse repetition rate	100	Hz
Beam pulse length	12	ns
Beam pulse rise-time	3	ns
Pulse current	2.5	A
Average current	3	μA
Hor. and vert. emittance/ π	< 1.3	mm · mrad
Bunch length	< 23	degrees RF
Energy spread (beam loading)	< 10	%

a) Powers buncher V and buncher W

A.6.4 Linac W

Converter (e^+ source)

Target material	Tungsten	
Target thickness ($2 X_0$)	7	mm
e^- beam diameter on target	< 2	mm
Average incident power	600	W
e^+ focusing	pulsed 1/4 wave transformer	
Pulsed solenoidal field	1.5	T
Conversion efficiency	0.04	GeV ⁻¹
Radial acceptance of linac W ^{a)}	< 1.6	mm
Angular acceptance of linac W ^{a)}	< 0.27	rad
Mean energy of positrons	8	MeV
Energy acceptance	3	MeV

Electron source

Off-axis gun		
Beam energy	60	keV
Pulse current	150	mA
Inflection by 255 °C alpha-magnet		
On-axis electron buncher		
Type	SW	
Length	0.35	m
Power input	< 3	MW
Non-load energy gain	4	MeV
Pulse current	71	mA

Distribution of klystrons and TW sections

1 klystron without LIPS feeding	2 sections
1 klystron with LIPS feeding	4 sections
1 klystron with LIPS feeding	4 sections
1 klystron without LIPS feeding	2 sections

Focusing 2 solenoids (0.3 T)	on first two sections
1 triplet + 3 singlets	in matching part
30 quadrupoles	FODO channel

a) At target exit

A.6.5 Accelerating sections

Type	TW, quasi-constant gradient	
Mode	$2\pi/3$	
Length including coupling cavities	4.605	m
Number of accelerating cavities including		
2 coupling cavities	138	
Range of iris diameter	25 to 18	mm
Filling time	1.22	μ s
Attenuation	0.75	Np
Shunt impedance per unit length ^{a)}		
beginning/end of section	64/74	M $\Omega \cdot m^{-1}$
Nominal energy gain per section		
Section 1 and 2	32	MeV
Others	54	MeV

a) Linac convention

A.6.6 Klystrons and modulators

Maximum RF power	35	MW
Maximum RF pulse length (−3 dB)	4.5	μs
Maximum cathode voltage	280	kV
Cathode current	295	A
Modulator peak power	90	MW
Modulator average power	50	kW

A.6.7 Quadrupoles

Type	Matching and FODO	
Total number	33	
Max. gradient	3.2	T · m ^{−1}
Inscribed radius	78.5	mm
Magnetic length	0.30	m

A.7 BEAM TRANSFER

Machine	Circumference/C(EPA)	RF/RF(LEP)
EPA	1	$(33/58) \times (4/7) \times (1/6)$
PS	1×5	$(33/58) \times (4/7)^a$
SPS	$1 \times 5 \times 11$	$(33/58)$
LEP	$1 \times 5 \times 11 \times (27/7)$	1

a) 114.5 MHz in PS

Beam transfer mode			
Linac–EPA	Continuous injection advancing in EPA by 3 bucket-to-bucket distances after every linac pulse		
EPA–PS	Single turn injection of 8 bunches		
PS–SPS	Single turn injection of 4 bunches, kicker reloading and rephasing (30 ms), single turn injection of 4 bunches		
SPS–LEP	Transfer sequence depending on LEP injection mode (betatron or synchrotron-stacking)		
Beam transfer	Minimum between two bunch transfers		
	Turns	Time	
LIL–EPA ^{a)}		10	ms
EPA–PS	$(1/8) \times \text{PS}$	0.262	μs
PS–SPS	$4\frac{1}{4} \times \text{SPS}$	97.982	μs
SPS–LEP	$1 \times \text{LEP}$	88.925	μs

a) Pulse transfers

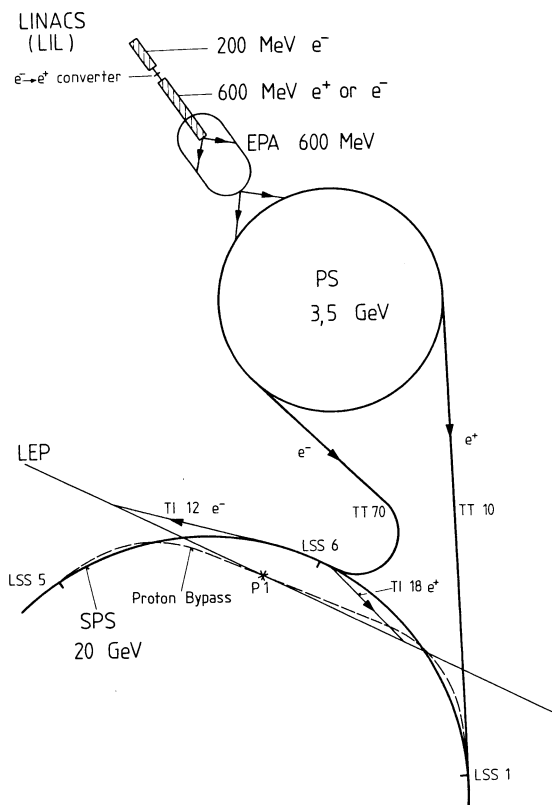


Fig. 2.1 Schematic layout of the LEP injector chain. The existing parts are drawn with a thick line; the dashed line indicates the possible future SPS bypass of the ep option. Of LEP, only the part around the crossing point 1 (P1) is shown.

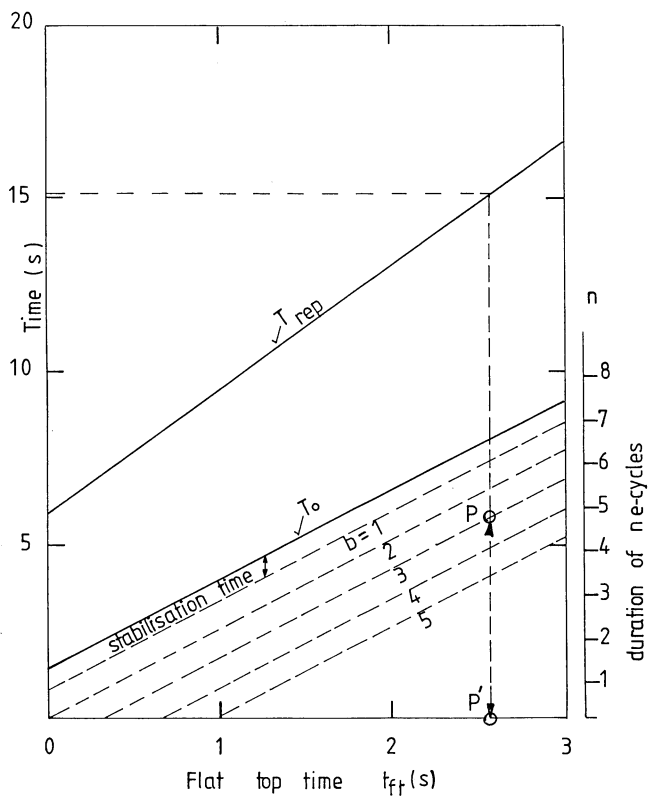


Fig. 2.2 Dead-time T_0 and repetition time T_{rep} of the SPS supercycle versus flat-top time at 450 GeV of the proton cycle. Example of the time remaining for e-cycles after stabilisation time and injection of three proton batches ($b = 3$) is indicated (PP') for the nominal SPS supercycle. On the right: duration of n e-cycles.

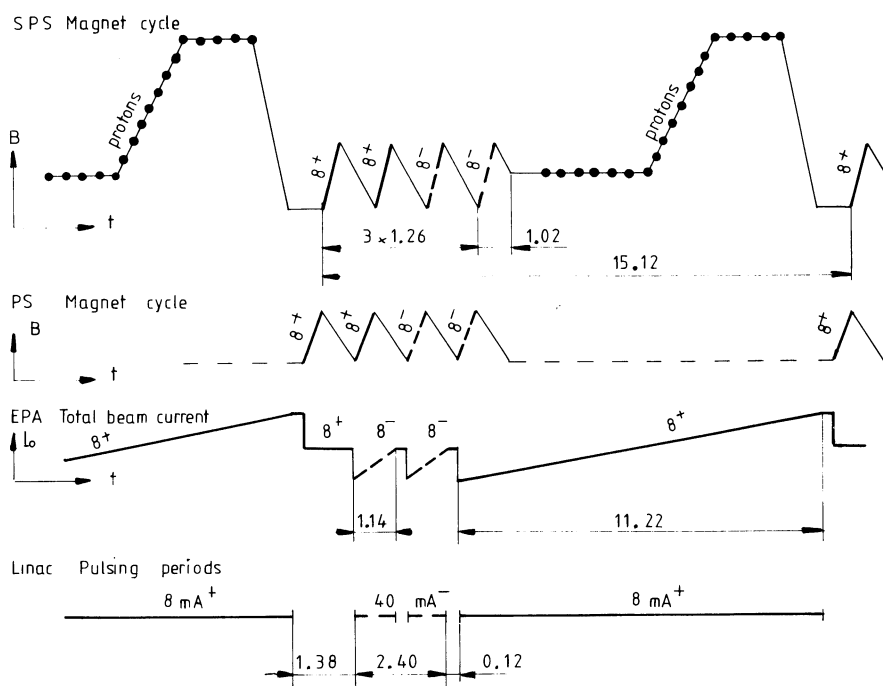


Fig. 2.3 Schematic diagram of the SPS and the PS magnet cycle, the EPA total beam current, and the linac pulsing periods versus time for the basic scheme. The numbers on the lines refer to the number of bunches used, and the sign of bunch charge is indicated. For the linac, the peak current defined as the average current during the 12 ns pulse is given.

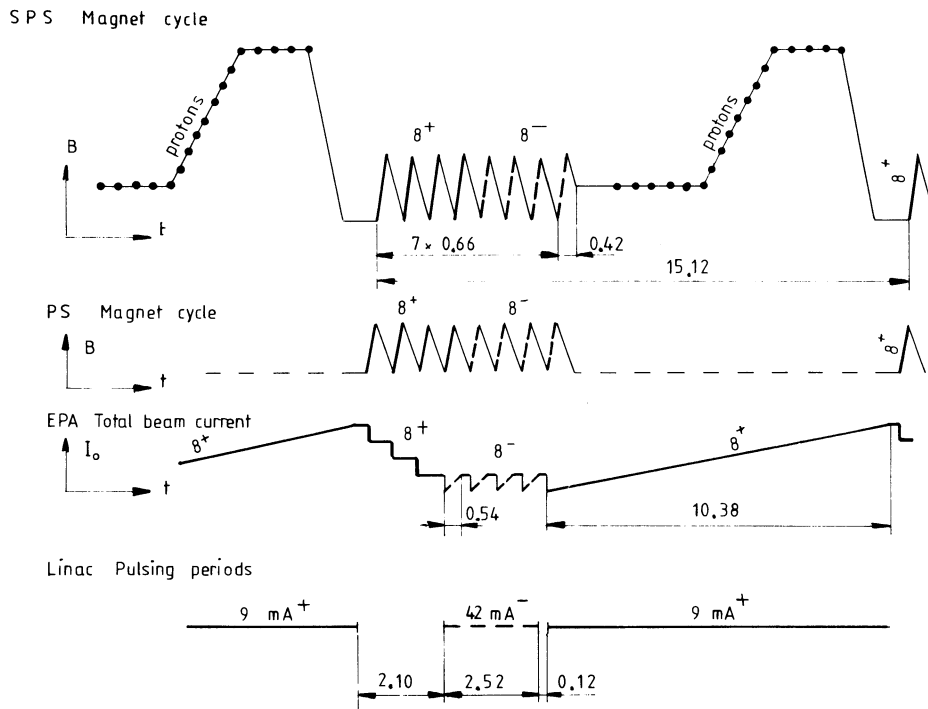


Fig. 2.4 Schematic diagram, as Fig. 2.3, of variant scheme with reduced bunch intensity.

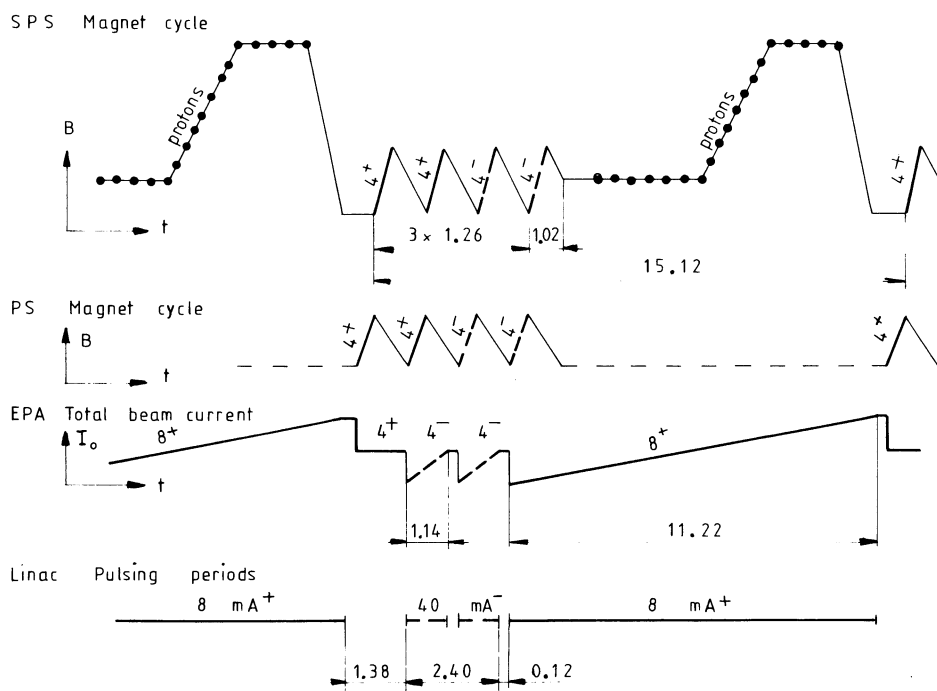


Fig. 2.5 Schematic diagram, as Fig. 2.3, of variant scheme providing four-bunch operation in the PS and the SPS.

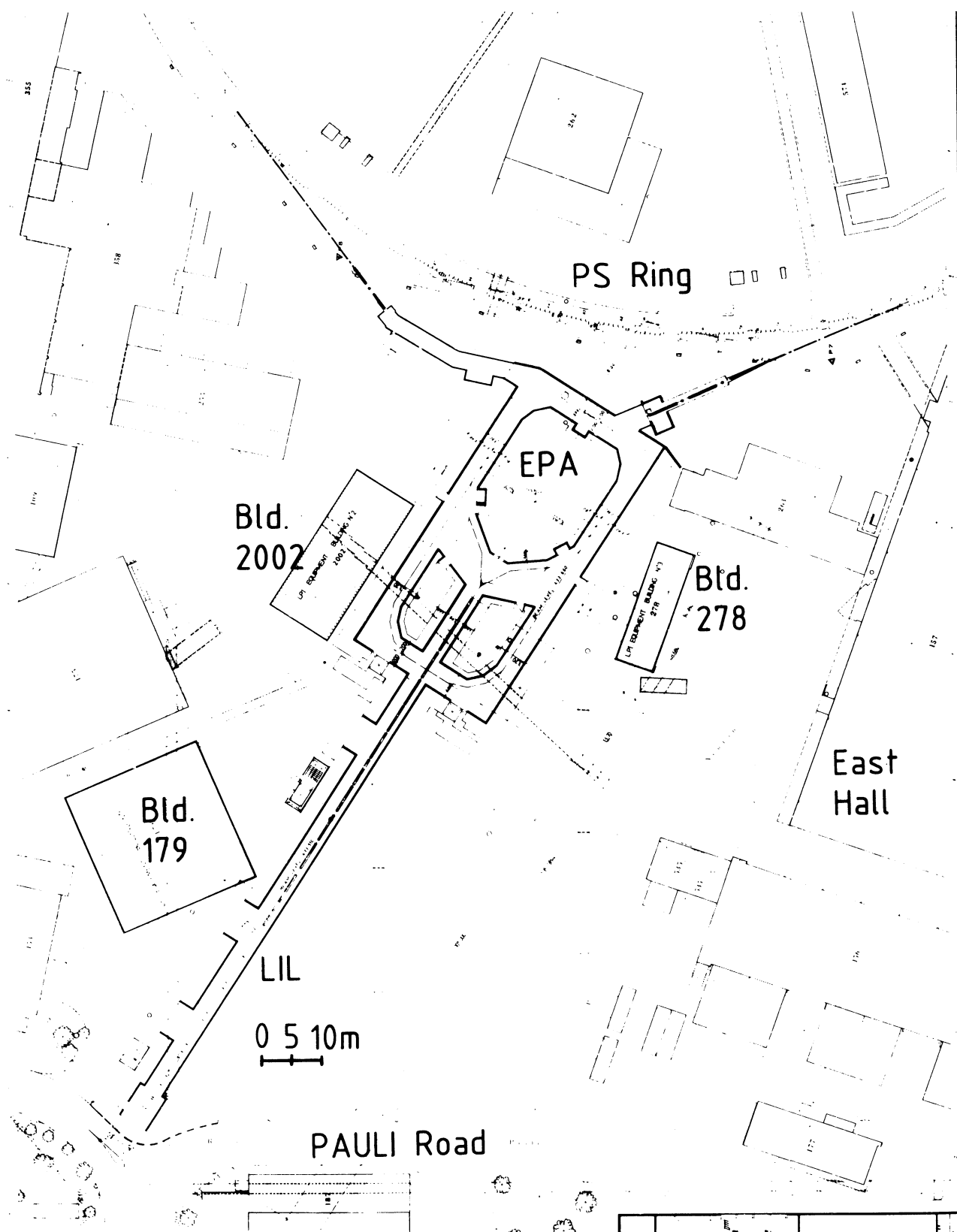


Fig. 3.1 Layout of the LEP pre-injector at the PS.

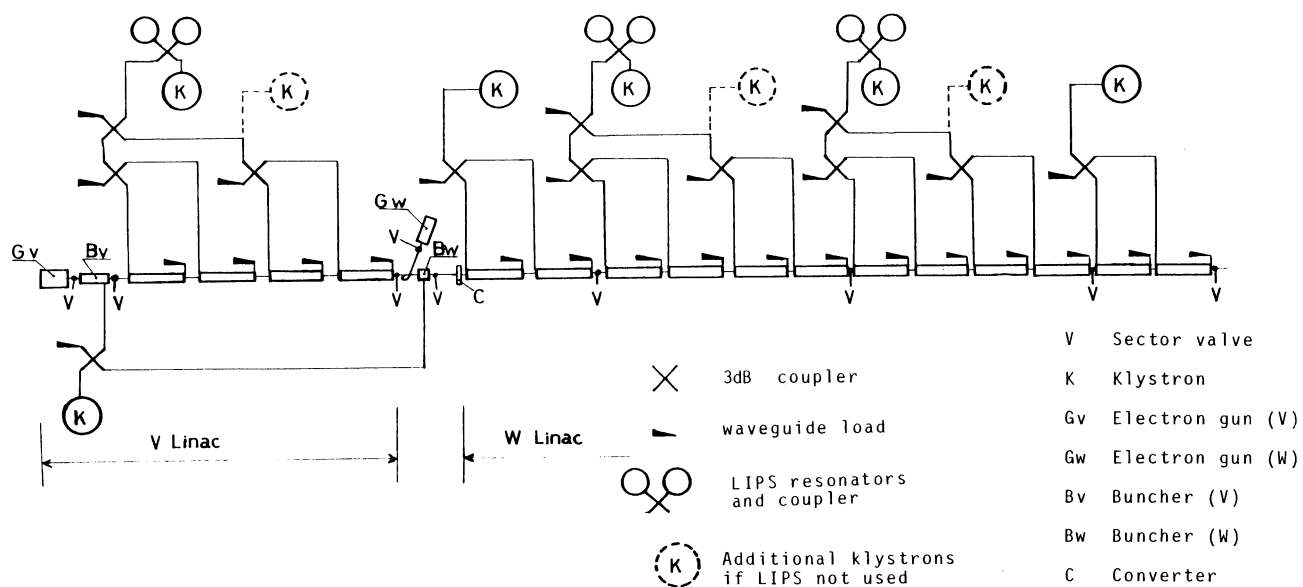


Fig. 3.2 Schematic layout of the LIL showing RF power distribution and position of sector valves.

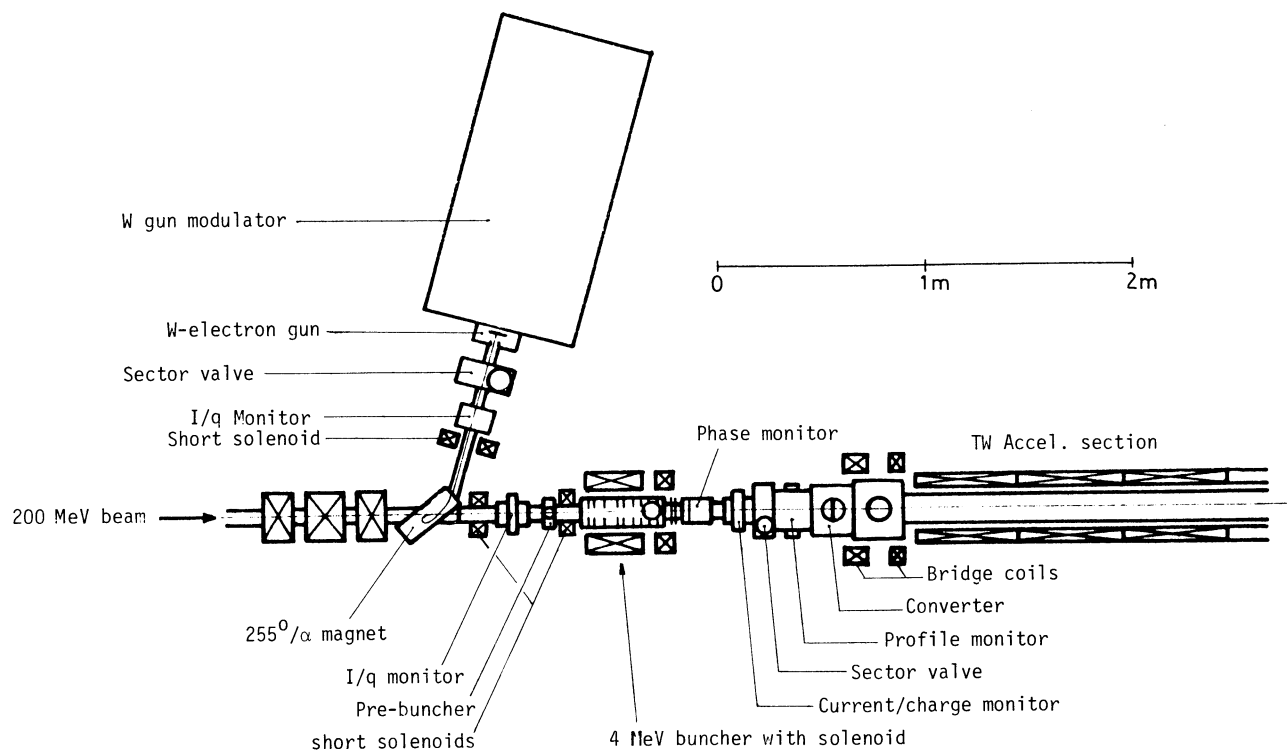


Fig. 3.3 Injection into linac W. Electron gun and converter.

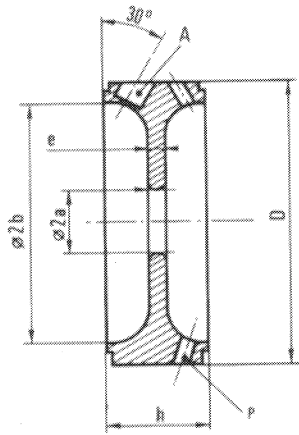


Fig. 3.4 Mechanical features of the LIL unit cell. There are four pumping holes (P) and four tuning recesses (A).

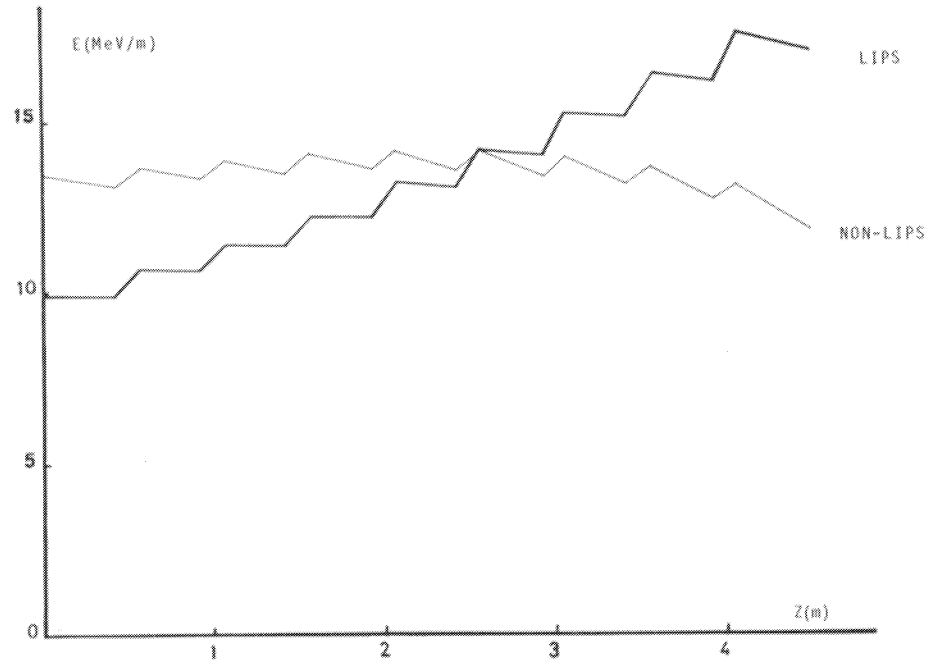


Fig. 3.5 Computed acceleration rate versus longitudinal particle position in the LIL TW accelerating section for LIPS and non-LIPS. Main parameters: for non-LIPS as in Table 3.3; for LIPS $Q(\text{spheres}) = 150\,000$, τ_p (RF pulse length) = $3.9\,\mu\text{s}$, π phase-switch at τ_p minus $1.2\,\mu\text{s}$.

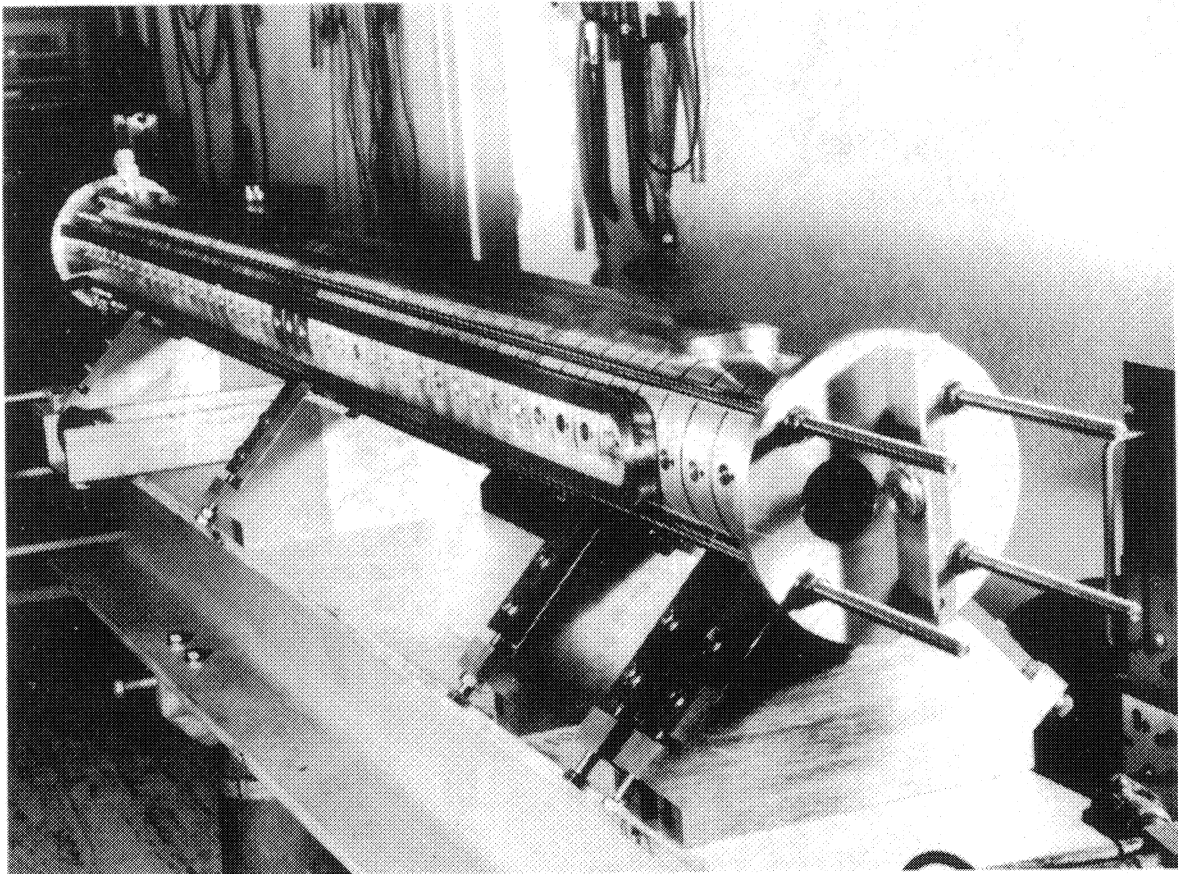


Fig. 3.6 Prototype 1.5 m long TW accelerating section (without couplers) of the LIL.

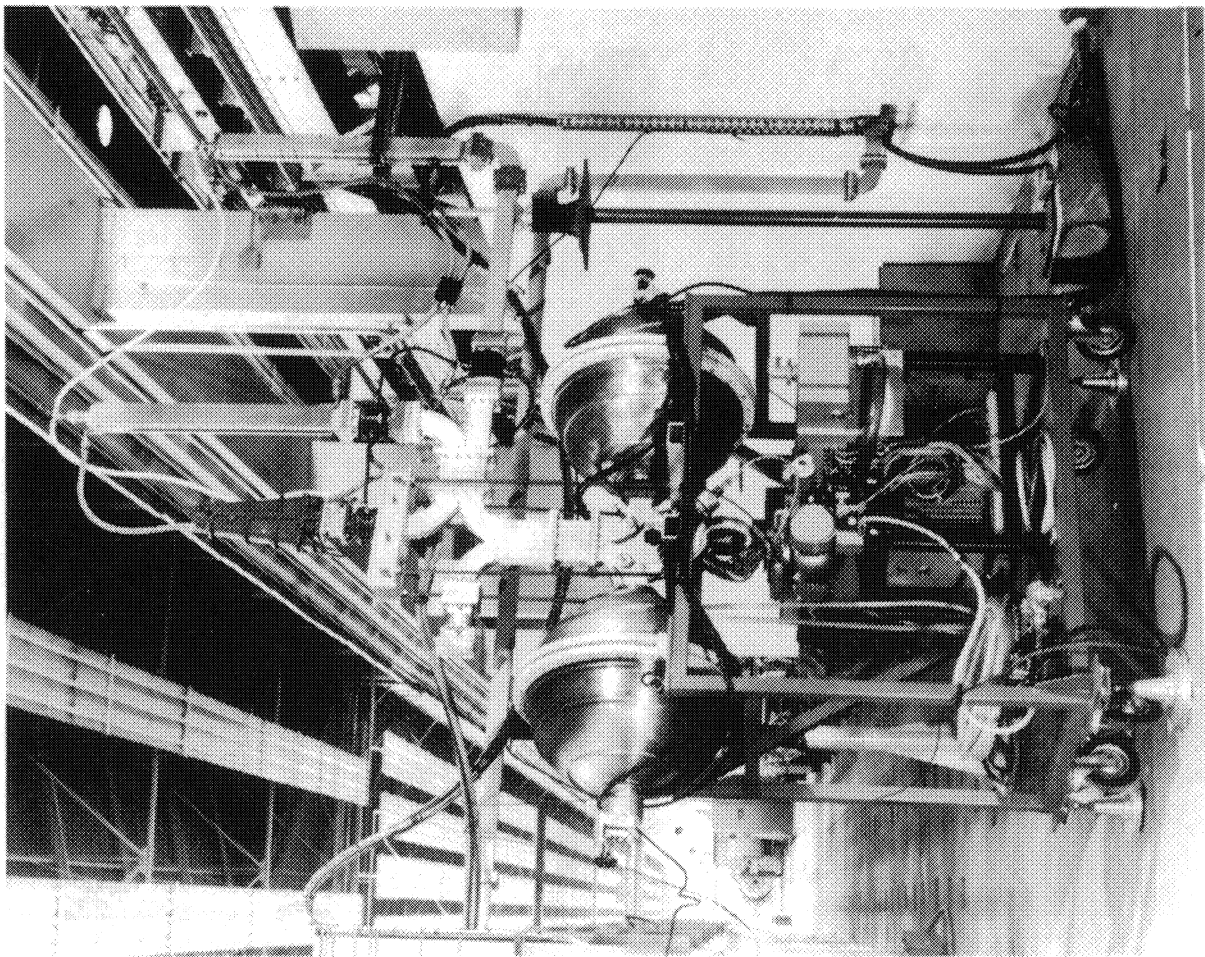


Fig. 3.7 Test set-up for prototype LIPS system at LAL. Two spherical, S-band storage cavities are shown with input waveguide (from left) and output waveguide (to right).

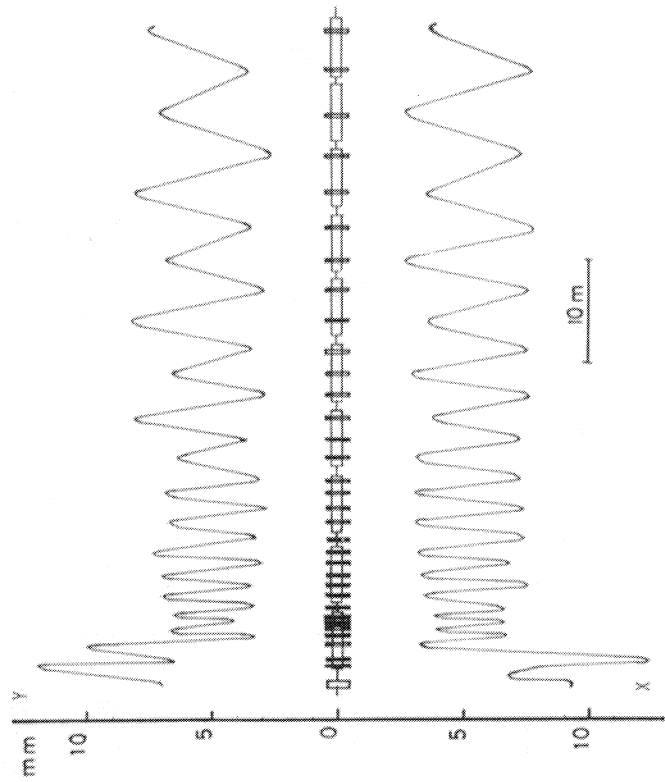


Fig. 3.8 Beam envelopes for positrons in linac W for ϵ (600 MeV) = $4.8 \pi \cdot \text{mm} \cdot \text{mrad}$: matching and FODO channel. Quadrupole positions on sections indicated in the middle.

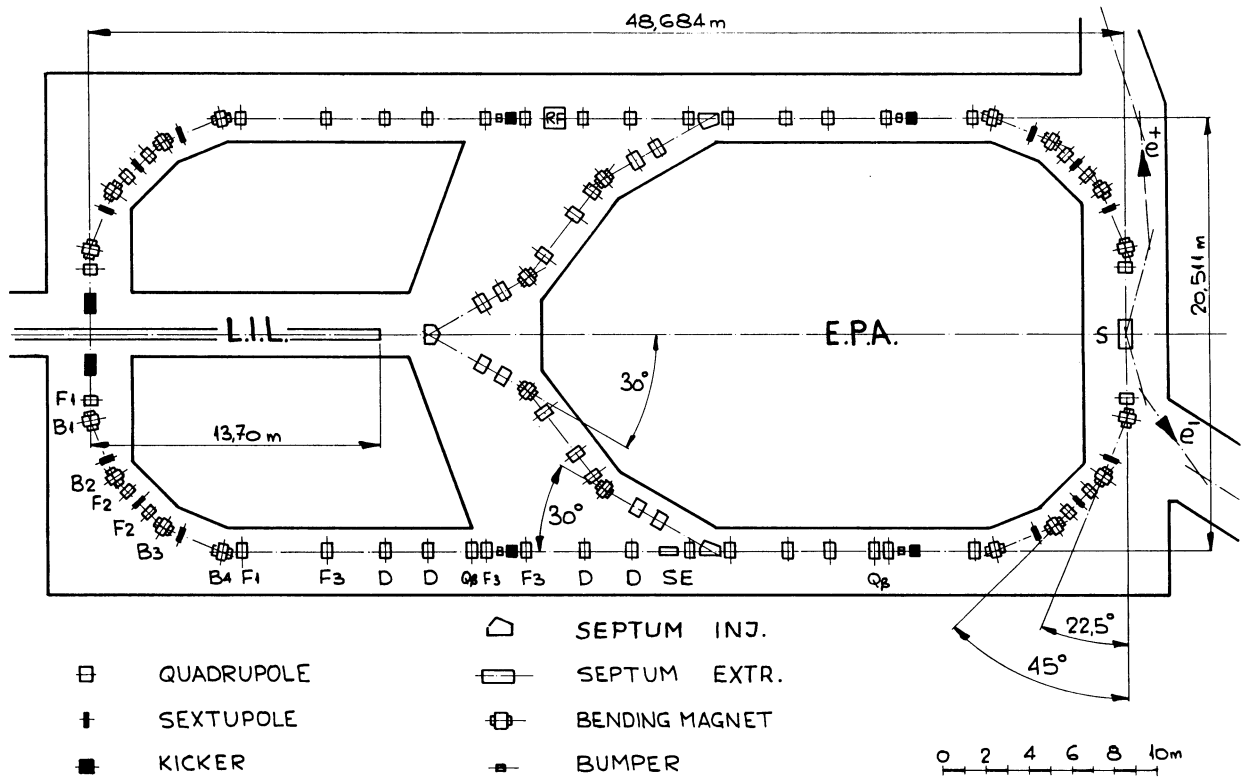


Fig. 3.9 Layout of the magnetic elements of the EPA including the transfer lines from LIL to EPA. S: extraction septum; SE: electrostatic septum.

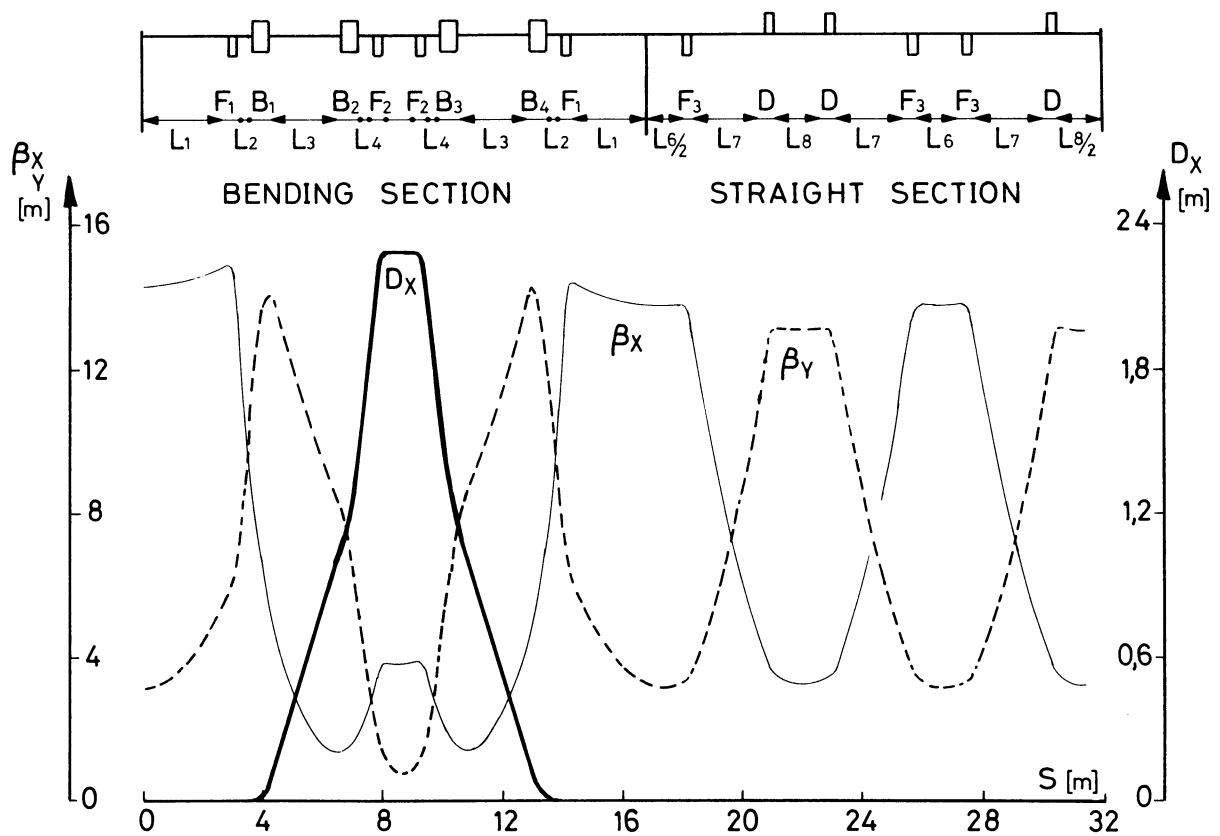


Fig. 3.10 Lattice functions in one EPA quadrant.

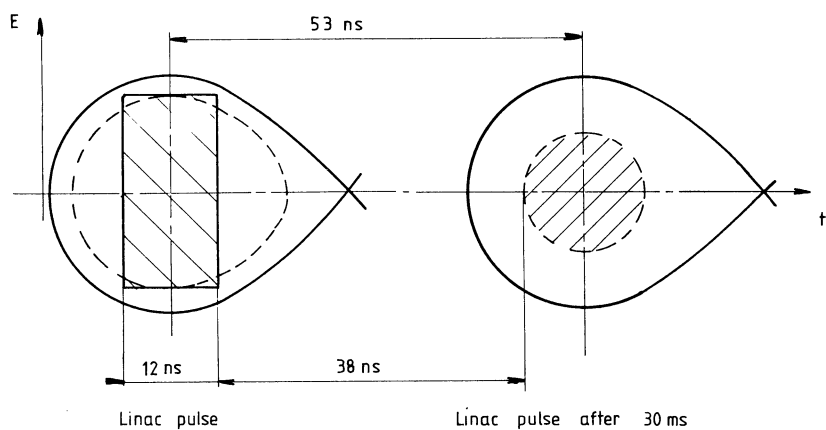


Fig. 3.11 Longitudinal phase plane in the EPA at the moment of injection into the bucket at the left. The bucket to the right contains a previously injected linac pulse. Three linac repetition times (3×10 ms) have already elapsed for this pulse. The bucket (not shown) to the left of the picture contains a pulse for which 5×10 ms have passed.

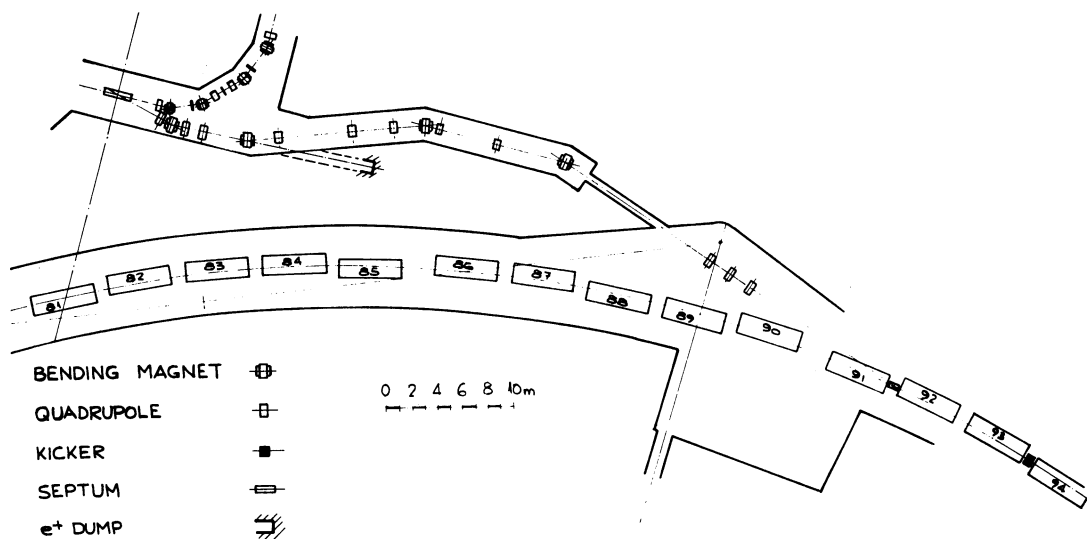


Fig. 3.12 Schematic layout of positron transfer line EPA → PS.

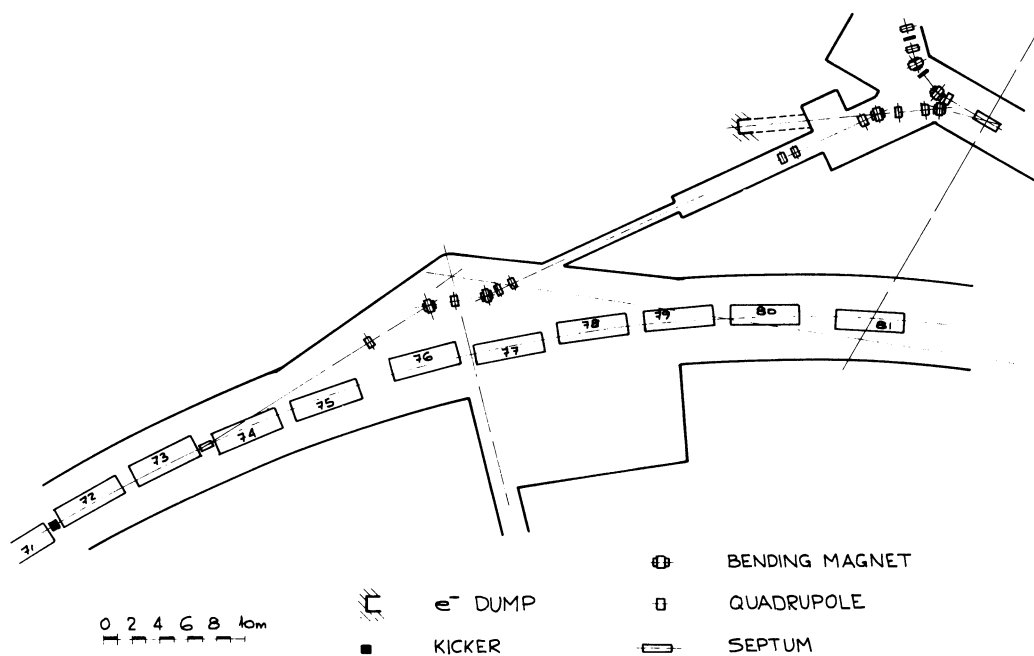


Fig. 3.13 Schematic layout of electron transfer line EPA → PS.

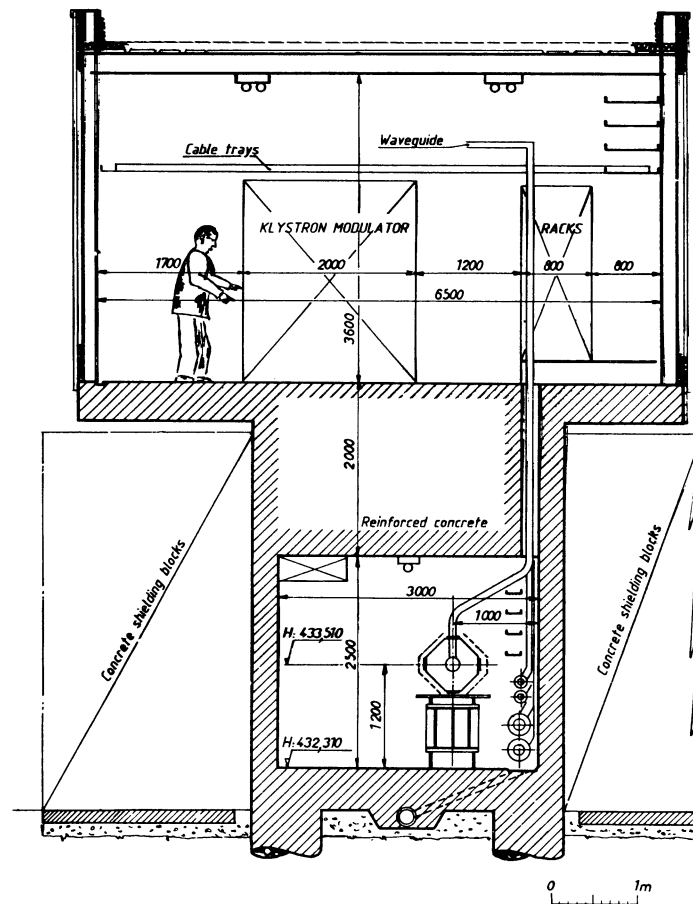


Fig. 3.14 Cross-section of linac building; klystron and modulator gallery at top, linac tunnel below.

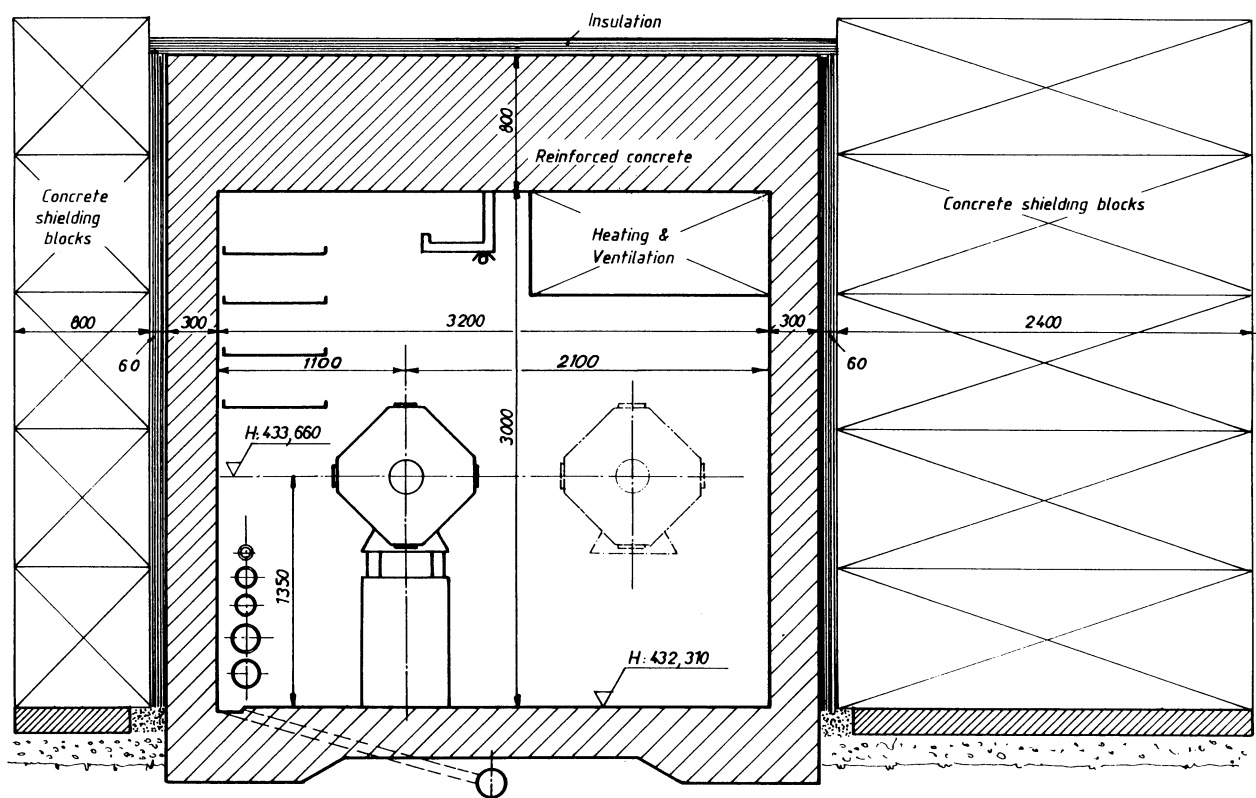


Fig. 3.15 Cross-section of the EPA tunnel.

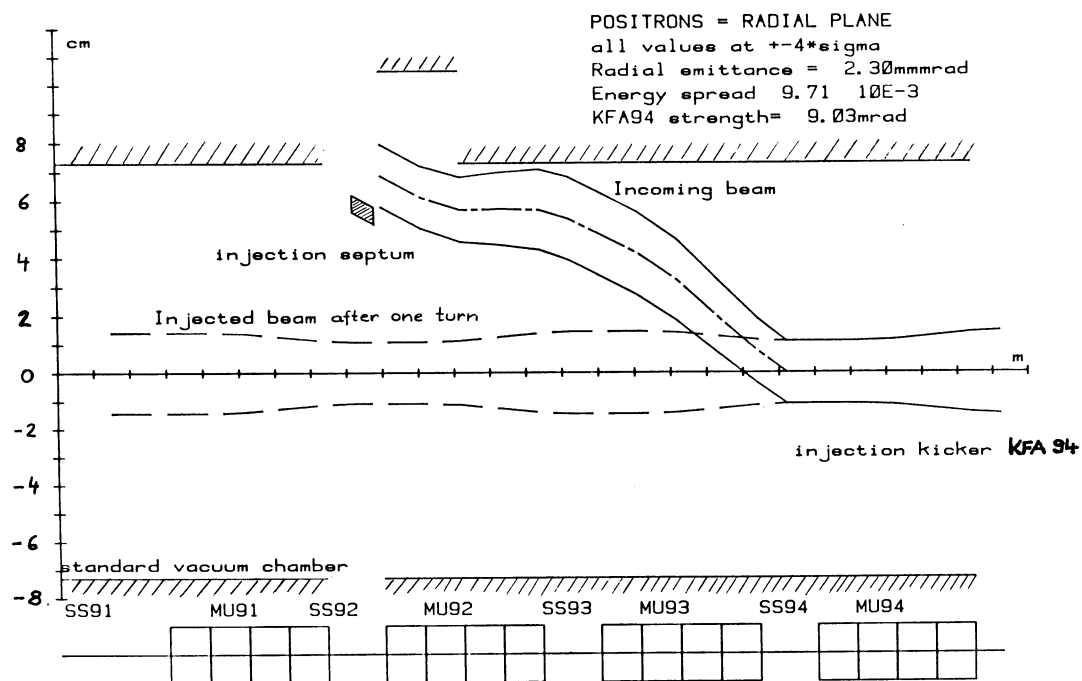


Fig. 3.16 Beam envelope at the PS injection point swept out by the injected positron bunch.

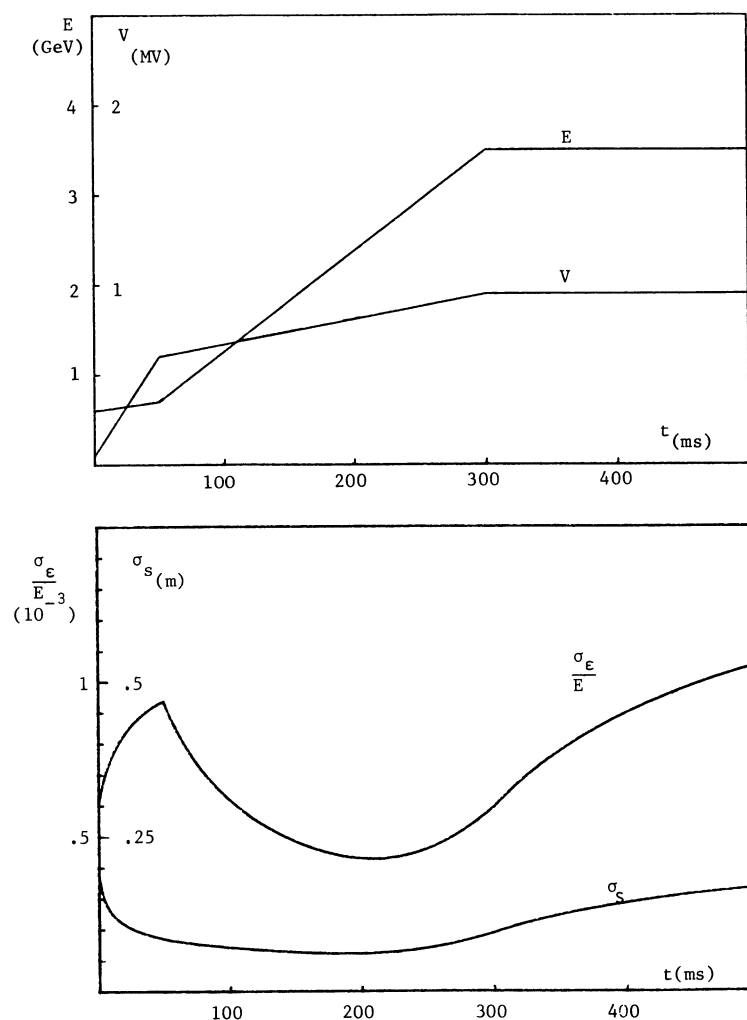


Fig. 3.17 Example of RF voltage program; evolution of bunch length and relative energy spread during acceleration in the PS with bunch expansion. Ejection takes place after 430 ms.

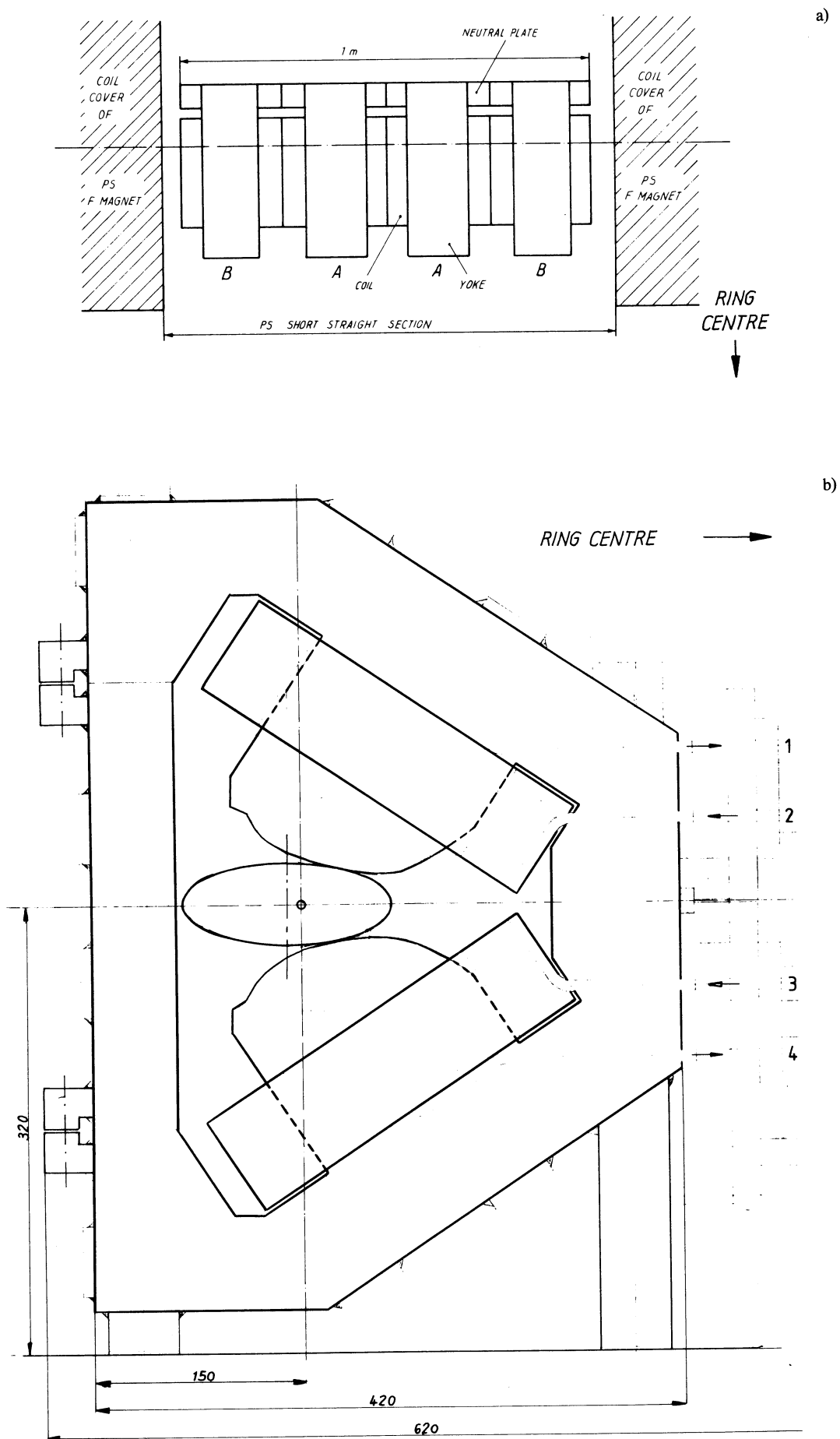


Fig. 3.18 Robinson wiggler magnet in the PS: a) plane view of wiggler layout in short F straight section; b) side view of one wiggler block.

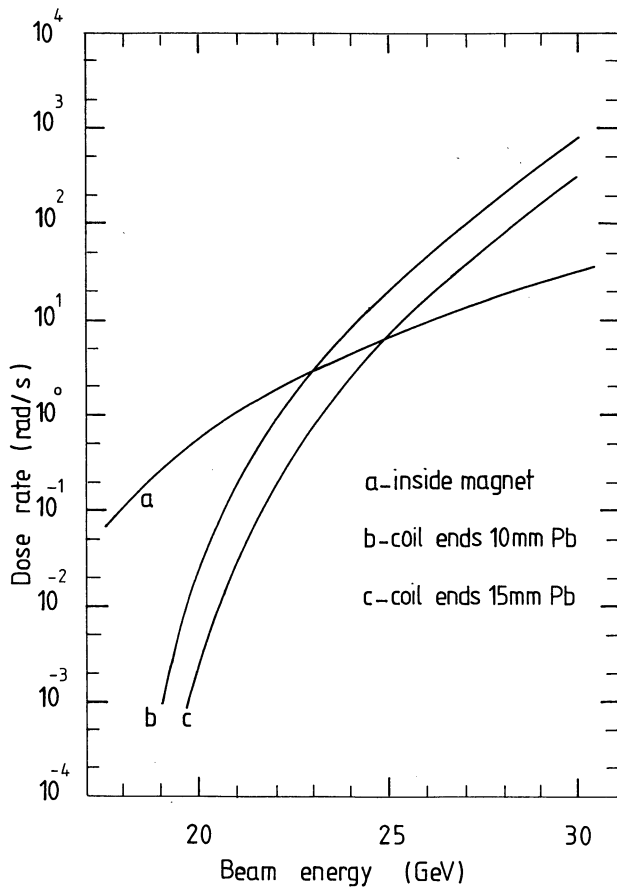


Fig. 3.19 Dose rate to coil insulation of the SPS dipole magnet MBB during electron cycles with 0.45 mA circulating beam.

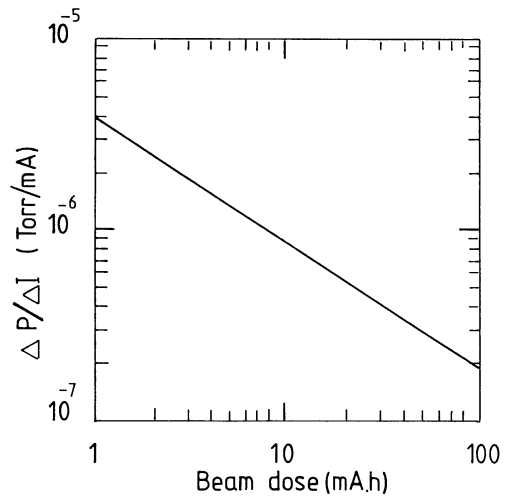


Fig. 3.20 Pressure rise factor $\Delta P/\Delta I$ (Torr/mA) versus beam dose ($\text{mA} \cdot \text{h}$) for a linear pumping speed of $S = 3.5 \text{ l s}^{-1} \text{ m}^{-1}$ and steady-state operation at 20 GeV in the SPS.

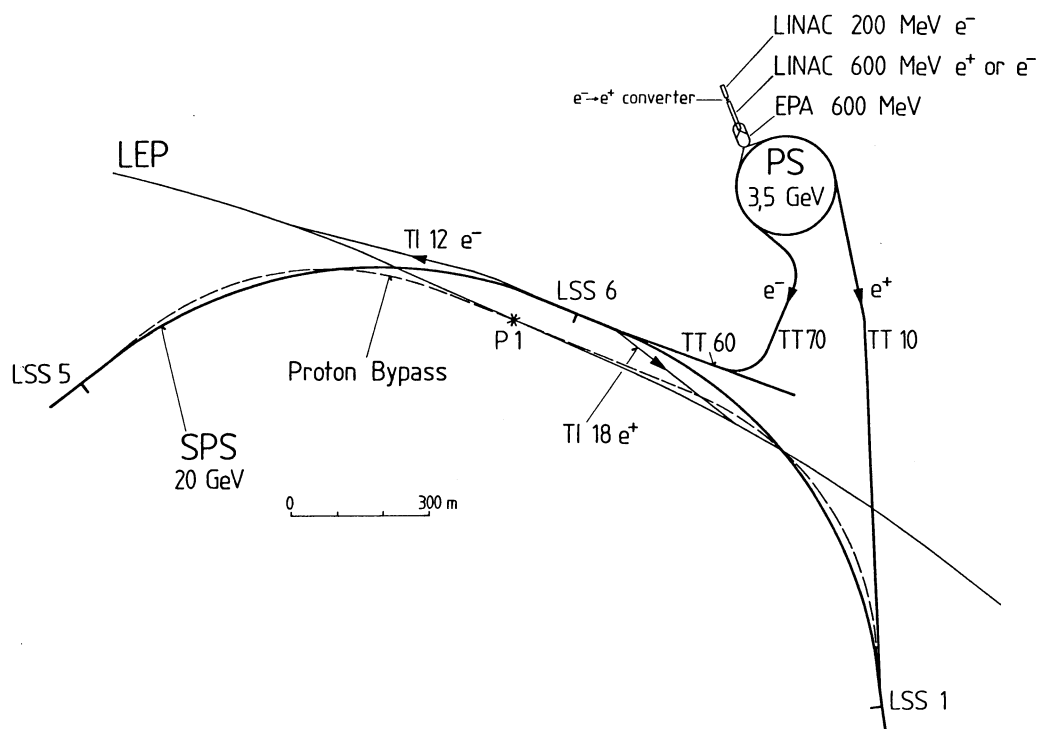


Fig. 3.21 Layout of transfer lines from the PS to SPS and the SPS to LEP. Possible proton bypass of the SPS is indicated by the dashed line.

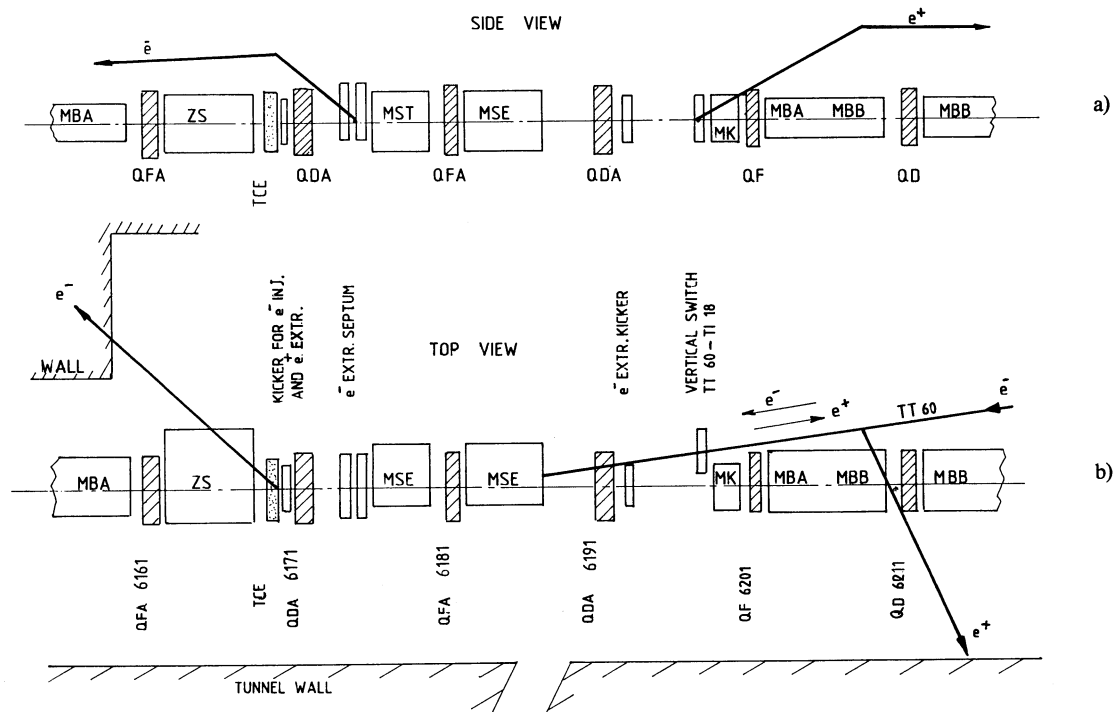


Fig. 3.22 Schematic layout of e^- injection and e^+ extraction in LSS6 of the SPS: a) elevation; b) plan view.

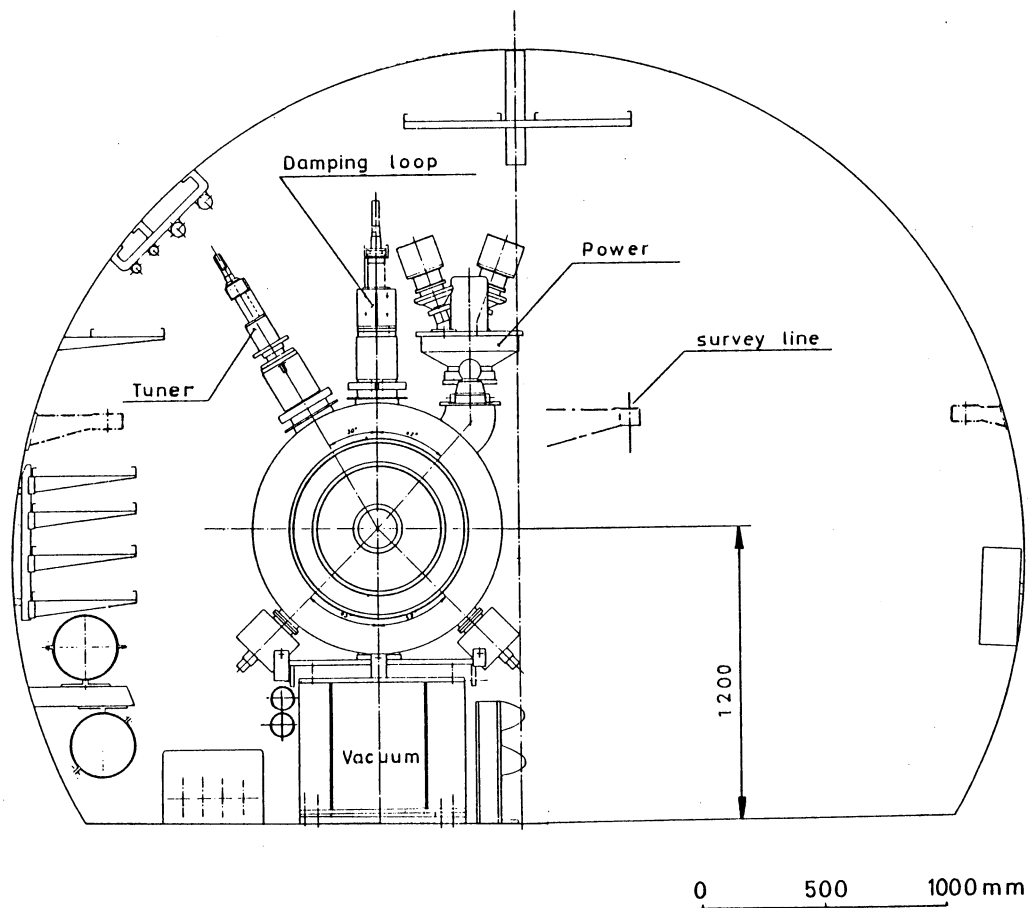


Fig. 3.23 Cross-section of the SPS tunnel in LSS3 showing a new 200 MHz single-cell cavity with amplifier and auxiliary devices.

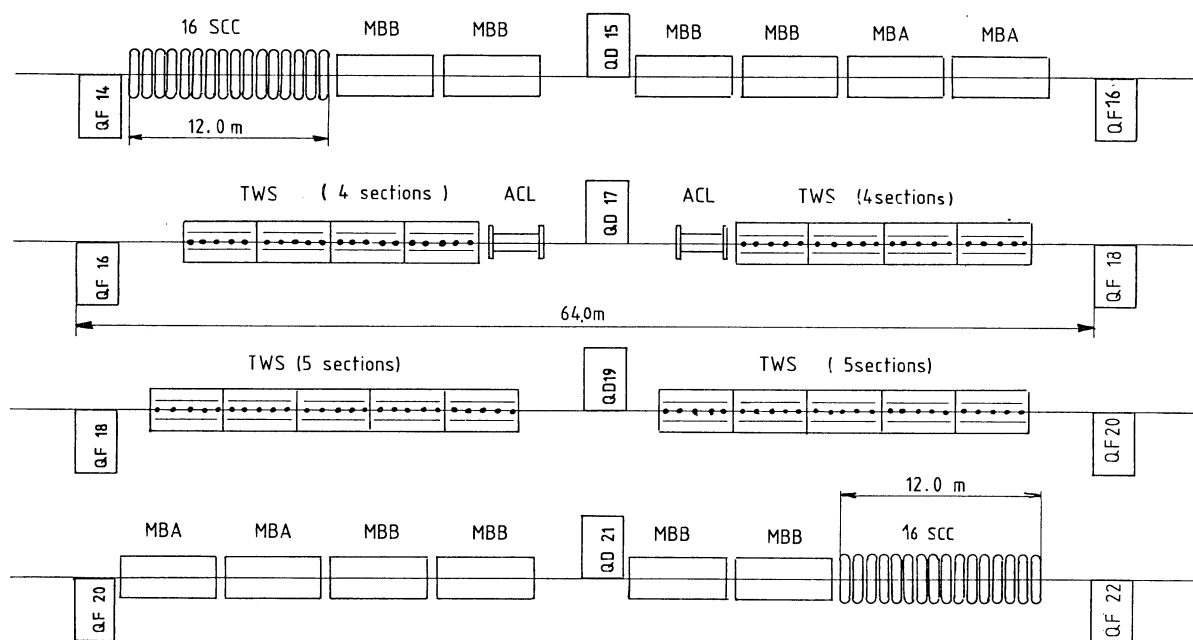


Fig. 3.24 Schematic layout of the SPS LSS3. TWS: travelling wave structure (200 MHz); ACL: travelling wave structure for Landau damping (800 MHz); SCC: new single-cell cavity (200 MHz); MBA, MBB: dipole magnets.

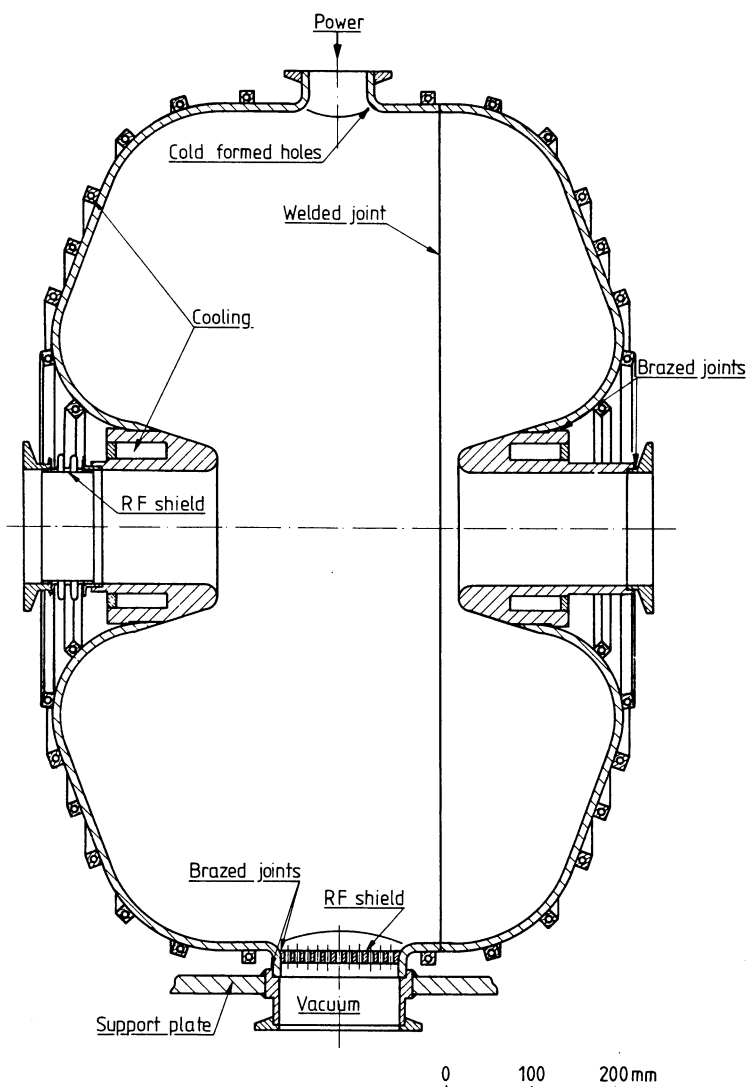


Fig. 3.25 Cross-section of new single-cell 200 MHz RF cavity for the SPS.

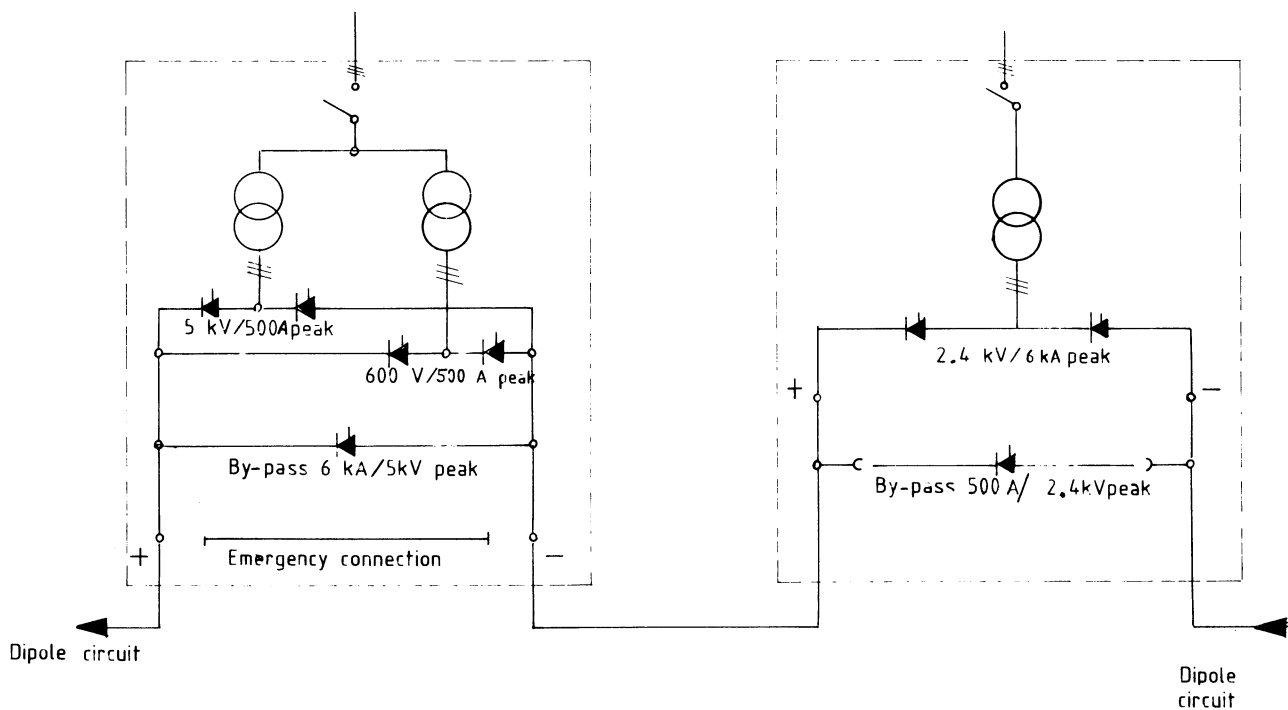


Fig. 3.26 Schematic layout of the new rectifiers and the existing ones for the SPS dipoles. Left: one of the 2 new dipole rectifiers for electron acceleration; right: one of the 14 existing dipole rectifiers for proton acceleration.

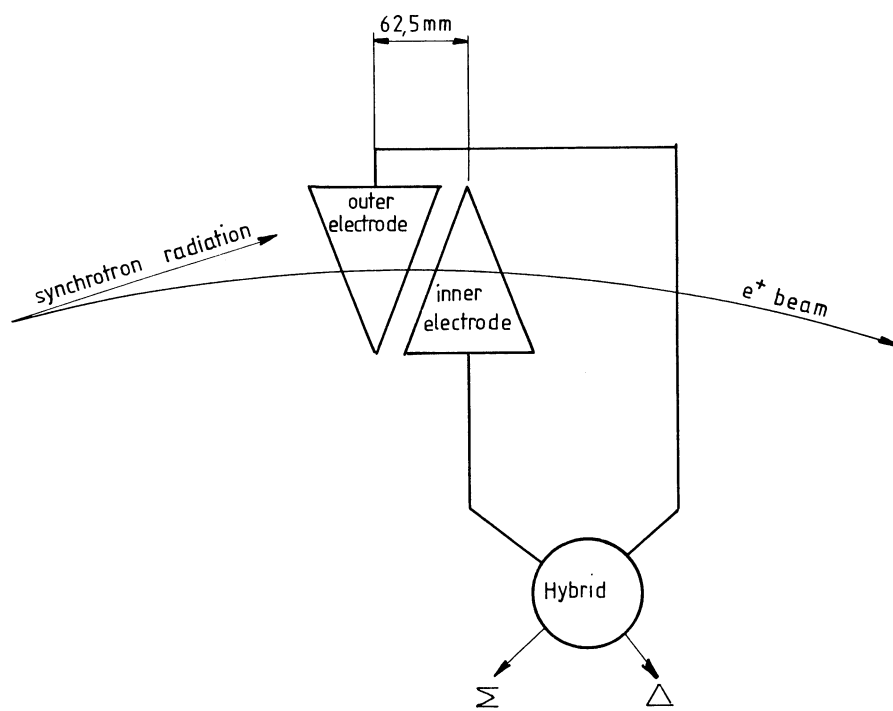


Fig. 3.27 Operating principle of the SPS electrostatic pick-ups.

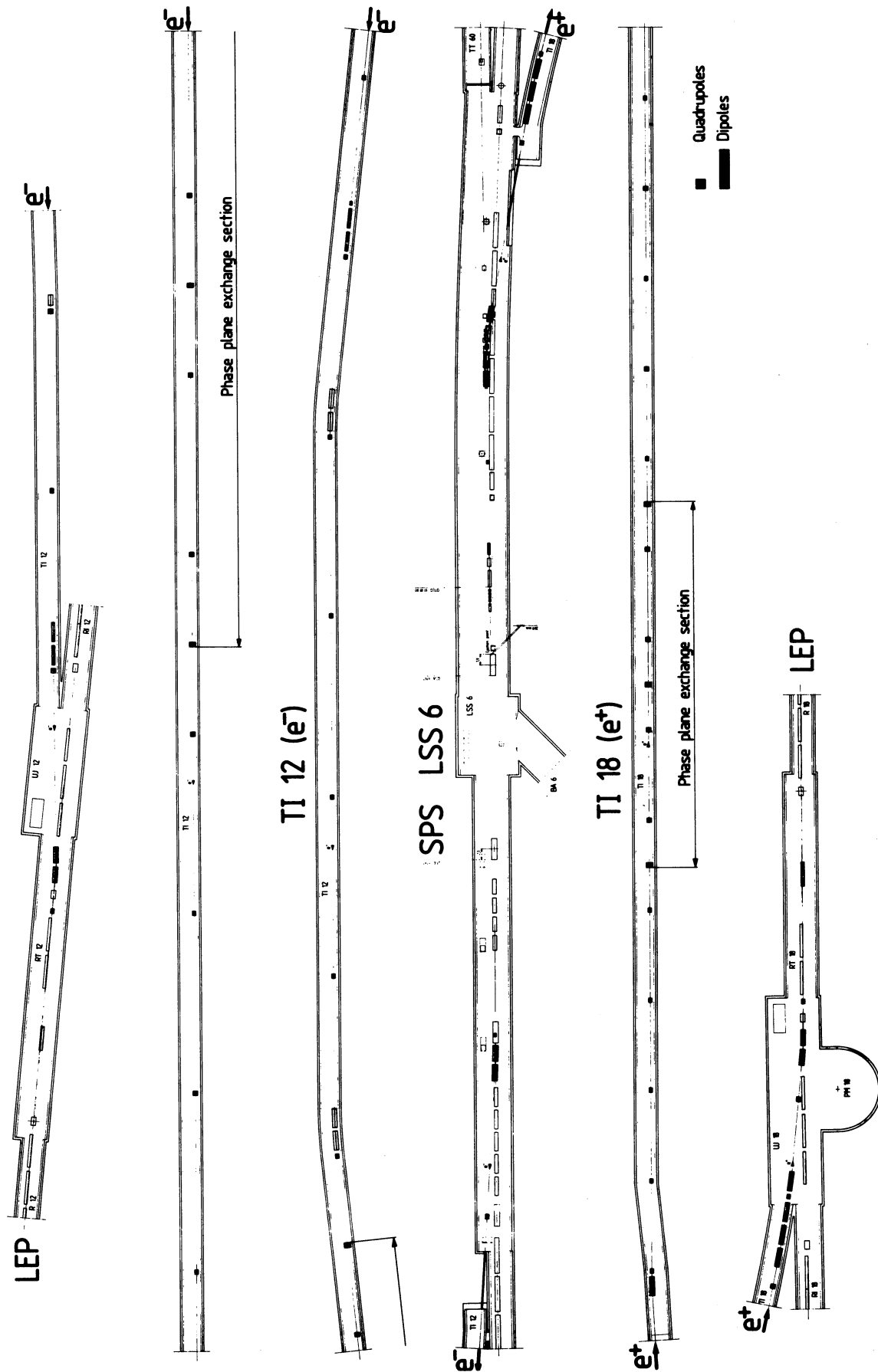


Fig. 3.28 Plan view of the e^+ and e^- beam transfer lines from the SPS to LEP. Extraction points from LSS6 of the SPS are shown in the middle.

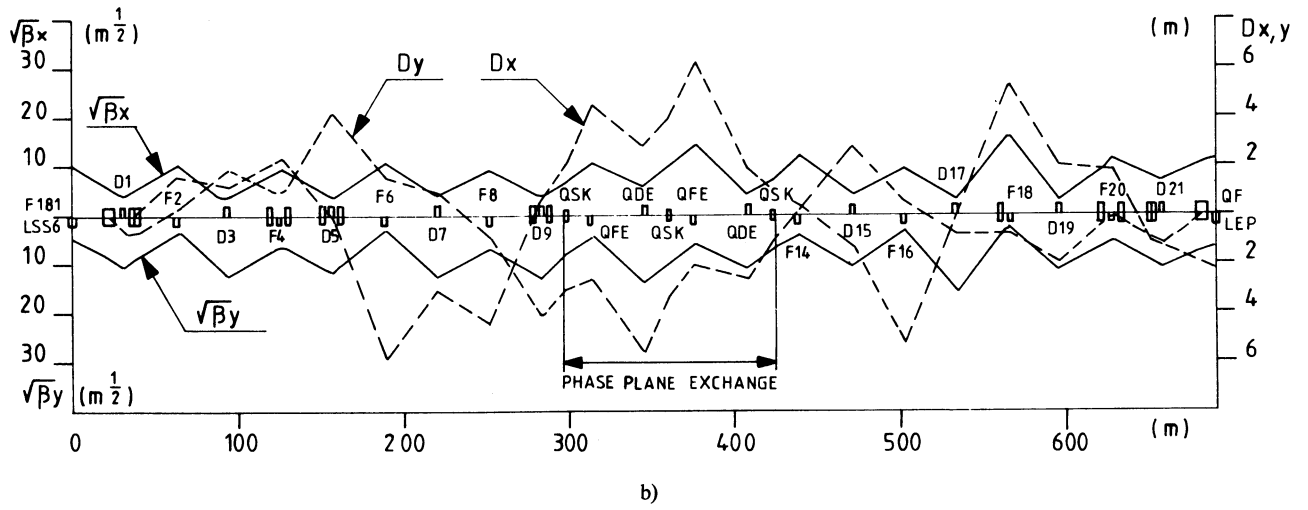
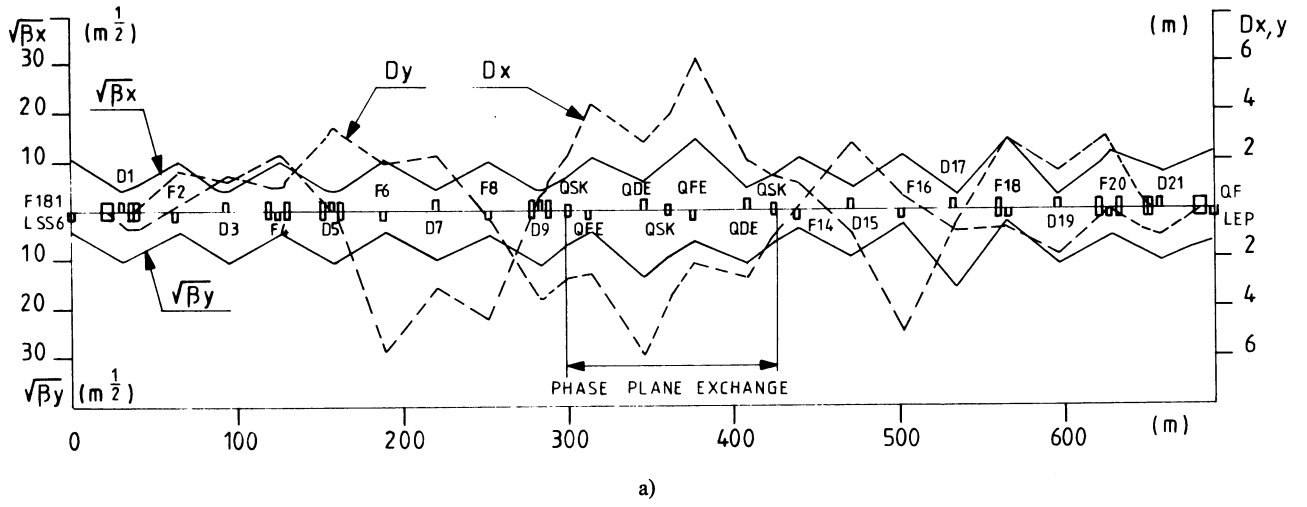


Fig. 3.29 Dispersion and betatron functions in beam transfer line from the SPS to LEP (TI12) with phase-plane exchange section: a) betatron functions matched and dispersion zero at QF20 in LEP; b) same as (a) but dispersion also matched to LEP.

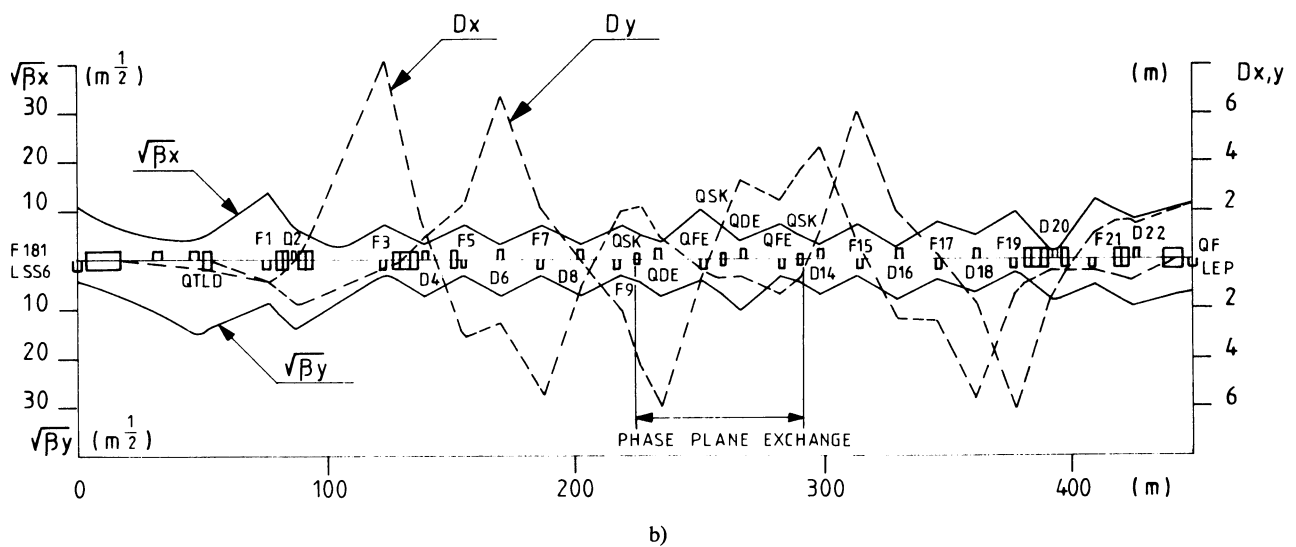
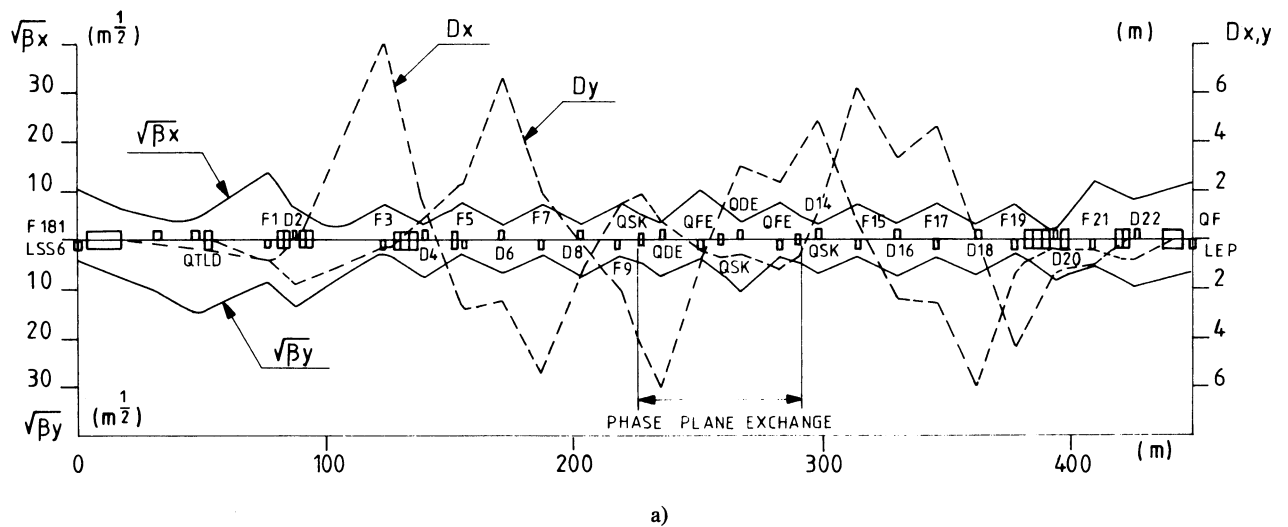


Fig. 3.30 Dispersion and betatron functions in beam transfer line from the SPS to LEP (TI18) with phase-plane exchange section: a) betatron functions matched and dispersion zero at QF20 in LEP; b) same as (a) but dispersion also matched to LEP.

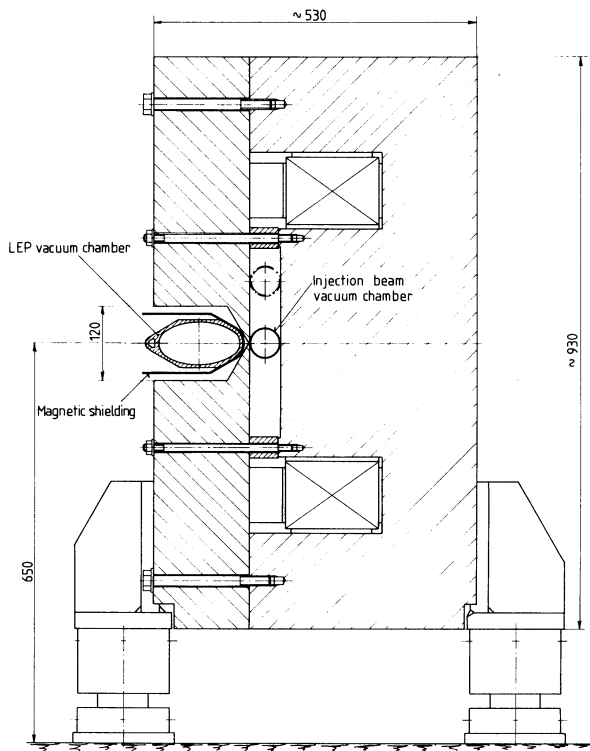


Fig. 3.31 Schematic cross-section of a steel-septum magnet for the LEP injection system.

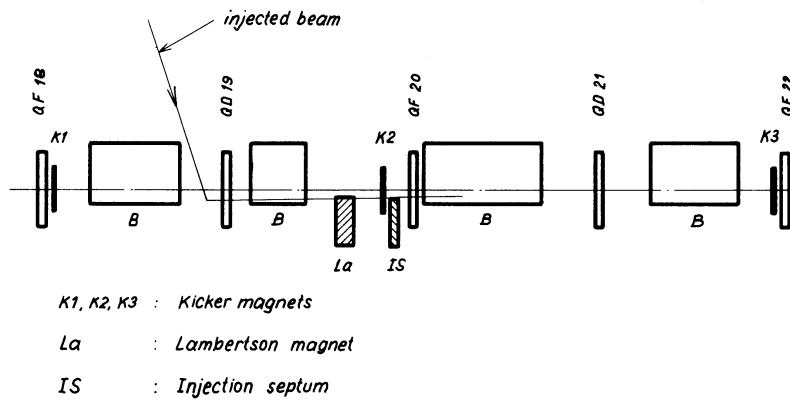


Fig. 3.32 Schematic layout of the LEP injection system (plan view). K_i : kickers; La : Lambertson magnet (steel-septum magnet); IS : injection septum magnet; B : bending magnets. Septa are on the inner side of LEP.

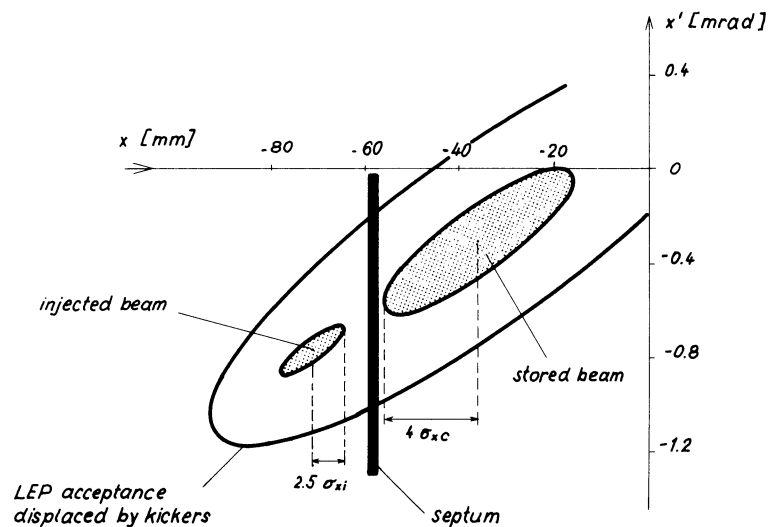


Fig. 3.33 Beam disposition in the horizontal phase plane at the exit of the injection (copper) septum magnet in LEP.

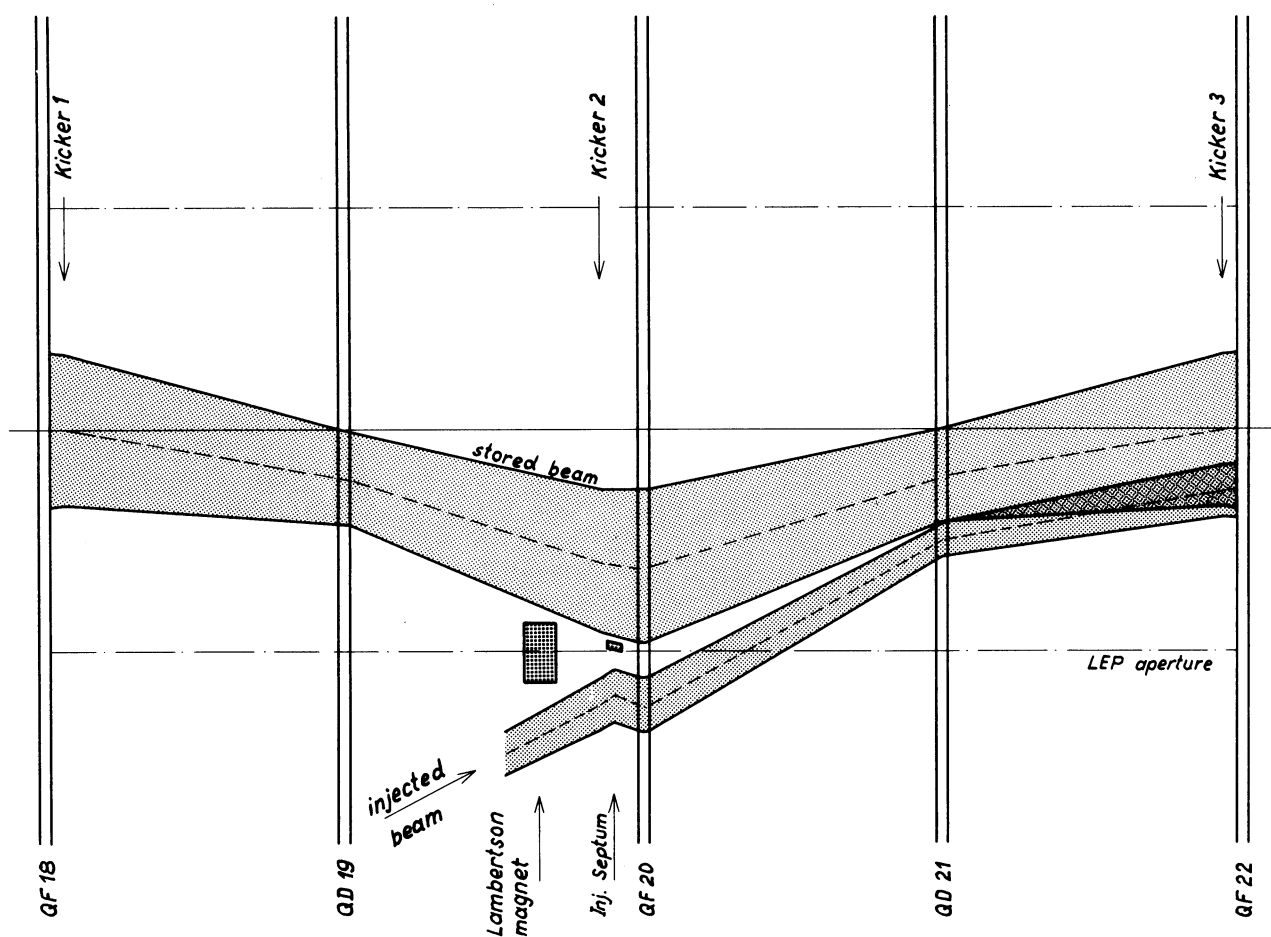


Fig. 3.34 Horizontal beam envelopes swept out by the stored and the injected bunch at LEP injection point. Example drawn for betatron accumulation and 60° phase advance in LEP.

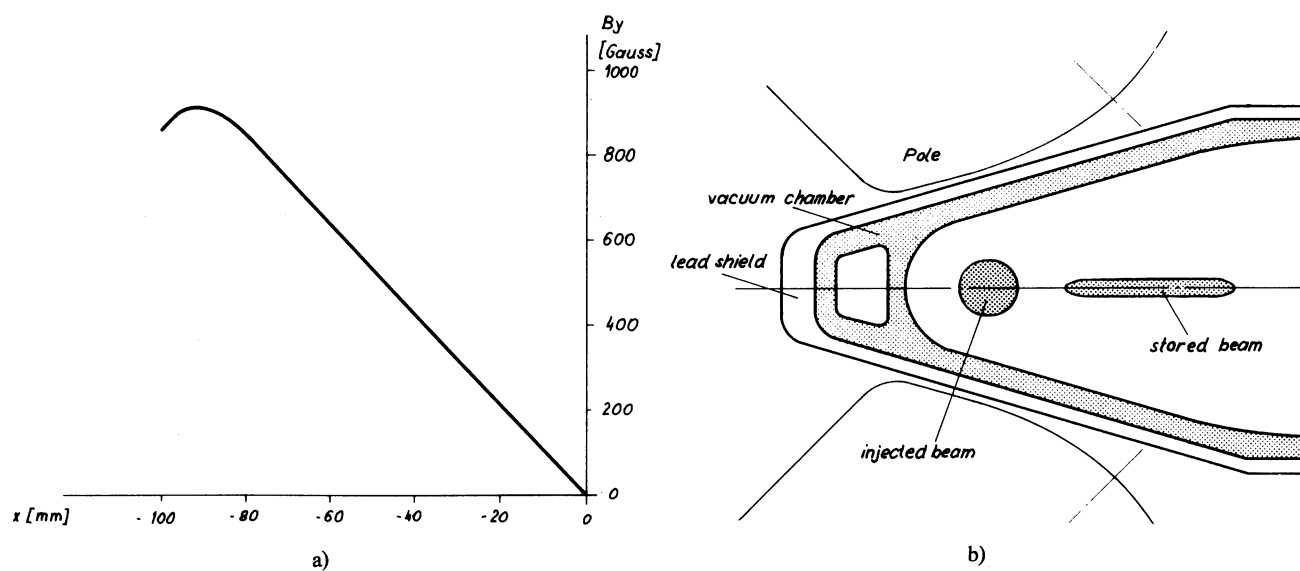


Fig. 3.35 a) Magnetic field distribution in LEP quadrupole QF20 at injection. b) Position of the injected and the stored beam in vacuum chamber of LEP quadrupole QF20 during injection.